Spring 2022

Characterization of high cycle fatigue and laser-aided machining and polishing of additively manufactured materials

Mohammad Masud Parvez

Department: Mechanical and Aerospace Engineering

CHARACTERIZATION OF HIGH CYCLE FATIGUE AND LASER-AIDED MACHINING AND POLISHING OF ADDITIVELY MANUFACTURED MATERIALS

by

MOHAMMAD MASUD PARVEZ

A DISSERTATION

Presented to the Graduate Faculty of the

MISSOURI UNIVERSITY OF SCIENCE AND TECHNOLOGY

In Partial Fulfillment of the Requirements for the Degree

DOCTOR OF PHILOSOPHY

in

MECHANICAL ENGINEERING

2022

Approved by

Dr. Frank Liou, Advisor
Dr. Lokeswarappa R. Dharani
Dr. K. Chandrashekhara
Dr. Ashok Midha
Dr. Joseph W. Newkirk

PUBLICATION DISSERTATION OPTION

This dissertation consists of the following three article which have been published as follows:

Paper I: Pages 8 - 33, "A Displacement Controlled Fatigue Test Method for Additively Manufactured Materials", was published in Applied Sciences Journal.

Paper II: Pages 34 - 60, "High Cycle Fatigue Performance of LPBF 304L Stainless Steel at Nominal and Optimized Parameters", was published in Materials Journal.

Paper III: Pages 61 - 89, "A Novel Laser-Aided Machining and Polishing Process for Additive Manufacturing Materials With Multiple Endmill Emulating Scan Patterns", was published in Applied Sciences Journal.

All the above papers have been prepared in the Missouri University of Science and Technology dissertation format.

ABSTRACT

Additive manufacturing (AM) and laser-aided machining and polishing (LAMP) of materials are emerging manufacturing processes both for research and industrial sectors. The AM process can manufacture near-net-shape parts with complex geometries. Meanwhile, the LAMP process integrated with an AM system offers a high processing rate, minimum heat-affected zone, and easily adjustable process parameters during machining and polishing. In mechanical properties characterization of AM metals and alloys, fatigue is a vitally important test method to understand the behavior of materials in cycling loading and unloading circumstances since most mechanical failures of structures are due to fatigue. To characterize AM metal fatigue behavior, it is also crucial to understand and analyze how the fabrication process parameters, build orientations, and defect formations affect the ability of materials to resist fatigue failure. This research aims to study the needed fundamental knowledge for a high-speed fatigue testing method with miniature specimens and investigate the effect of build process parameters on the high cycle fatigue performance of AM materials. In this study, the implementation of miniature specimens with increased surface area and uniform stress distribution within gauges captures a large population of surface and subsurface defects, reduces the stress gradient effect, maintains symmetric loading, minimizes material and test equipment costs, and decreases sample preparation and test time. The acquired knowledge from this study helps understand the influence of defects on the fatigue behavior of AM materials and determine the high fatigue strength yielding process parameters. Since the fatigue strength of materials can be improved by machining and polishing part surfaces, the objectives of this research also include developing a multilaser LAMP process and investigating the effect of different process parameters on part surface quality improvements. The research results lead to new knowledge that could benefit a wide range of manufacturing industries.

ACKNOWLEDGMENTS

All praise goes to the almighty Allah for giving me the strength and perseverance to continue this arduous and extensive journey. I would like to take a moment to acknowledge all the important individuals who helped me along the way.

First, I must thank my supervisor, Dr. Frank Liou, for his constant support and guidance in achieving such academic accomplishment. My sincere gratitude also goes to the Ph.D. advisory committee members: Dr. Chandrasekhara, Dr. Midha, Dr. Dharani, and Dr. Newkirk for their interest in my work and serving as the dissertation committee. I would also like to thank NSF, Department of Energy's Kansas City National Security Campus (KCNSC) operated by Honeywell Federal Manufacturing Technologies, Intelligent Systems Center (ISC), Material Research Center (MRC), and Mechanical and Aerospace Engineering Department (MAE) at Missouri University of Science and Technology. I also appreciate the helps I received from the members of LAMP lab.

I want to express my gratitude to my siblings: Mamun, Moon, and Nishi in fulfilling all my responsibilities towards our parents in my absence. I am indebted to them especially to my elder brother. This expedition would never be possible without his help and support. My other family members: Sumona, Afia, Ahyan, and my parents in law; and friends: Galib, Shaheen, Palash also deserve my wholehearted thanks as well. Finally, I am thankful to my wife, Musarrat and to be born junior Hasan. I am fortunate to have Musarrat beside me throughout the journey. Her patience and understanding strengthened me through tough times.

I would like to acknowledge Hasan Engineering and Shaheen Engineering Works for aspiring me to be an engineer and bringing the enthusiasm for science and technology.

I dedicate this dissertation to my parents with heartfelt gratefulness for their constant support, prayers, sacrifices, and unconditional love.

TABLE OF CONTENTS

Page

LIST OF ILLUSTRATIONS

PAPER II

PAPER III

LIST OF TABLES

SECTION

1. INTRODUCTION

1.1. BACKGROUND

Additive manufacturing (AM) is a layer-by-layer material deposition process. There are several techniques recently developed for metal and alloy deposition i.e. laser powder bed melting (LPBF), electron beam melting (EBM), direct energy deposition (DED), wire and arc melting (WAAM), etc. LPBF and DED are two popular and widely accepted methods to fabricate metals and alloys [1, 2, 3, 4, 5, 6, 7, 8]. While both processes are capable of depositing near-net-shape internal and external complex geometries, DED process can also be used to repair damaged and worn parts.

In mechanical properties characterization of materials, fatigue is a very important test method to understand the property of a material in cycling loading and unloading conditions. The practical implementation of any material or alloy in application fields significantly depends on the fatigue properties. Fatigue of a material is defined as a progressive and permanent structural change due to fluctuating stresses or strains. During cyclic loading, progressive and localized structural damage and the growth of cracks cause fatigue failure of a part. To avoid metal fatigue failure, it is crucial to understand and analyze how the characteristic of metals affects its ability to resist fatigue failure.

The major drawbacks of the materials deposited in the AM process are the presence of surface irregularities, residual stress, and defects such as porosity, microcracks, inclusions, dislocations, and others. They significantly influence the static and dynamic mechanical properties of a material including fatigue strength. Several studies have been carried out recently to assess the fatigue behavior of different AM materials i.e. AlSi10Mg

[9, 10, 11, 12], Ti6Al4V [13, 14, 15, 16, 17, 18], Ni-based alloy [19], 15-5 PH stainless steel [20], steel [21], stainless steel [22]. Unlike wrought materials, defects such as porosity, shrinkage cavities, lack of fusion, voids, inclusion, etc. are formed arbitrarily during a material deposition in the AM process. These defects are substantially detrimental to the fatigue performance of a material. The other important factor influential in reducing the fatigue life of AM materials is the surface anomalies i.e. high surface roughness and irregularities due to the presence of contaminants, such as spatter, balling, and partially melted powder [23, 24, 25]. These defects behave as a micro notch or stress intensity raiser. Stress intensity factor (SIF) due to volumetric defect depends on the size, shape, location, and orientation of the defect with respect to the loading direction, and proximity of multiple pores. Larger defects result in higher stress concentration, therefore, reduced fatigue life. Based on Murakami's root area method, the stress concentration is proportional to the overall area of the defect perpendicular to the loading direction. Non-spherical or defects elongated along the crack propagation direction are more detrimental than spherical defects [16]. Subsurface defect location is found to be the most critical location in nucleating fatigue cracks [26, 23]. However, the fatigue life is predicted to be the lowest when multiple defects are present within close proximity. Since in AM, the formation of porosity, lack of fusion, keyhole, voids, and others is substantially influenced by the fabrication process parameters, the effect of process parameters on the fatigue behavior is yet to be investigated. While minimum energy input for a dense part originates lack of fusion type defects most, keyhole defects are dominant at high energy input [27, 28, 29].

Due to the layer-by-layer deposition process in AM technique, another downside of the AM material is the anisotropy issue in mechanical behaviors such as tensile performance [30, 31, 32, 33, 34, 35, 36], impact toughness [37] and fatigue properties [38]. Among the potential variables causing the anisotropy issue, both layer thickness and overlap rate were found to have an insignificant effect on the tensile properties on account of the similar metallurgical bonding and microstructure while build direction and hatch angle

revealed strong impacts on mechanical properties by influencing stress concentration and microstructure [31]. Columnar grain structure with a higher length-width ratio induced by the rapid cooling rate of the AM process could be the main reason for the mechanical anisotropies [32, 35]. The possible reason for anisotropy issue in impact toughness could be the difficulty level of crack propagation along the interlayer track boundaries [37]. While AM materials exhibit anisotropic fatigue behavior [38], the effect of anisotropy on the nucleation and propagation phase in fatigue assessment is yet to be investigated.

Fatigue test is indispensable in the characterization of materials, but both the AM process and fatigue testing is time-consuming and very expensive [39, 40]. The implementation of a miniature specimen can minimize the overall expenses to a great extent. In conventional wrought materials, miniature specimens demonstrate higher fatigue strength than standard specimens due to the lower probability of larger material defects. Statistically, large specimens contain more extreme defects. The presence of larger defects leads to crack growth and failure at lower stress levels. AM materials have a higher defect population within a definite volume compared to wrought materials. Additionally, the impact of the size effect on mechanical properties depends on the type and local feature of the material structure i.e., grain size, microcracks, inclusions, discontinuities, dislocations, and other defects [41, 42, 43]. Therefore, miniature specimens have been proved to be instrumental in characterizing AM material properties reliably [44, 45, 46].

There are several techniques already developed to monitor the crack nucleation and propagation during the fatigue test. These techniques include the acoustic emission diagnostic method [47, 48, 49], electrical resistance change method [50, 51], meandering winding magnetometer (MWM)-array eddy current sensing [52], and thermographic method [53]. All these techniques require an additional sensor with intensive signal processing. Whether a displacement or load control approach is applied in the fatigue test, there is a variation in the control signal during the test due to the stiffness variation of the specimen which

provides a unique insight into identifying the nucleation and propagation phase. A new method named control signal monitoring (CSM) will be introduced in this study to identify the nucleation and crack propagation life cycle.

In most applications especially for the usages critical to fatigue [54], post-fabrication surface treatments such as machining, grinding, and polishing are preferred for AM metal parts. Conventional machining and polishing processes are usually employed to improve the part surface finish and bring it within GD&T. Besides conventional surface quality improvement processes, laser aided machining and polishing (LAMP) can also be an effective method to achieve dimensional accuracy and minimize roughness [55, 56, 57, 58, 59]. LAMP offers a high processing rate, minimum heat-affected zone (HAZ), and easily adjustable process parameters [60, 61]. This method can also repair cracks and pores, ablate metallic globules, and improve the fatigue performance of AM materials [62, 63]. This technique is also advantageous over commonly used processes since the size of the tools used in conventional methods for machining and polishing has limitations to reach critical locations. Additionally, while a hybrid manufacturing process combined with AM system makes the entire process unwieldy and complicated, LAMP can be easily integrated with any existing laser-enabled AM process. Among different AM techniques available, laser-aided AM processes are very popular methods to fabricate ferrous and nonferrous materials. Toward improving the surface finish and obtaining GD&T for AM parts, by utilizing the same laser employed to fabricate AM parts, surface roughness can be improved in the same build chamber or machine. While different techniques and methods have been presented using both CW laser and/or PL for the laser aided polishing process [55, 56, 57, 58, 59, 64, 65, 66], further investigation is required to come up with a comprehensive and combined process while selecting the scan patterns and types of lasers for machining and polishing AM materials. To address the issues mentioned above, this dissertation will conduct research focusing on the fabrication, machining, polishing, and fatigue characterization of AM materials.

1.2. RESEARCH OBJECTIVES

The main objective of this research is to advance the fundamental knowledge of employing miniature specimens for fatigue testing of AM materials and investigating the effect of build process parameters on the high cycle AM metal fatigue behavior. A part of this research also includes studying the state of combining multiple lasers for both additive and subtractive manufacturing processes. To achieve this goal, three research tasks are carefully conducted.

In detail, research task 1 first addresses the key issues in conducting fatigue tests effectively with miniature specimens. Geometrically, the size effect is related to the nonlinear distribution of the stress [67, 68, 69]. The stress gradient occurring under bending and shear stress has a higher influence on the size effect for a bending type test compared to an axially loaded cyclic test but the axial fatigue test on mini specimens suffers buckling. In this study, the transverse bending fatigue test with a constant stress distribution within the gauge section in a miniature specimen minimizes the size effect and stress gradient effect. A noble dual gauge Krouse type specimen designed in task 1 can increase the overall surface area of the gauge to capture critical defects of AM parts since surface and subsurface defects are found to be the most critical defects in influencing the fatigue characteristic of an AM material.

The objective of task 2 is to attain a fundamental understanding of the effect of fabrication process parameters and build orientation on the high cycle fatigue characteristic of AM materials. In AM, the presence of surface irregularities, residual stress, and defects such as porosity, microcracks, inclusions, dislocations, and others significantly affects the fatigue strength of the material. The formation of different types of defects is substantially influenced by the fabrication process parameters. To obtain the high fatigue strength yielding process parameters, fatigue testing of metals fabricated with all different sets of process

parameters is a very expensive and time-consuming process. Therefore, identifying the set of nominal and optimized process parameters is an imperative topic of study to investigate the fatigue characteristic of AM material at different process parameters.

The analysis of the fatigue fracture surface of AM materials, and the size, and location of the defects nucleating fatigue cracks reveal that surface and subsurface defects are the most influential in affecting the fatigue strength of an AM material. The fatigue behavior of a material is sensitive to surface roughness. The rough surface of material behaves as a micro notch with high-stress concentration; hence, parts fail earlier. The fatigue strength of a material can be increased by machining and polishing the part. Therefore, task 3 focuses on researching the required fundamental knowledge for laser-aided machining and polishing and investigating the effects of process parameters on surface quality improvement.

1.3. ORGANIZATION OF DISSERTATION

This dissertation has correlative tasks with the core goal of characterizing fatigue properties of AM materials through conducting fatigue tests on miniature specimens and investigating the effect of LAMP process parameters on surface roughness optimization. Three research papers addressing the overall objectives are included in this dissertation.

In Paper-I, a noble dual gauge Krouse type miniature specimen including a fatigue test setup was proposed. The objective of using a custom test setup and a miniature specimen was to minimize the sample manufacturing cost and time and reduce the test equipment cost and power requirements. A high cycle fatigue test was performed on LPBF 304L stainless steel samples with wrought materials included. In this study, a unique CSM method was also introduced to identify nucleation and propagation phase during metal fatigue. The nucleation and propagation phase differences between AM and wrought materials were explained by fracture surface analysis. Previous studies show that miniature specimens exhibit higher mechanical strength both for monotonic and cyclic loading compared to standard specimens due to the lower probability of capturing large defects which affect the

strength of materials, especially fatigue. Therefore, the test results were also compared with the results from previous studies to validate the performance of the designed miniature specimen and to demonstrate the effective implementation of the test bench in fatigue testing of AM materials.

Paper-II emphasized the investigation of the high cycle fatigue performance of laser powder bed fused (LPBF) 304L stainless steel at different build process parameters. In AM, the effect of the process parameters and build orientation could lead to a fatigue property difference within the same part. The variation of the fabrication process parameters influences the mechanical properties of a material such as tensile strength, impact toughness, hardness, fatigue strength, and so forth, but fatigue testing of metals fabricated with all different sets of process parameters is a very expensive and time-consuming process. Therefore, in this study, first, a design of experiment (DOE) was implemented for the selection of build process parameters. Then the nominal and optimized process parameters were obtained from part density, tensile, and impact toughness test results for different process parameters and build orientation. Later, the fatigue test was performed on the horizontal, vertical, and inclined specimens built with nominal and optimized process parameters. The test results including the fractography of the specimens were analyzed and compared to obtain high fatigue strength yielding process parameters for LPBF 304L stainless steel.

Paper-III proposed a novel laser aided machining and polishing process for AM materials using multilaser technology in the same build chamber. An aluminum alloy was deposited using the DED process. High power continuous-wave laser was used for deposition and macro-polishing while a high scan speed pulsed laser was used for machining and fine finishing the deposited material. The part surface was machined and micro-polished with a unique scan pattern emulating multiple end-mills of different diameters. A design of experiments was implemented to optimize machining and polishing parameters. Later, the material removal rate was modeled and factors influencing the surface roughness were discussed.

PAPER

I. A DISPLACEMENT CONTROLLED FATIGUE TEST METHOD FOR ADDITIVELY MANUFACTURED MATERIALS

Mohammad Masud Parvez[1,*], Yitao Chen[1], Sreekar Karnati[1], Connor Coward[1], Joseph W. Newkirk[2], and Frank Liou[1]

[1] Department of Mechanical and Aerospace Engineering

[2] Material Science and Engineering

Missouri University of Science and Technology, Rolla, MO 65401, USA

[*] Correspondence: mphf2@umsystem.edu; Tel.: +1-573-202-1506

ABSTRACT

A novel adaptive displacement-controlled test setup was developed for fatigue testing on mini specimens. In property characterization of additive manufacturing materials, mini specimens are preferred due to the specimen preparation, and manufacturing cost but mini specimens demonstrate higher fatigue strength than standard specimens due to the lower probability of material defects resulting in fatigue. In this study, a dual gauge section Krouse type mini specimen was designed to conduct fatigue tests on additively manufactured materials. The large surface area of the specimen with a constant stress distribution and increased control volume as the gauge section may capture all different types of surface and microstructural defects of the material. A fully reversed bending ($R = -1$) fatigue test was performed on simply supported specimens. In the displacement-controlled mechanism, the variation in the control signal during the test due to the stiffness variation of the specimen provides a unique insight into identifying the nucleation and propagation phase.

The fatigue performance of the wrought 304 and additively manufactured 304L stainless steel was compared applying a control signal monitoring (CSM) method. The test results and analyses validate the design of the specimen and the effective implementation of the test bench in fatigue testing of additively manufactured materials.

Keywords: adaptive control; fatigue testing; simply supported bending; mini specimen; additive manufacturing; 304L stainless steel

1. INTRODUCTION

Fatigue is a progressive and permanent structural change due to fluctuating stresses or strains subjected to a material. 50% to 90% of mechanical failures of structures are due to fatigue [1, 2]. Fatigue test is indispensable in the characterization of materials but the test is both time-consuming and very expensive [3, 4]. In this research, a unique test setup was designed and developed to reduce the test cost using mini specimen. The measured strength of a material subjected to monotonic or cyclic loading depends inversely on the specimen size. The impact of the size effect on mechanical properties depends on the type and local feature of the material structure i.e., grain size, microcracks, inclusions, discontinuities, dislocations, and other defects [5, 6, 7]. Extended studies were carried out to investigate the effect of specimen size and loading condition on fatigue behavior of metallic materials [8, 9, 10, 11, 12, 13, 14, 15]. Statistically, large specimens contain more extreme defects. The presence of larger defects leads to crack growth and failure at lower stress levels. Sun [16] proposed a probabilistic method to correlate the effects of specimen geometry and loading condition on the fatigue strength based on the Weibull distribution. Tomaszewski [4] performed comparative tests on mini specimens and normative specimens, and verified the monofractal approach based on Basquin's equation along with the Weibull weakest link model. There are some other statistical methods proposed to evaluate the size effect on the fatigue test [17, 18, 19, 20, 21]. All of these approaches epitomize that standard specimens demonstrate lower fatigue strength than mini specimens due to the higher probability of

larger material defects. Additively manufactured materials have a higher probability of defects compared to wrought materials. In this paper, the implementation of a dual gauge section Krouse type mini specimen increases the surface area to capture all different types of surface and microstructural defects since most of the fatigue failures are initiated at the surface or subsurface due to the presence of defects.

Geometrically, the size effect is related to the nonlinear distribution of the stress [22, 23, 24]. The stress gradient occurring under bending and shear stress has a higher influence on the size effect for a bending type test compared to axially loaded cyclic test but the axial fatigue test on mini specimens suffers buckling. In this study, the transverse bending test with a constant stress distribution within the gauge section in a specimen eliminates the stress gradient effect.

There are several techniques already developed to monitor the crack nucleation and propagation during the fatigue test. These techniques include the acoustic emission diagnostic method [25, 26, 27], electrical resistance change method [28, 29], meandering winding magnetometer (MWM)-array eddy current sensing [30], and thermographic method [31]. All of these techniques require an additional sensor with intensive signal processing. In the current work, we introduce a simple but effective control signal monitoring (CSM) method to identify the nucleation and propagation phase. In a displacement-controlled mechanism, the control signal decreases with the decrease in the structural stiffness of the specimen. The change in the control signal provides insight in estimating the nucleation and propagation phase. In this study, the fatigue test was conducted on wrought 304 and additively manufactured 304L stainless steel specimens. The CSM method was applied to identify the nucleation and propagation phase. The test results were compared to validate the design of the specimen and the test setup performance in high cycle fatigue testing.

2. METHODOLOGY

In this study, a fully reversed bending (R = −1) fatigue test was performed on simply supported specimens. A simply supported testing methodology has several advantages over a fully clamped type of loading mechanism. The maximum deflection in a simply supported and a fully clamped beam with a concentrated load F at the center are given by Equations (1) and (2) respectively [32, 33],

$$\delta_{max} = \frac{Fl^3}{48EI} \tag{1}$$

$$\delta_{max} = \frac{Fl^3}{192EI} \tag{2}$$

where F, δ_{max}, l, E, and I are the applied force, maximum deflection, length, modulus of elasticity, and moment of inertia of the beam respectively. For a given load, the displacement is four times higher in a simply supported bending than in a fully clamped bending. During the fatigue test, investigators attempt to actuate the specimen at its natural frequency to achieve maximum displacement. However, the dynamics of the actuator coupled with the specimen limit the operation. Therefore, as an alternate, we adopted a simply supported bending mechanism as the testing methodology.

3. SPECIMEN DESIGN, ANALYSIS AND PREPARATION

3.1. DESIGN OF THE SPECIMEN

A dual gauge section Krouse type mini specimen was designed for simply supported loading. The specimen is a modified form of the ASTM (American Society for Testing and Materials) International standard B593-96(2014)e1, definition E206, and practice E468 [34]. Some authors already reported on the modification and implementation of the specimen in miniature form [35, 36, 37, 38]. Since the specimens are miniature size, Haydirah

[39] performed an error analysis based on the effect of specimen's dimension. Figure 1 shows the dimension of our specimen. The effective length between both clamping ends is 25.4 mm. Each gauge is 4.34 mm long. The total gauge covers 34.17% of the total effective length of the specimen. The dual gauge increases the overall surface area. The failure is expected to be within the gauges. Another reason for choosing the dual gauge is to maintain symmetry. In a single cantilever beam, the actuator follows a curved path during excitation. To keep the path of the actuator one dimensional, and to distribute the load symmetrically along with the specimen, the dual gauge concept is opted.

3.2. STRESS CALCULATION

Previous studies showed that simple beam equation is applicable to calculate the stress in miniature wedge shaped specimen [34, 35, 36, 39, 37, 38]. The stress in a simply supported bending beam with a point load at the center can be expressed as [40],

$$\sigma = \frac{M(x)}{I(x)} \frac{h}{2} \tag{3}$$

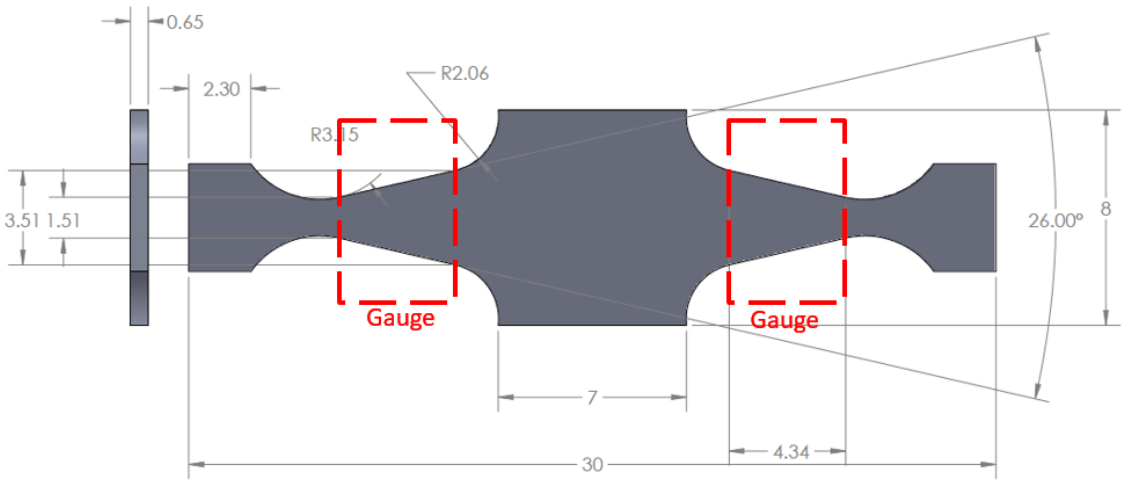

Figure 1. Drawing of the dual gauge section Krouse type mini specimen, all units are in mm.

where, σ, $M(x)$, $I(x)$, and h are the stress, moment, second moment of inertia, and the thickness of the specimen, respectively. For a simply supported beam, $M(x) = \frac{Fx}{2}$, and $I(x) = \frac{b(x)h^3}{12}$ where, F, and b are the point load, and the width of the specimen, respectively. For a Krouse type specimen $b(x) = 2kx$ where, k is the slope of the specimen. Inserting $M(x)$, and$I(x)$ in Equation (3), we get,

$$\sigma = \frac{3F}{2kh^2} = j(F, h) \tag{4}$$

where, j is the stress function. The nominal stress σ within the gauge in Equation (3) depends on the force applied and the thickness of the specimen, not on the distance x. Ideally, a constant stress distribution is expected but in reality at the defect zone or at the lower strength site, the actual local stress will be higher than the nominal stress.

3.3. SENSITIVITY AND UNCERTAINTY ANALYSIS

The specimen is a miniature size compared to the standard one. The necessity of sensitivity and uncertainty analysis is inevitable to determine the optimal thickness of the specimen. The stress calculation is sensitive to the force and thickness of the specimen according to Equation (3). Uncertainty in force measurement depends on the sensor's accuracy, calibration, and set up. The thickness is sensitive to the machining and polishing process. For a higher thickness, a higher force is required to attain particular stress. This leads to the necessity of a high power system and actuator. An optimal thickness was determined to eliminate the necessity of high power fatigue machine and external cooling. Partially differentiating Equation (3) we get,

$$\nabla \bar{j} = \begin{bmatrix} \frac{F}{\sigma} \times \frac{\partial \sigma}{\partial F} \\ \frac{h}{\sigma} \times \frac{\partial \sigma}{\partial h} \end{bmatrix} = \begin{bmatrix} 1 \\ -2 \end{bmatrix} \tag{5}$$

From Equation (5), we can see 1% variation in specimen thickness produces 2% change in stress value. To estimate the thickness uncertainties, 10 specimens were prepared. The thickness was measured using a high precision laser displacement sensor. The uncertainty was calculated obtaining overall standard deviation (std) using Equation (6).

$$std = \frac{1}{n}\sum_{j=1}^{n}(x_j - \bar{x})^2 = \frac{1}{n}\left[\sum_{i=1}^{g} n_i S_i^2 + \sum_{i=1}^{g}(\bar{x}_i - x)^2\right] where, \bar{x} = \frac{\sum_{i=1}^{g} n_i x_i}{n} \tag{6}$$

where, $\bar{x}_i$, S_i, and n_i are the mean, standard deviation, and the number of scanned data points of i th specimen respectively. $\bar{x}$ is the overall mean, and n is the total number of data points. For ±5% stress variation, the calculated optimal thickness of the specimen was 0.509 mm with three sigma quality level. Including a factor of safety, the specimen thickness used in this study is 0.65 mm.

3.4. FINITE ELEMENT ANALYSIS

Finite element analysis was performed using ABAQUS 2018 software (Dassault Systèmes Simulia Corp; Providence, RI, USA) to demonstrate the constant stress distribution within gauge sections. According to the specimen design, as shown in Figure 2, the 3D prototype of the specimen was simply supported at both sides which are marked by red lines ($U_z = 0$). To ensure a symmetric deformation, the displacement on center-lines along the x -axis (green line) and y-axis (blue line) are restricted in y direction ($U_y = 0$) and x direction ($U_x = 0$), respectively. A constant displacement $U_z = 0.150$ mm was applied on the 3 mm × 7 mm dark grey rectangular area at the center of the specimen, which indicates the rectangular plate washer in the machine setup. Boundary conditions are listed in the box under the 3D prototype of the specimen. The Young's modulus and Poisson's ratio set for the wrought 304 stainless steel were 200 GPa and 0.3 respectively. A linear elastic model was applied to observe the mechanical response under this static condition, as the deformation is

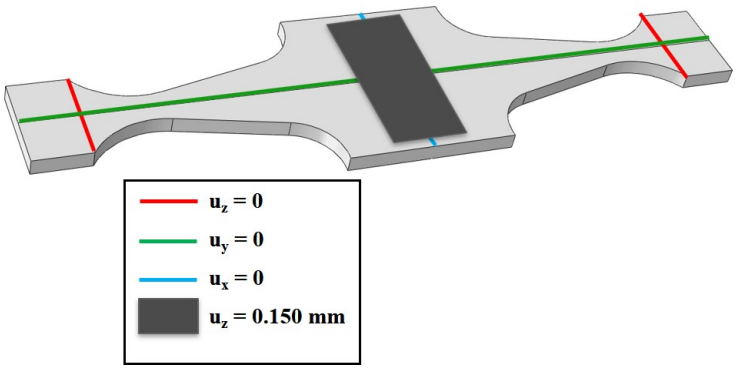

Figure 2. FEA simulation setup for wrought 304 stainless steel specimen.

within the elastic regime. The distribution of the nominal stress S11 on the whole specimen is then obtained by the simulation, as shown in Figure 3. A constant nominal stress within triangular gauge sections can be observed, and it reaches the maximum value at the surface. Convergence study was also performed by selecting 6 different mesh sizes which result in the number of elements ranging from 1263 to 166,506. The data points in Figure 4 shows that the nominal stress converges to approximately 177.7 MPa as the number of elements increases to 166,506, since when the number of mesh elements increases from 76,698 to 166,506, the change in nominal stress value is less than 0.2%. Figure 3 exhibits the nominal stress distribution with the number of elements of 166,506. The sole purpose of using FEA analysis is to demonstrate the stress distribution within the gauge.

3.5. MATERIALS AND SPECIMEN PREPARATION

The materials tested in this study are hot rolled and annealed 304 stainless steel bulk material and additive manufacturing (AM) fabricated 304L SS bar. These materials were chosen because they are economical and widely used due to their strength and high resistance to corrosion. The chemistry of both the wrought material and powder used as the feedstock for AM is listed in Table 1. The relatively close chemistry of both materials except Ni which is 2% higher but not expected to make a significant difference in the test results

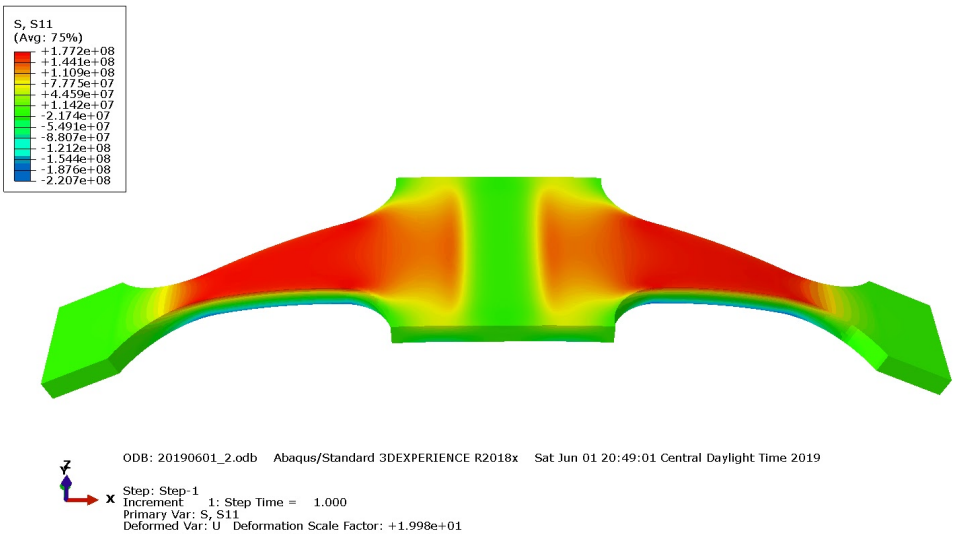

Figure 3. FEA simulation result of the specimen.

may aid a better understanding of the comparative study. Rough finish (average R_a = 3.82 µm) and fine finish (average R_a = 0.482 µm, average R_z = 4.242 µm) wrought specimens were machined using W-EDM, while additively manufactured fine finish specimens were cut along Z axis from a bar fabricated using the selective laser melting (SLM) process. A

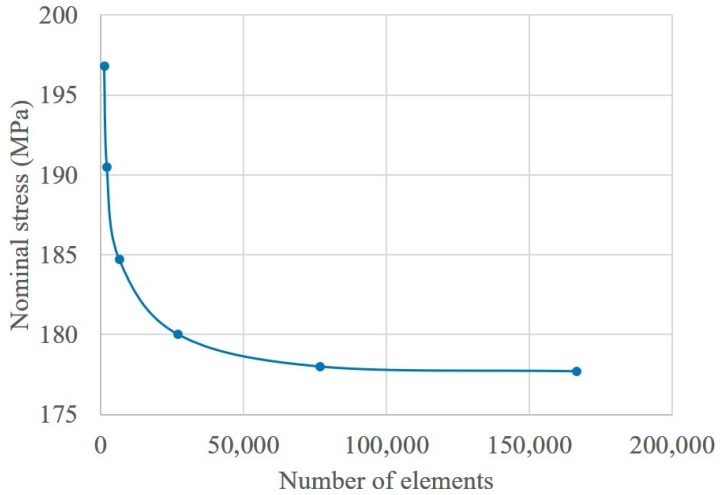

Figure 4. Convergence analysis of the FEA simulation results.

Table 1. Chemical properties (wt%) of 304L stainless steel powder and bulk 304 stainless steel.

Material	C	Mn	Si	S	P	Cr	Ni	Cu	Mo	Co	N	O
Wrought	0.023	1.69	0.43	0.020	0.034	18.10	8.02	0.63	0.24	0.15	0.084	-
Powder	0.015	1.40	0.63	0.004	0.012	18.50	9.90	<0.1	-	-	0.090	0.02

Renishaw AM250 machine was used to build the part. An optimal process parameter listed in Table 2 was applied to yield maximum part density. A total of 10 specimens for each type were manufactured with no additional surface preparation.

4. EXPERIMENTAL SETUP

4.1. MINI FATIGUE TESTING MACHINE

The mini fatigue testing machine consists of six major parts: (i) an electromagnetic actuator, (ii) a non-contact displacement sensor, (iii) a load cell, (iv) a controller, (v) a power amplifier or driver, and (vi) a test bench. The voice coil of a subwoofer was used as the actuator. The sub-woofer behaves as a low audio frequency shaker. The mathematical model of an electrodynamic shaker and a sub-woofer is relatively similar though the moving elements of a shaker are more rigid than a subwoofer. Higher rigidity multiplies the power requirements. To design a low power system, a soft mechanical suspension of the sub-woofer was implemented to transfer maximum energy to the specimen. The actuator is

Table 2. Parameters used to build additively manufactured part using selective laser melting (SLM) process.

Parameter Set	Power (watt)	Hatch Space (μm)	Point Distance (μm)	Exposure Time (millisecond)	Energy Density (MJ/m^3)	Raster Rotation (degree)
Nominal	200	85	60	75	58.8	67

made of a high Curie temperature ferrite magnet with a cast aluminum frame of 10 inches diameter. The larger diameter of the voice coil (3 inches) than the length (1 inch) of the specimen supports the one-dimensional movement. The dust cap of the voice coil was replaced with a plastic flange. A load cell was mounted in-line between the central clamp and the flange to measure the tensile and compressive force. To measure the displacement of the specimen, a high-speed non-contact laser displacement sensor was fixed with a guide rail. Figure 5 illustrates the test bench setup. First, the specimen was clamped at the center. The specimen sits on the bearings at both ends as shown in Figure 5. Spacers were used at both ends to ensure no preload on the specimen. Then, the other bearing holders were placed and clamped using heavy load toggle clamps on top. To ensure line contact at both ends, bearings were used. Bearings also minimize the friction during the simply supported vibration test. By sliding the displacement sensor using the guide rail, the sensor was pointed at the center of the specimen. The displacement measured by the sensor was processed using a microcontroller to determine the amplitude and mean of the displacement. The data was sent to a computer from the microcontroller using a serial port. An adaptive controller was implemented in the Python development environment to estimate the required amplitude of the sinusoidal control signal. The signal from the computer was sent to a waveform generator via Ethernet. A linear power amplifier connected with the waveform generator drives the actuator. All process and manipulated variables were stored for further analysis to identify the nucleation and propagation phase.

4.2. ADAPTIVE CONTROLLER DESIGN

An adaptive proportional and derivative (PD) controller was designed to control the displacement amplitude. A conventional PID controller was avoided since the system parameters change due to the structural stiffness change of the specimen during the test. Material hardening or softening may occur too. There may also be a possibility of overshoot

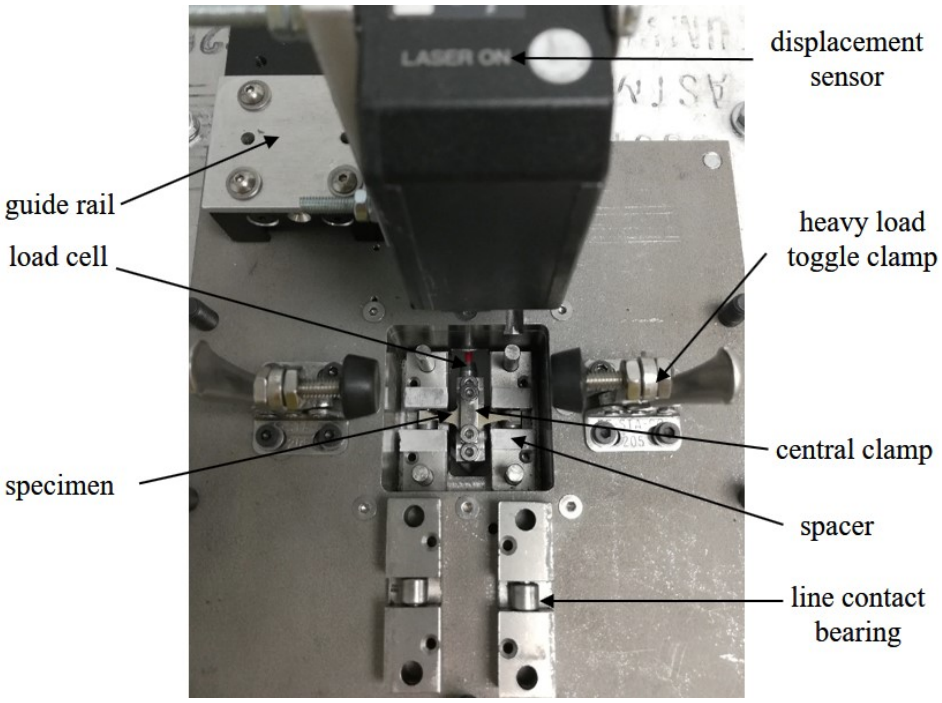

Figure 5. Fatigue test bench with a specimen mounted.

above the set point during the transient condition. Overshoot may affect the test results. Therefore, an adaptive controller was designed. The design of an adaptive controller follows Equation (7).

$$u(k) = u(k-1) + P * error + D * \frac{error(k) - error(k-1)}{\Delta t} \tag{7}$$

where, $u(k)$, and $u(k-1)$ are the control signal amplitudes at time k, and $(k-1)$ respectively. P, and D are the proportional and derivative gain respectively, and Δt is the time step. The proportional controller offsets the current value linearly with the error, and the derivative controller adds in controlling the actuation based on the rate of the change of error. The error is defined as,

$$error = d_{p-p}^{set} - d_{p-p}^{current} \tag{8}$$

where, d_{p-p}^{set} and $d_{p-p}^{current}$ are the desired and current displacement amplitude respectively. The controller values were chosen by manual tuning with caution that no overshoot occurs above the set point. The controller values need to be varied with the test frequency and test material as well. The P and D controllers were set at 5.0 and 0.5 respectively for 304 materials at 56 Hz test frequency.

5. RESULTS AND DISCUSSION

The closed-loop displacement-controlled fatigue test was performed on wrought 304 and SLM fabricated 304L SS specimens. The sinusoidal excitation frequency was set at 56 Hz. Figure 6 shows the displacement amplitude of a specimen actuated at 0.100 volts control signal amplitude for different frequencies. The system response is a window function with 39 Hz cutoff frequency. In terms of system dynamics, the fatigue test is a harmonic forced vibration of two mass-spring systems. One is the actuator, and another is the specimen. At cutoff frequencies, the system behaves like a shock absorber. A detailed explanation can be found in the literature [41]. The frequency response shows that the displacement amplitude is maximum at 56 Hz, 95 Hz, and 134 Hz. The test frequency was chosen 56 Hz since external cooling may be required at higher frequencies. All experiments were conducted for simply supported fully reversed bending test at room temperature. During the test, the temperature of the specimen was monitored using an infrared temperature sensor. The deviation in the temperature remains within ± 2° C at 56 Hz test frequency.

In a Krouse type specimen, the fatigue failure can occur at any location within the gauge. All the specimens tested in this study failed within the gauge as expected. The random failure location is due to the defects present randomly within the gauge. The nominal stress distribution is supposed to be constant while the local stress is expected to be high at the defect zone. Figure 7 exhibits the failure location of wrought specimens. Figure 8 illustrates the displacement and control signal amplitude for the wrought specimen actuated at 0.200 mm amplitude which corresponds to 514.26 MPa nominal stress. During

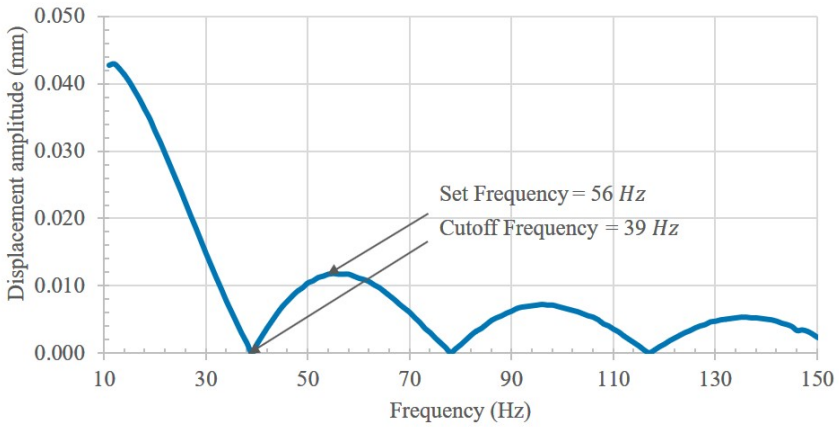

Figure 6. The frequency response of a specimen actuated at 0.100 volts control signal amplitude.

the test, the stiffness of the specimen decreases as the crack grows, propagates, and final failure occurs. The control signal amplitude decreases with the reduction of stiffness to maintain the desired set displacement. The displacement amplitude increases suddenly during the final failure. The test was stopped automatically when the amplitude was above a threshold. The test result at different displacements illustrated in Figure 9 validates the effective performance of the adaptive controller.

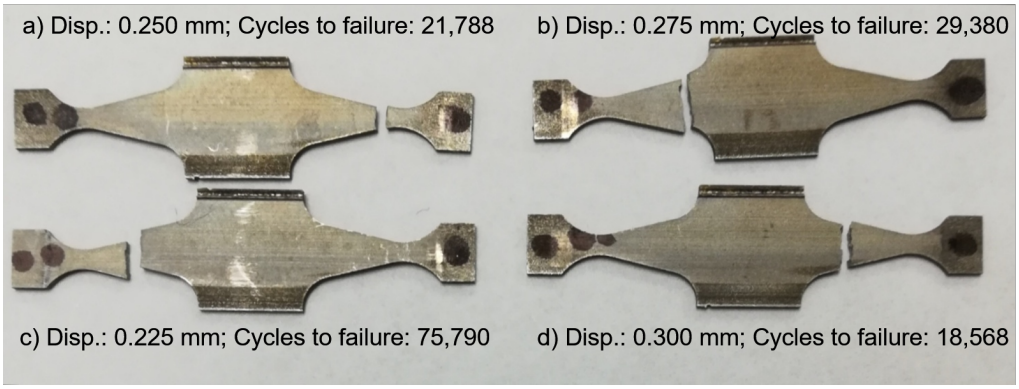

Figure 7. Fatigue failure of specimens actuated at different displacement amplitude.

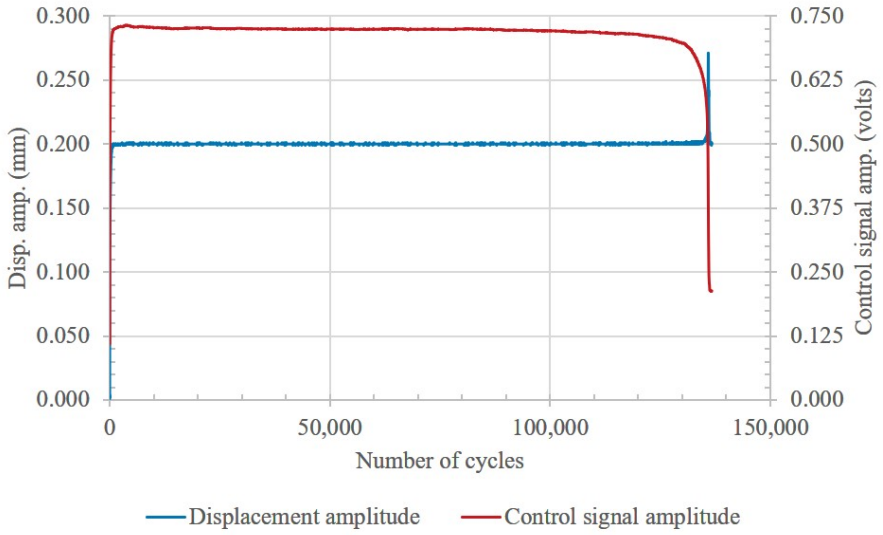

Figure 8. Displacement and control signal amplitude up to the entire fatigue life cycle of a fine finished wrought specimen.

In this study, we introduce a control signal monitoring (CSM) method to identify the nucleation and propagation stage. During the fatigue test, the crack first grows slowly, which is termed as nucleation. When the nucleation process ends, the crack starts propagating

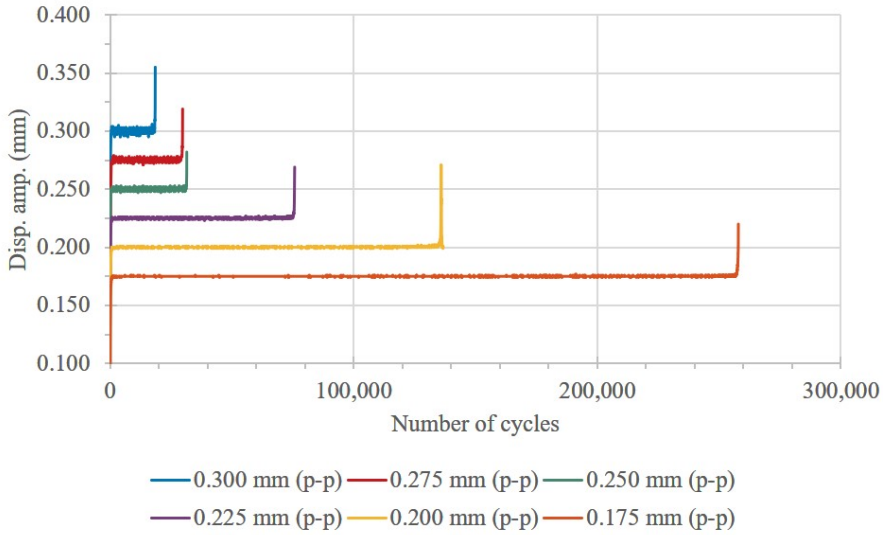

Figure 9. Displacement amplitude control of fine finished wrought specimens up to the entire fatigue life cycle.

and the final failure occurs. The stiffness of the specimen decreases at all stage, but the rate of the stiffness change is different. Wang [42] reported for carbon fiber polymer-matrix composite that the stiffness of the material has an inverse analogous relation with the change in resistance up to the end of nucleation phase while performing the electrical potential technique on fatigue test to identify the nucleation and propagation phase. Grammatikos [31] implemented the linear regression analysis on the relative potential change as a function of fatigue life fraction to identify different stages. Similarly, this is possible to identify the phases using linear regression analysis on the control signal. First linear regression was applied on the control signal. Then the peak amplitude of the signal near the end of regression line was marked as the end of nucleation phase, as shown in Figure 10. Here the regression helps in choosing the peak of the signal. Current study demonstrates the implementation of CSM method. Future study includes the sensitivity analysis on the monitoring signal. The implementation of the CSM method on other wrought and SLM specimens is shown in Figure 11. To determine the maximum nominal stress, the average

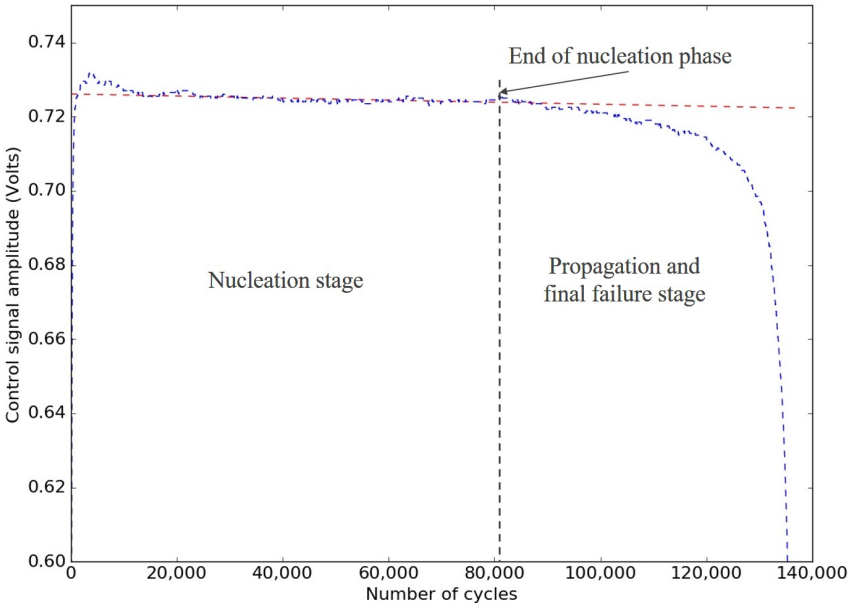

Figure 10. Nucleation and propagation stage of a fine finished wrought specimen displaced at 0.200 mm amplitude.

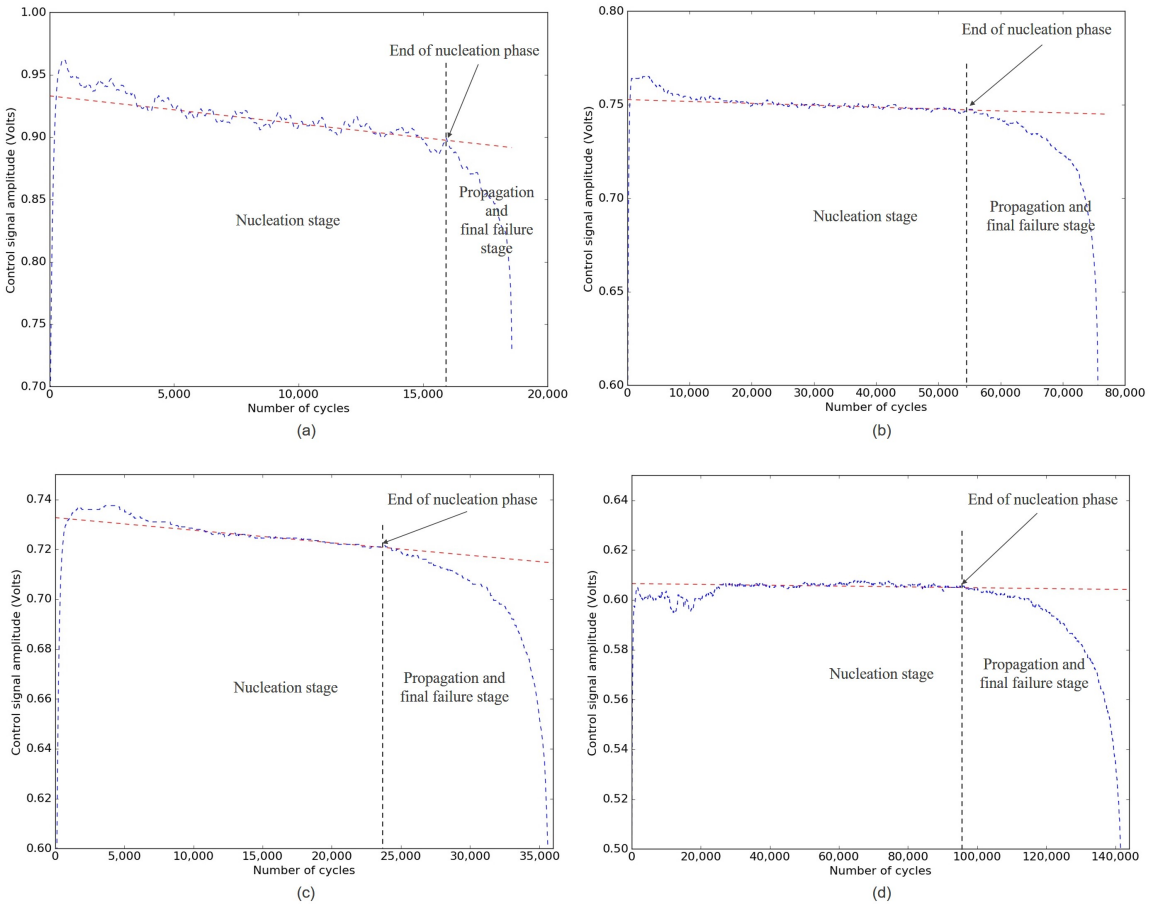

Figure 11. Nucleation and propagation stage of fine finished specimens.

of the peak load was calculated up to the end of the nucleation phase. Inserting the average in Equation (3), the nominal stress was calculated. Figure 12 shows the tensile and compressive load response up to the final failure for the wrought specimen displaced at 0.200 mm amplitude.

The fatigue life of a specimen in terms of the number of cycles is the sum of cycles during nucleation and propagation stages. Materials demonstrate a higher life cycle at low-stress value. Figure 13 shows the end of the nucleation phase cycle and cycles to failure for fine finished wrought and SLM specimens. The trend of nucleation and propagation presented in the literature [43, 44] supports the results. Both the wrought and SLM specimens demonstrate an increase in the nucleation and propagation cycle as the

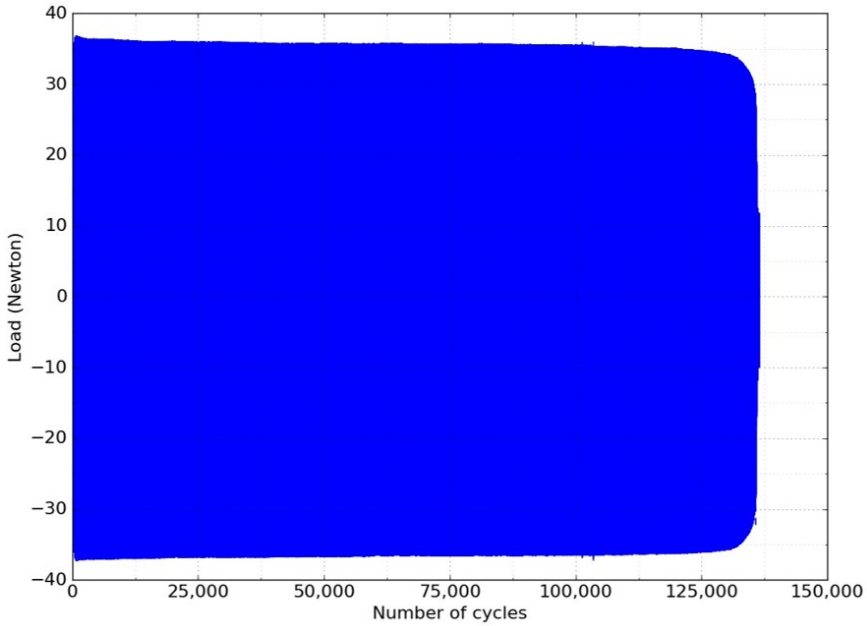

Figure 12. Load values for the specimen displaced at 0.200 mm amplitude.

stress goes low, but for a particular stress value, both the nucleation and propagation cycles for the SLM material is lower than those for the wrought material. A possible reason is that additively manufactured materials have a higher probability of different types of defects. The fracture surface analysis of wrought and SLM specimens is shown in Figure 14. In the SLM specimen, the crack is initiated at the lack of fusion defect near the top surface while surface defect is the crack initiation source for wrought specimens. We observed similar type of defects to be the crack nucleation site for other SLM specimens. The crack starts growing earlier in SLM materials than in wrought materials. Therefore, the nucleation life cycle is less. The presence of other defects such as micro-cracks, pores, and lack of fusion within the volume enhance the propagation rate. Additionally, some authors reported that inter-layer bonding is weak in SLM materials [45, 46]. Therefore, SLM fabricated 304 L SS demonstrate lower fatigue strength than bulk material.

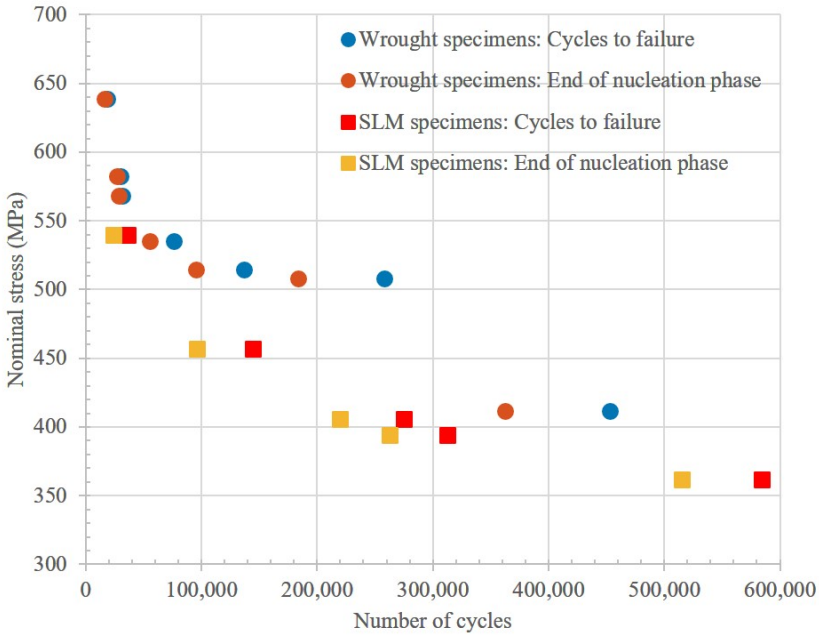

Figure 13. End of nucleation phase and cycles to failure for fine finished wrought and SLM fabricated specimens.

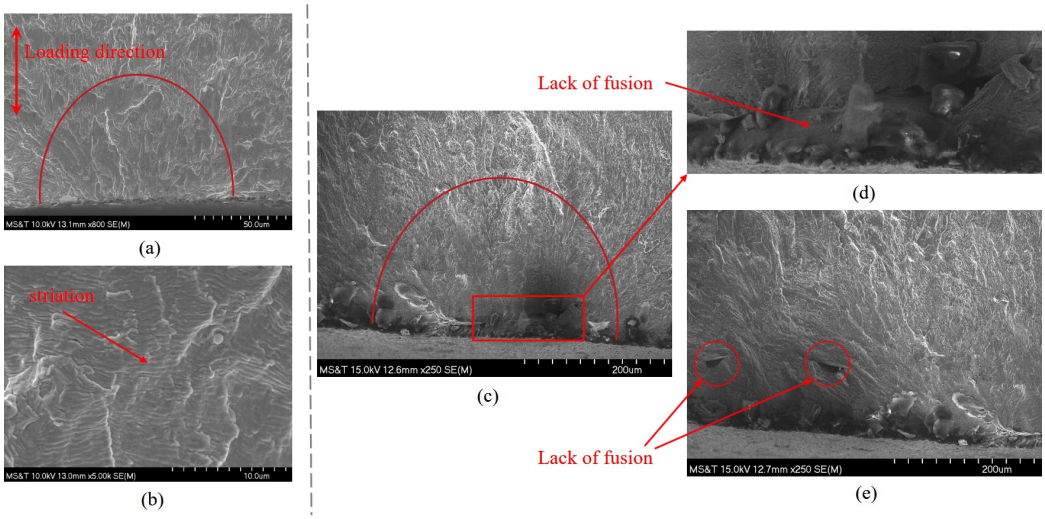

Figure 14. Fracture surface analysis of fine finished wrought and SLM fabricated materials.

Further analysis was performed to evaluate the CSM method in identifying nucleation and propagation phase. Rough finished and notched rough finished wrought specimens were prepared to conduct fatigue test. Rough finished specimens were chosen because these

are easy to prepare. Figure 15 shows the notch location in the specimen. Figure 16 illustrates the nucleation and propagation phase identified using the CSM method for the specimens. As we know, notched specimens have higher stress concentration, hence, they fail earlier. The number of cycles decreases more in nucleation phase due to the notch while the influence of notch on the propagation is minimal. This attributes to the proper implementation of the CSM method in identifying the end of nucleation phase. In future, the method will be validated determining the crack length at the end of nucleation phase.

The Wohler curve for fine finished and rough finished wrought specimens, and fine finished SLM specimens was plotted as shown in Figure 17. Both fine finished SLM and rough finished wrought materials exhibit low fatigue strength compared to the fine finished wrought material. The endurance limit (10^7) of the fine finished, rough finished wrought specimen and fine finished SLM specimen reported here are 404.26, 344.62 and 336.52

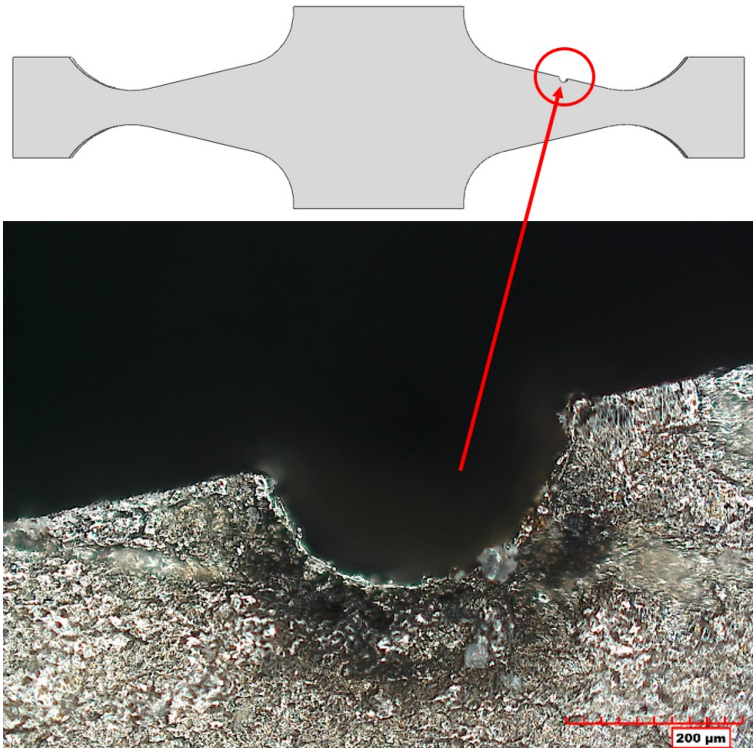

Figure 15. Notched rough finished wrought specimens prepared with a W-EDM wire radius of 0.125 mm.

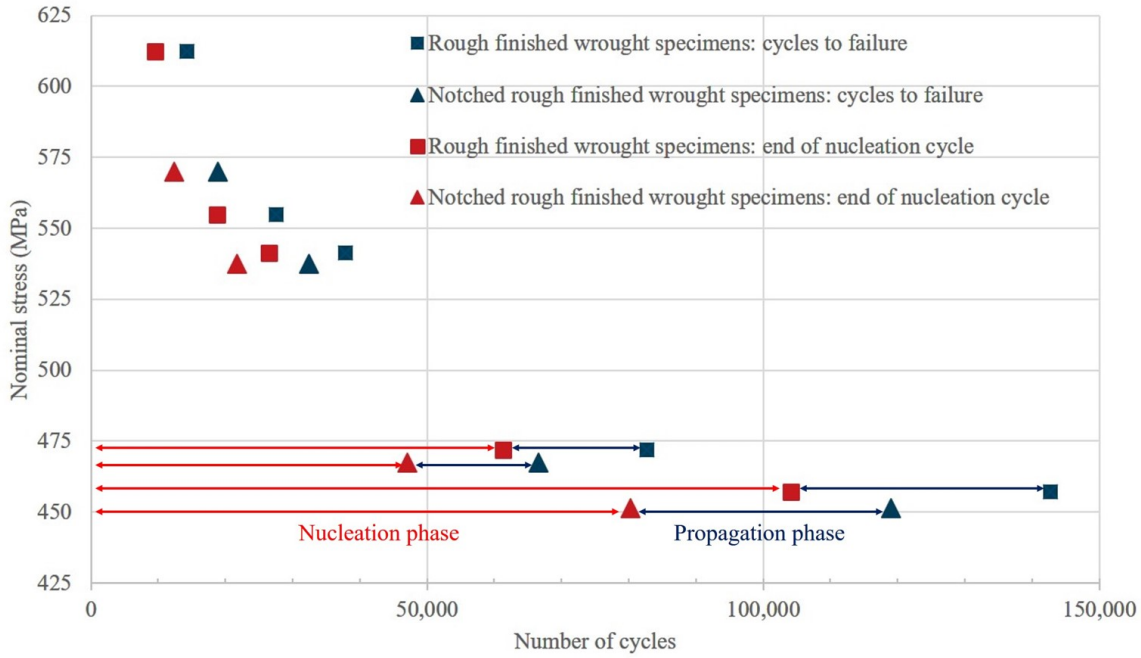

Figure 16. Nucleation and propagation phase of rough finished wrought and notched rough finished wrought specimens.

MPa respectively. The yield tensile strength (YTS) and ultimate tensile strength (UTS) for the wrought material used in this study are 582.5 and 780.9 respectively while for the SLM material with the same process parameter used, they are 368.4 and 536.7 MPa respectively [47]. These results are in good agreement with the general relationship between fatigue limit and ultimate tensile strength [43]. The endurance limit is also comparable with the results reported by other authors [38, 48].

6. CONCLUSIONS

In this study, a dual gauge section Krouse type mini specimen was designed to achieve a constant stress distribution with increased volume to conduct fatigue test. The test was performed with a simply supported loading mechanism on wrought and additively manufactured materials using a unique adaptive displacement controlled mini fatigue test set up. A new diagnosis method named control signal monitoring (CSM) was employed to

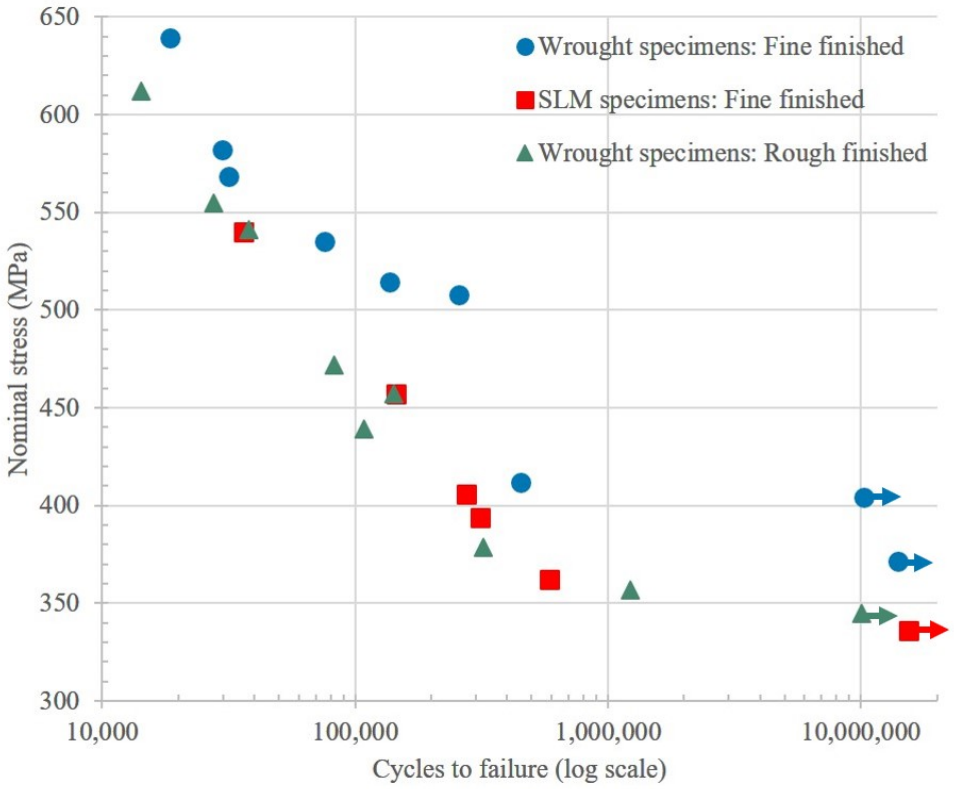

Figure 17. Wohler curve plot of wrought and SLM fabricated specimens.

identify the nucleation and propagation stages. The test results and analyses illustrate that SLM fabricated 304L stainless steel demonstrate lower fatigue strength in terms of both the nucleation and propagation cycles compared to bulk wrought material. The test method developed here can be applied in the extensive study on other additively manufactured materials in the future.

ACKNOWLEDGMENT

This research was supported by National Science Foundation Grant CMMI-1625736. Part of the work was also funded by the Department of Energy's Kansas City National Security Campus which is operated and managed by Honeywell Federal Manufacturing Technologies, LLC under contract number DE-NA0002839.

REFERENCES

[1] E. Santecchia, A. Hamouda, F. Musharavati, E. Zalnezhad, M. Cabibbo, M. El Mehtedi, and S. Spigarelli, "A review on fatigue life prediction methods for metals," *Advances in Materials Science and Engineering*, vol. 2016, 2016.

[2] F. C. Campbell, *Elements of metallurgy and engineering alloys*. ASM International, 2008.

[3] J. Sempruch and T. Tomaszewski, "Application of mini specimens to high-cycle fatigue tests," *Journal of Polish CIMAC*, vol. 6, no. 3, pp. 279–287, 2011.

[4] T. Tomaszewski and J. Sempruch, "Verification of the fatigue test method applied with the use of mini specimen," in *Key Engineering Materials*, vol. 598, pp. 243–248, Trans Tech Publ, 2014.

[5] Z. P. Bažant, "Size effect in blunt fracture: concrete, rock, metal," *Journal of Engineering Mechanics*, vol. 110, no. 4, pp. 518–535, 1984.

[6] T. Hirose, H. Sakasegawa, A. Kohyama, Y. Katoh, and H. Tanigawa, "Effect of specimen size on fatigue properties of reduced activation ferritic/martensitic steels," *Journal of Nuclear Materials*, vol. 283, pp. 1018–1022, 2000.

[7] H. Haftirman, "The size effect on fatigue strength of structural steel materials in high-humidity environment," *Jurnal Mekanikal*, vol. 32, no. 1, 2011.

[8] S. Beretta, A. Ghidini, and F. Lombardo, "Fracture mechanics and scale effects in the fatigue of railway axles," *Engineering fracture mechanics*, vol. 72, no. 2, pp. 195–208, 2005.

[9] M. Nakajima, K. Tokaji, H. Itoga, and T. Shimizu, "Effect of loading condition on very high cycle fatigue behavior in a high strength steel," *International Journal of Fatigue*, vol. 32, no. 2, pp. 475–480, 2010.

[10] Y. Akiniwa, N. Miyamoto, H. Tsuru, and K. Tanaka, "Notch effect on fatigue strength reduction of bearing steel in the very high cycle regime," *International Journal of Fatigue*, vol. 28, no. 11, pp. 1555–1565, 2006.

[11] A. Wormsen, B. Sjödin, G. Härkegård, and A. Fjeldstad, "Non-local stress approach for fatigue assessment based on weakest-link theory and statistics of extremes," *Fatigue & Fracture of Engineering Materials & Structures*, vol. 30, no. 12, pp. 1214–1227, 2007.

[12] W. Findley, "An explanation of size effect in fatigue of metals," *Journal of Mechanical Engineering Science*, vol. 14, no. 6, pp. 424–428, 1972.

[13] S.-P. Zhu, S. Foletti, and S. Beretta, "Evaluation of size effect on strain-controlled fatigue behavior of a quench and tempered rotor steel: Experimental and numerical study," *Materials Science and Engineering: A*, vol. 735, pp. 423–435, 2018.

[14] A. Diemar, R. Thumser, and J. Bergmann, "Determination of local characteristics for the application of the weakest-link model," *Materialwissenschaft und Werkstofftechnik: Entwicklung, Fertigung, Prüfung, Eigenschaften und Anwendungen technischer Werkstoffe*, vol. 36, no. 5, pp. 204–210, 2005.

[15] M. Leitner, C. Garb, H. Remes, and M. Stoschka, "Microporosity and statistical size effect on the fatigue strength of cast aluminium alloys en ac-45500 and 46200," *Materials Science and Engineering: A*, vol. 707, pp. 567–575, 2017.

[16] C. Sun and Q. Song, "A method for predicting the effects of specimen geometry and loading condition on fatigue strength," *Metals*, vol. 8, no. 10, p. 811, 2018.

[17] M. Leitner, M. Vormwald, and H. Remes, "Statistical size effect on multiaxial fatigue strength of notched steel components," *International Journal of Fatigue*, vol. 104, pp. 322–333, 2017.

[18] D. B. Lanning, T. Nicholas, and A. Palazotto, "Hcf notch predictions based on weakest-link failure models," *International journal of fatigue*, vol. 25, no. 9-11, pp. 835–841, 2003.

[19] Z. P. Bažant and D. Novák, "Probabilistic nonlocal theory for quasibrittle fracture initiation and size effect. i: Theory," *Journal of Engineering Mechanics*, vol. 126, no. 2, pp. 166–174, 2000.

[20] M. Makkonen, "Statistical size effect in the fatigue limit of steel," *International journal of fatigue*, vol. 23, no. 5, pp. 395–402, 2001.

[21] G. Härkegård and G. Halleraker, "Assessment of methods for prediction of notch and size effects at the fatigue limit based on test data by böhm and magin," *International Journal of Fatigue*, vol. 32, no. 10, pp. 1701–1709, 2010.

[22] H. Brown, C. Mischke, and J. Shigley, "Standard handbook of machine design," *Raleigh, North Carolina*, 2004.

[23] Y.-L. Lee, J. Pan, R. Hathaway, and M. Barkey, *Fatigue testing and analysis: theory and practice*, vol. 13. Butterworth-Heinemann, 2005.

[24] Y. Nakai, A. Hashimoto, T. Imanishi, and C. Hiwa, "Size effect on fatigue strength of metallic micro-materials," in *Proceedings of Asian-Pacific Conference on Fracture and Strength*, vol. 99, 1999.

[25] M. Biancolini, C. Brutti, G. Paparo, and A. Zanini, "Fatigue cracks nucleation on steel, acoustic emission and fractal analysis," *International Journal of Fatigue*, vol. 28, no. 12, pp. 1820–1825, 2006.

[26] J. Meriaux, M. Boinet, S. Fouvry, and J. Lenain, "Identification of fretting fatigue crack propagation mechanisms using acoustic emission," *Tribology International*, vol. 43, no. 11, pp. 2166–2174, 2010.

[27] L. Lin and F. Chu, "Hht-based ae characteristics of natural fatigue cracks in rotating shafts," *Mechanical Systems and Signal Processing*, vol. 26, pp. 181–189, 2012.

[28] J. Meriaux, S. Fouvry, K. Kubiak, and S. Deyber, "Characterization of crack nucleation in ta6v under fretting–fatigue loading using the potential drop technique," *International Journal of Fatigue*, vol. 32, no. 10, pp. 1658–1668, 2010.

[29] A. Todoroki, Y. Mizutani, Y. Suzuki, and D. Haruyama, "Fatigue damage detection of cfrp using the electrical resistance change method," *International Journal of Aeronautical and Space Sciences*, vol. 14, no. 4, pp. 350–355, 2013.

[30] V. Zilberstein, D. Schlicker, K. Walrath, V. Weiss, and N. Goldfine, "Mwm eddy current sensors for monitoring of crack initiation and growth during fatigue tests and in service," *International Journal of Fatigue*, vol. 23, pp. 477–485, 2001.

[31] S. Grammatikos, E. Kordatos, T. Matikas, and A. Paipetis, "Real-time debonding monitoring of composite repaired materials via electrical, acoustic, and thermographic methods," *Journal of materials engineering and performance*, vol. 23, no. 1, pp. 169–180, 2014.

[32] E. ToolBox, "Beams-fixed at both ends-continuous and point loads," 2004.

[33] E. ToolBox, "Beams-supported at both ends-continuous and point loads," 2009.

[34] ASTM, *B593-96(2014)e1 Standard Test Method for Bending Fatigue Testing for Copper-Alloy Spring Materials*. West Conshohocken, PA: ASTM International, 2009.

[35] P. De, C. Obermark, and R. Mishra, "Development of a reversible bending fatigue test bed to evaluate bulk properties using sub-size specimens," *Journal of Testing and Evaluation*, vol. 36, no. 4, pp. 402–405, 2008.

[36] P. Gohil, H. N. Panchal, S. M. Sohail, and D. V. Mahant, "Experimental and fea prediction of fatigue life in sheet metal (is 2062)," *MH*, vol. 1, p. 1.

[37] A. S. Haidyrah, C. Castano, and J. W. Newkirk, "An experimental study on bending fatigue test with a krouse-type fatigue specimen," in *2014 ANS Winter Meeting and Nuclear Technology Expo*, pp. 1–4, 2014.

[38] A. S. Haidyrah, J. W. Newkirk, and C. H. Castaño, "Characterization a bending fatigue mini-specimen technique (krouse type) of nuclear materials," in *TMS 2015 144th Annual Meeting & Exhibition*, pp. 1225–1232, Springer, 2015.

[39] A. S. Haidyrah, J. W. Newkirk, and C. H. Castaño, "Weibull statistical analysis of krouse type bending fatigue of nuclear materials," *Journal of Nuclear Materials*, vol. 470, pp. 244–250, 2016.

[40] F. P. Beer, E. R. Johnston, J. T. DeWolf, and D. F. Mazurek, *Statics and mechanics of materials*. McGraw-Hill Education, 2017.

[41] W. Thomson, *Theory of vibration with applications*. CrC Press, 2018.

[42] X. Wang and D. Chung, "Real-time monitoring of fatigue damage and dynamic strain in carbon fiber polymer-matrix composite by electrical resistance measurement," *Smart materials and structures*, vol. 6, no. 4, p. 504, 1997.

[43] R. I. Stephens, A. Fatemi, R. R. Stephens, and H. O. Fuchs, *Metal fatigue in engineering*. John Wiley & Sons, 2000.

[44] H. Mughrabi, "Microstructural mechanisms of cyclic deformation, fatigue crack initiation and early crack growth," *Philosophical Transactions of the Royal Society A: Mathematical, Physical and Engineering Sciences*, vol. 373, no. 2038, p. 20140132, 2015.

[45] E. O. Olakanmi, R. Cochrane, and K. Dalgarno, "A review on selective laser sintering/melting (sls/slm) of aluminium alloy powders: Processing, microstructure, and properties," *Progress in Materials Science*, vol. 74, pp. 401–477, 2015.

[46] B. Zhang, Y. Li, and Q. Bai, "Defect formation mechanisms in selective laser melting: a review," *Chinese Journal of Mechanical Engineering*, vol. 30, no. 3, pp. 515–527, 2017.

[47] S. Karnati, I. Axelsen, F. Liou, and J. W. Newkirk, "Investigation of tensile properties of bulk and slm fabricated 304l stainless steel using various gage length specimens," in *Proceedings of the 27th Annual International Solid Freeform Fabrication Symposium–An Additive Manufacturing Conference*, pp. 592–604, 2016.

[48] S. Al-Shahrani and T. Marrow, "Effect of surface finish on fatigue of stainless steels," in *ICF12, Ottawa 2009*, 2009.

II. HIGH CYCLE FATIGUE PERFORMANCE OF LPBF 304L STAINLESS STEEL AT NOMINAL AND OPTIMIZED PARAMETERS

Mohammad Masud Parvez[1,*], Tan Pan[1], Yitao Chen[1], Sreekar Karnati[1], Joseph W. Newkirk[2], and Frank Liou[1]

[1] Department of Mechanical and Aerospace Engineering

[2] Material Science and Engineering

Missouri University of Science and Technology, Rolla, MO 65401, USA

[*] Correspondence: mphf2@umsystem.edu; Tel.: +1-573-202-1506

ABSTRACT

In additive manufacturing, the variation of the fabrication process parameters influences the mechanical properties of a material such as tensile strength, impact toughness, hardness, fatigue strength, and so forth, but fatigue testing of metals fabricated with all different sets of process parameters is a very expensive and time-consuming process. Therefore, the nominal process parameters by means of minimum energy input were first identified for a dense part and then the optimized process parameters were determined based on the tensile and impact toughness test results obtained for 304L stainless steel deposited in laser powder bed fusion (LPBF) process. Later, the high cycle fatigue performance was investigated for the material built with these two sets of parameters at horizontal, vertical, and inclined orientation. In this paper, displacement controlled fully reversed (R = -1) bending type fatigue tests at different levels of displacement amplitude were performed on Krouse type miniature specimens. The test results were compared and analyzed by applying the control signal monitoring (CSM) method. The analysis shows that specimen built-in horizontal direction for optimized parameters demonstrates the highest fatigue strength while the vertical specimen built with nominal parameters exhibits the lowest strength.

Keywords: additive manufacturing; 304L stainless steel; tensile test; impact toughness test; fatigue test; nucleation and propagation; miniature specimen; simply supported bending

1. INTRODUCTION

Additive manufacturing (AM) has recently attained much popularity both in research and application fields such as aerospace, automobile, maritime, biomedical, and other industrial sectors [1, 2, 3, 4]. Among different additive manufacturing process available, laser powder bed fusion (LPBF) also known as selective laser melting (SLM) is a widely accepted method to fabricate metals and alloys [5, 6, 7, 8, 9]. LPBF is capable of depositing near-net-shape internal and external complex geometries but the major drawbacks of the AM materials are the surface irregularities, residual stress, and defects such as porosity, microcracks, inclusions, dislocations, and others. They significantly influence the static and dynamic mechanical properties of a material including fatigue strength. Several studies have been carried out recently to assess the fatigue behavior of different AM materials, that is, AlSi10Mg [10, 11, 12, 13], Ti6Al4V [14, 15, 16, 17, 18, 19], Ni-based alloy [20], 15-5 PH stainless steel [21], steel [22], stainless steel [23]. Nasab et al. [24] studied the effect of surface and subsurface defects on the fatigue behavior of AlSi10Mg. They also investigated the combined effect of surface anomalies and volumetric defects on fatigue life of AlSi7Mg fabricated via laser powder bed fusion [25]. Romano [26] investigated the effect of sub-surface porosity and surface roughness on the high cycle fatigue behavior of AM 17-4 PH stainless steel. Chan et al. [27] developed a methodology to predict the surface crack nucleation mechanism in a nickel-based superalloy AM 718Plus and proposed that fatigue life enhancement can be achieved by machining and polishing the surface. Zhan et al. [28] proposed a fatigue damage model considering AM effects and investigated the variation of fatigue life with the volumetric energy density and the variation of damage evolution rate. Biswal et al. [29] studied the effect of internal porosity on the fatigue strength of Ti-6Al-4V and proposed a modified Kitagawa-Takahashi diagram and a critical pore diameter to

initiate crack applying Murakami's approach. Since in AM, the formation of different types of porosity, that is, lack of fusion, keyhole, voids, and others is substantially influenced by the fabrication process parameters, the effect of process parameters on the fatigue behavior is yet to be investigated. While minimum energy input for a dense part originates lack of fusion type porosity most, keyhole defects are dominant at high energy input [30, 31, 32].

Due to the layer-by-layer deposition process in AM technique, another downside of the AM material is the anisotropy issue in mechanical behaviors that is, tensile performance [33, 34, 35, 36, 37, 38, 39], impact toughness [40] and fatigue properties [41]. Guan et al. [34] investigated the potential variables causing the anisotropy issue. They reported that both layer thickness and overlap rate showed an insignificant effect on the tensile properties on account of the similar metallurgical bonding and microstructure while build direction and hatch angle revealed strong impacts on mechanical properties by influencing stress concentration and microstructure. Hatch angle is the laser scan path angle with the x-axis. Wang et al. [35] and Yu et el. [38] further confirmed the anisotropy in tensile properties with different build orientations and proposed that columnar grain structure with higher length-width ratio induced by the rapid cooling rate of AM process could be the main reason for the mechanical anisotropies. Karnati et al. [40] investigated the anisotropy issue in impact toughness of AM printed AISI 304L stainless steel with different build orientations where vertical Charpy specimens exhibited the lowest toughness while horizontal specimens provided the highest. They explained the difficulty level of crack propagation along the interlayer track boundaries could be the possible reason. While Blinn et al. [41] studied the anisotropic fatigue behavior of AISI 316L stainless steel, the effect of anisotropy on the nucleation and propagation phase in fatigue assessment is yet to be investigated.

In this paper, the effect of build process parameters and anisotropy issues on the fatigue behavior of laser powder bed fused AISI 304L stainless steel was investigated. For fatigue testing, two sets of process parameters were selected to fabricate parts at horizontal, vertical, and inclined build direction. Nominal parameters were chosen for minimum

energy input for a dense part while the optimized parameters were determined by performing tensile and impact toughness tests. The fatigue test was conducted on miniature specimens. Since fabricating standard specimen is very expensive and time-consuming in the AM process, miniature specimens are recently employed in mechanical properties characterization of an AM material. Sreekar et al. [42] showed the miniature specimens to be instrumental in characterizing both bulk and AM material properties reliably. Dzugan et al. [43] demonstrated the implementation of miniaturized tensile test specimens instead of standard specimens in determining the local properties characterization of AM material Ti-6Al-4V. Wan et al. [44] addressed the reasons, necessities, and potential strategies to evaluate and qualify the fatigue performance of AM material using miniature specimens.

A modified Krouse type specimen with a dual gauge section was implemented for the bending fatigue test in this paper. The Krouse type specimen is a wedge-shaped ASTM (American Society for Testing and Materials) International standard B593-96(2014)e1 specimen, definition E206, and practice E468 [45]. The advantage of using such specimens is that nominal stress distribution remains uniform within the gauge. Haidyrah et al. [46, 47] and Gohil et al. [48] applied finite element analysis method on different modified versions of Krouse type specimens to confirm the uniform nominal stress distribution within the gauge. The uniform stress distribution eliminates the stress gradient effect in the bending type test of miniature specimens [49, 50]. Additionally, the increased surface area in a dual gauge specimen may also capture different surface and subsurface defects. A displacement controlled test was performed in this study since the displacement controlled fatigue test tends to be a more stable approach than load control and the driving force decreases with the crack growth in displacement control [51]. Later implementing the control signal monitoring (CSM) method [52, 53], the crack nucleation, and propagation phase were identified and compared for different build directions and process parameters.

2. MATERIALS AND METHODOLOGY

2.1. MATERIALS

The material used for this study was Ar gas atomized AISI 304L stainless steel (SS) powder purchased from LPW Technology (Imperial, PA 15126, USA) with a reported particle size distribution ranging from 15 to 45 μm and true powder density of 7.935 g/cm^3. The chemical composition provided by the vendor is listed in Table 1. From the chemistry of the material, this may be characterized as 304L SS due to its low content of interstitial, N, C, O, and so forth.

2.2. FABRICATION

The AM machine used in this study was Renishaw AM 250 (Renishaw Inc., Auburn Hills, MI 48326, USA) equipped with an Nd-YAG pulsed laser (IPG Photonics, Oxford, MA 01540, USA). The maximum power capacity of the laser is 200 W with a Gaussian intensity profile. A preheating process was employed prior to the initiation of the build. The substrate and powder were heated up and maintained 80°C temperature to reduce the thermal gradient and eliminate the water vapor inside powder particles. During the printing process, a recirculating Ar gas flow was maintained to remove the condensate generated. A design of experiment (DOE) was implemented for the selection of process parameters in this study in order to vary the energy density range. The energy density (ED) in AM is

Table 1. Chemical composition of AISI 304L stainless steel powder particles in weight percentage.

Element	**C**	**Cr**	**Cu**	**Fe**	**Mn**	**N**	**Ni**	**O**	**P**	**S**	**Si**
wt.%	0.018	18.4	<0.1	bal.	1.4	0.06	9.8	0.02	0.012	0.005	0.6

defined as

$$ED = \frac{P}{v \times h \times t} \quad (\mathrm{J/mm^3}), \quad (1)$$

where, P, v, h, and t are the laser power (W), scan speed (m/s), hatch spacing (µm), and layer thickness (µm), respectively. Hatch spacing is defined as the distance between two adjacent laser scan tracks. Scan speed was calculated using Equation (2)

$$v = \frac{\text{Point distance}}{\text{Exposure time}} \quad (\mathrm{m/s}). \quad (2)$$

Point distance and hatch spacing were identified as two variables where the scan speed of the laser traveling was linearly related to the point distance. A higher point distance determines a higher scan speed, hence a lower energy input is achieved and vice versa. Hatch spacing controls the overlap between adjacent laser track, which tends to cause the lack of fusion defects with less overlap and keyhole porosity with higher overlay. A previous study by Brown [54] proposed a nominal parameter for AISI 304L which originated from the optimization of bulk density and surface finish of downward skin. The parameters were selected in a range surrounding the nominal parameters. Three levels of point distance and five levels of hatch spacing were designated to obtain a 2-way full factorial experiment with 15 parameter combinations. The laser power was set at 200 W with a constant layer thickness of 50 µm and an exposure time of 88 µs. A stripe scan pattern was applied to guide the way laser scanned with a hatch angle of 67° rotating between two adjacent layers. The 15 parameter combinations are listed in Table 2 where ED #8 is for the nominal parameters mentioned here [54].

Table 2. Process parameters used to fabricate 304L stainless steel.

Laser Power (W)	Exposure Time (µs)	Layer Thickness (µm)	Point Distance (µm)	Scan Speed (m/s)	Hatch Spacing (µm)	Energy Density (J/mm^3)	ED #
			53	0.6	65	102.6	1
			53	0.6	75	88.8	2
			53	0.6	85	78.4	3
			53	0.6	95	70.2	4
			53	0.6	105	63.5	5
			70	0.8	65	76.9	6
			70	0.8	75	66.7	7
200	88	50	70	0.8	85	58.8	8
			70	0.8	95	52.6	9
			70	0.8	105	47.6	10
			88	1.0	65	61.5	11
			88	1.0	75	53.3	12
			88	1.0	85	47.1	13
			88	1.0	95	42.1	14
			88	1.0	105	38.1	15

2.3. PARAMETERS SELECTION

2.3.1. Nominal Parameters. In order to determine the nominal parameters, a density test was performed after the samples were printed with parameters listed in Table 2. All the samples were cut off from the substrate with a Sodick VZ300L Wire Electric Discharge Machine (EDM). The density test was performed on the as-printed samples based on the Archimedes principle. The mean relative density results are illustrated in Figure 1 with a

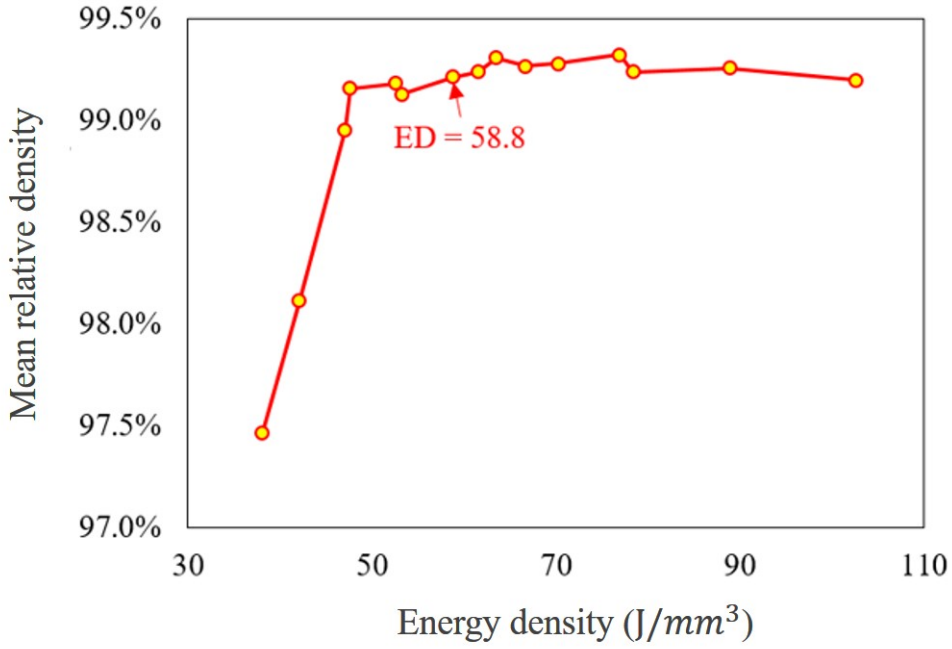

Figure 1. Relative density of the samples printed with the combination of all parameters.

true powder density of 7.935 g/cm^3 and the average of three samples. From the trend of the relative volumetric density along with the energy density indicated at the lower ED region, the relative density of the as-printed sample elevated with the increase of ED till 58.8 J/mm^3. After that, the relative density was almost consistent (>99.0%) with negligible fluctuation. Therefore, the set of parameters for ED #8 was chosen as the nominal parameters in this study [54].

2.3.2. Optimized Parameters. In order to determine the optimized parameters, tensile and impact toughness test was performed on the samples with ED above 58.8 J/mm^3 included. Tensile testing was performed with miniature dog bone specimen as shown in Figure 2 [42]. The samples fabricated were machined to size with a nominal thickness of 1 mm. Three specimens were prepared for each parameter combination with the gauge length perpendicular to the build direction (horizontal specimen). Prior to the testing, the specimens were polished with 800 grit sandpaper. The Instron UTM machine was employed in this study to do tensile testing. The strain was controlled using an extensometer

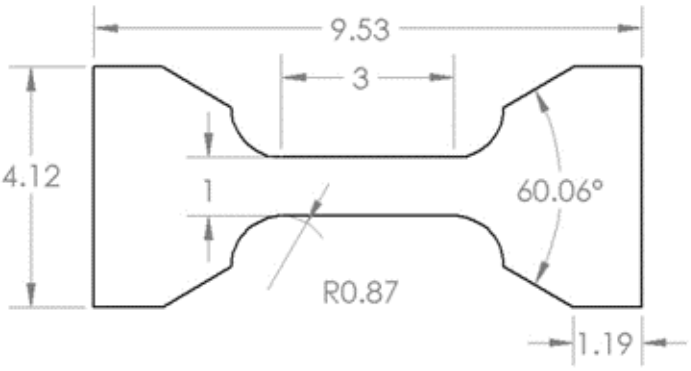

Figure 2. Dimension of the miniature tensile specimen.

with a strain rate of 0.015 mm/min to 1% strain value. After that, the extensometer was removed and the testing was run with a cross-head speed of 1.5 mm/min. The tensile properties of the tested samples were represented by 0.2% offset yield strength (YS) and ultimate tensile strength (UTS). From the tensile test result of horizontal specimens with different energy density combinations as shown in Figure 3, it can be seen that no significant differences in YS and UTS can be recognized within the current ED range though there is a large scatter in results at an energy density of 66.7 J/mm^3. The possible reason

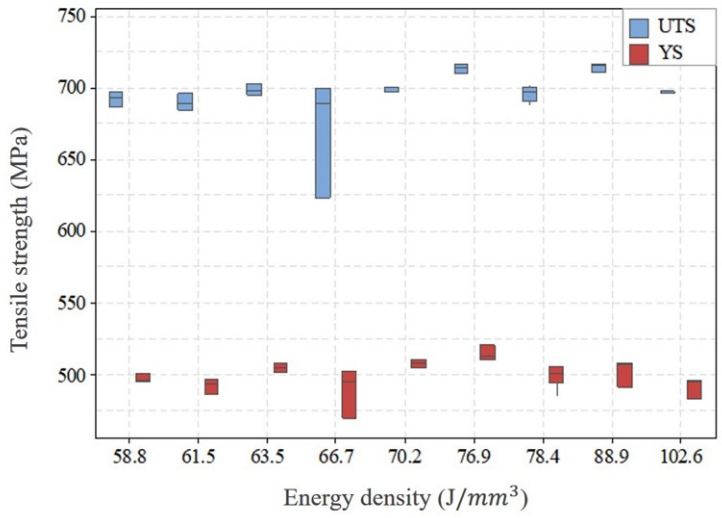

Figure 3. Tensile strength (yield strength (YS) and ultimate tensile strength (UTS)) of horizontal specimens with different parameters combination.

could be the quality of the printed part affected by the location on the build plate and the relative location of the gas flow [37]. However, the median of YS and UTS at horizontal orientation reached the maximum value at 76.9 J/mm^3 in comparison with other parameter combinations while the difference in UTS and YS for the vertical orientation (shown in Figure 4) at 58.8 and 76.9 J/mm^3 is negligible. Therefore, a further check was performed on vertical orientation by Charpy testing to the as-printed sample to demonstrate the parameter set optimized for impact toughness according to ASTM Standard E23. The longest axis of the Charpy specimen was printed along the build direction. A 2 mm "V" notch was machined with a standard broach. Three specimens were tested at each ED. The result of impact toughness from Charpy testing is illustrated in Figure 5. A relatively larger variation of impact toughness was observed for all ED. The median toughness achieved the optimal value at 76.9 J/mm^3. Hence, 76.9 J/mm^3 was demonstrated to be an optimized parameter set for both tensile strength and toughness.

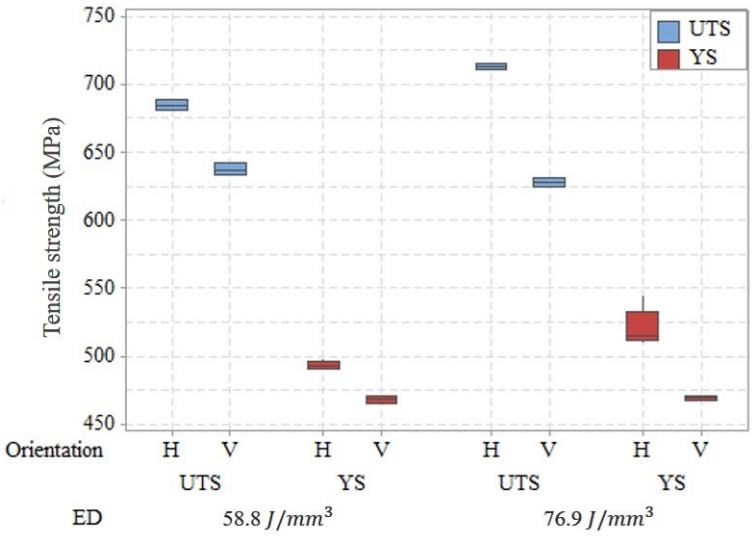

Figure 4. Tensile strength (YS and UTS) of horizontal and vertical specimens for energy densities 58.8 and 76.9 J/mm^3.

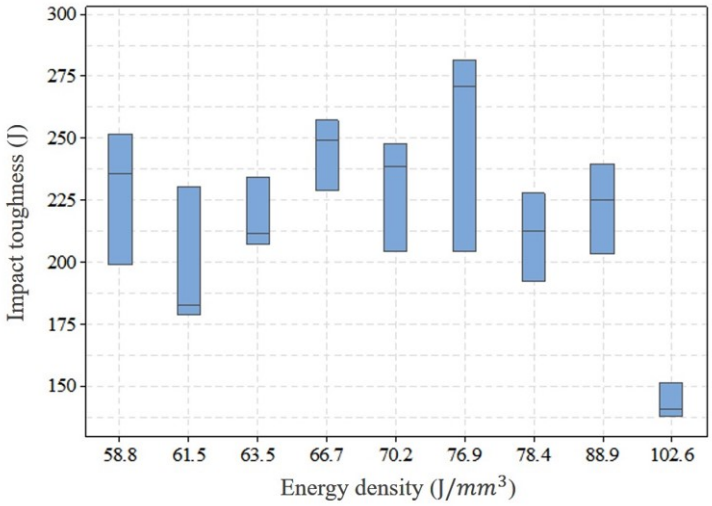

Figure 5. The impact toughness of as-built Charpy specimens printed in the vertical orientation with different parameters combination.

3. FATIGUE TEST

3.1. SPECIMEN DESIGN AND PREPARATION

The fatigue strength depends on the specimen size, dimension, and loading condition. Small specimens demonstrate higher fatigue strength compared to standard specimens while real parts exhibit even lower strength than the standard ones. While extended studies have been carried out to compare and evaluate the size effects on fatigue tests [55, 56, 57, 58, 59, 60, 61, 62, 63, 64, 65, 66, 67, 68, 69], recent studies show the implementation of miniature specimens to be instrumental in characterizing local properties of AM materials [42, 43, 44].

Since in AM, the effect of the process and build orientation could lead to fatigue property differences within the same part, therefore, a miniature specimen was designed. The dimension of the specimen is shown in Figure 6. The nominal thickness of the specimen was 0.67 mm. The Krouse type specimen with a dual gauge section was employed to conduct fatigue testing on the specimen fabricated using nominal and optimized parameters. While

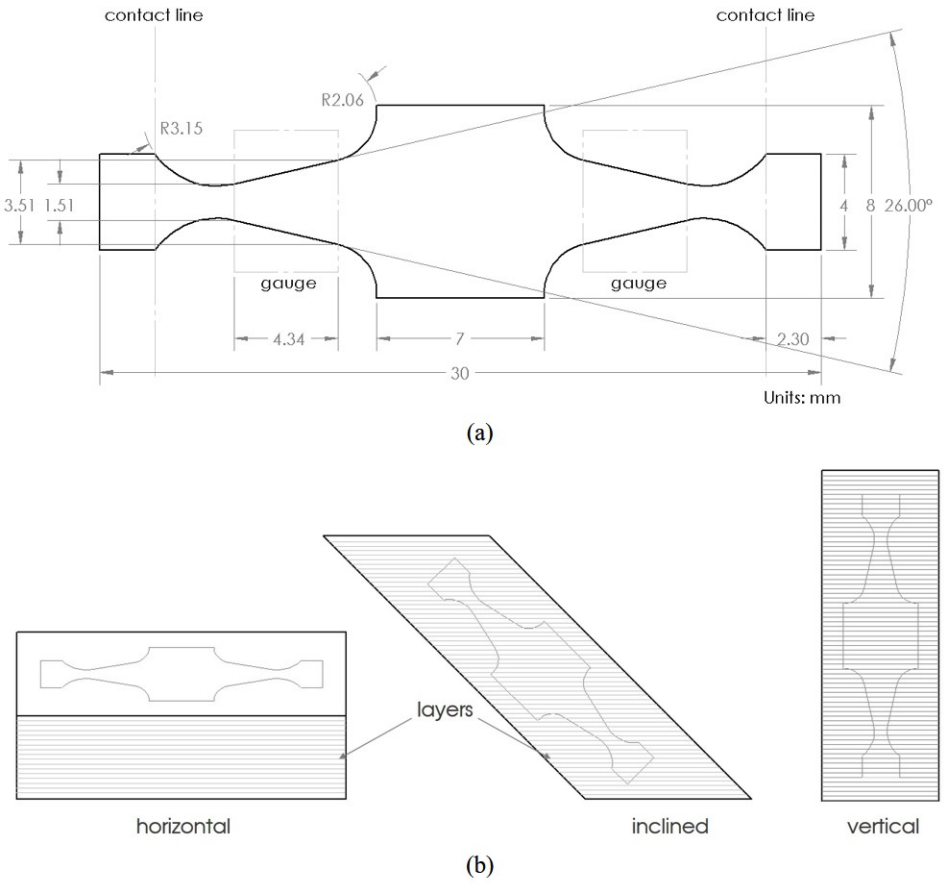

Figure 6. Schematic representation of miniature specimen including the dimensions with the dual gauge section and the specimens cut at horizontal, inclined, and vertical orientation

the Krouse type specimen ensures uniform stress distribution, the dual gauge with increased surface area enhances the probability of capturing different kinds of surface and subsurface defects since fatigue crack initiates at this location in most cases. The dual gauge also helps in distributing the load symmetrically and keeping the actuation path unidirectional, unlike a single cantilever beam. The specimen was specially designed for simply-supported test conditions. One of the advantages of using simply-supported is that the displacement is four times the displacement in a fully clamped mechanism. Since fatigue strength is also greatly influenced by the surface roughness of the test sample, therefore, finely finished (average roughness R_a = 0.482 µm, average R_z = 4.242 µm) specimens were machined

using a W-EDM. A total of 7 specimens for each build orientation and process parameters were prepared without any additional surface preparation. Detailed FEA simulation results and sensitivity analysis on the designed specimen can be found here [52].

3.2. TEST SETUP

An additional advantage of using miniature specimens is that it requires a lower range of force; thus it minimizes the test setup cost. A subwoofer with low power capacity was employed as an actuator in this study. The subwoofer is a low-frequency drive. The mechanical modeling of a subwoofer is relatively similar to an electrodynamic shaker but the shaker has more rigid moving parts. Since higher rigidity requires higher force, the subwoofer with soft mechanical suspension is a well fitted low-cost alternate of a shaker. In order to utilize the woofer as the actuator, a plastic flange of 76.2 mm diameter replaced the cap of the voice coil. The flange of relatively larger diameter (3 times) compared to the effective length of the specimen (25.4 mm) along with the cone (254 mm diameter) supports the one-dimensional movement of the specimen. On top of the flange, the moving parts were mounted. A load cell fixed between the flange and the clamp of the central part measures the force applied on the specimen. Figure 7 illustrates the test setup with a specimen installed for simply supported bending type fatigue testing. While the specimen at the center was in surface contact (7 mm along the width and 3 mm along at length) with the central fixture, both ends maintained a line contact with bearings to ensure simply supported condition. In order to avoid any preloading on the specimen, spacers were used at both ends. The other two bearing holders were placed on top of the spacers. Finally, the heavy load toggle clamps fixed both ends of the test setup with the structure well. A high-speed laser-based displacement sensor pointing at the central clamp measured the displacement of the specimen. A proportional derivative (PD) controller was implemented to maintain

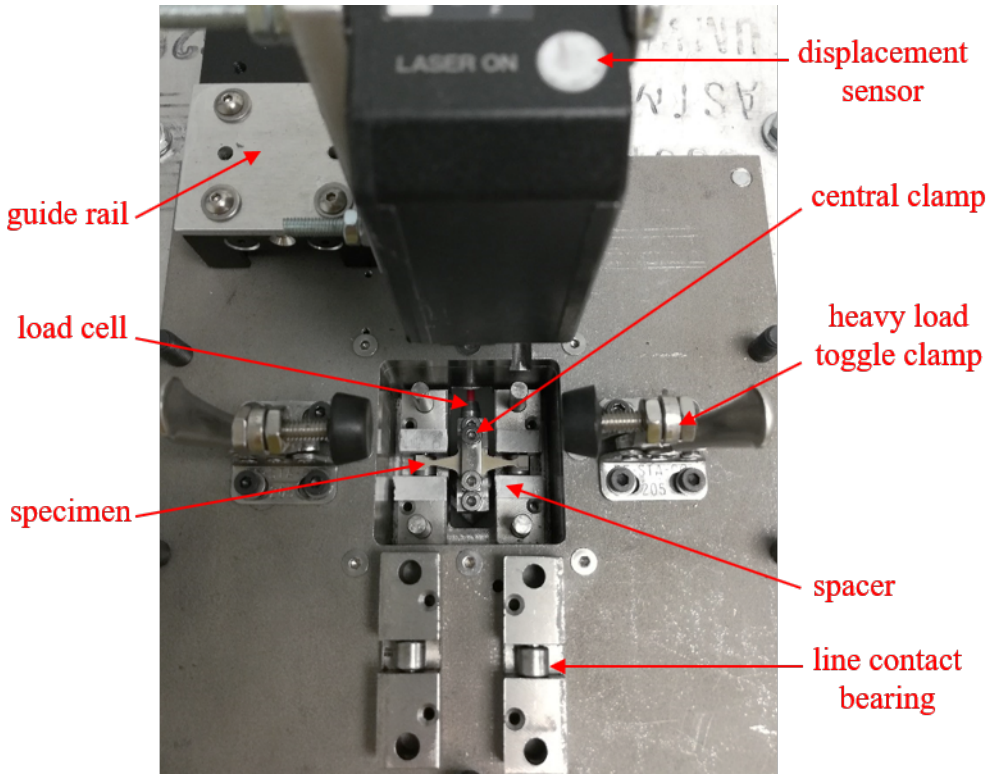

Figure 7. Fatigue testbench setup.

the required set displacement while the load cell was used to measure the amplitude of the force applied. For further analysis, the displacement, load, and control signal amplitudes were recorded in a computer until the final failure of the specimen.

4. RESULTS AND DISCUSSION

The fatigue test controlling the displacement was performed for simply-supported fully reversed (R = −1) type bending of the specimen with sinusoidal excitation at 56 Hz test frequency. All experiments were conducted at room temperature monitored with an infrared temperature sensor. The temperature variation reported here [52] remained within ±2° C. The specimens failed at random locations within the gauges since defects are present randomly in the material. In Krouse type specimens, the stress concentration near the defects within the gauges was expected to be high, though the nominal stress distribution

was assumed uniform. Figure 8 illustrates the controller performance in maintaining the set displacement of a horizontal specimen built with nominal parameters. During the test, the control signal amplitude was also monitored. In the fatigue test, with the crack initiation and propagation until the final failure happens, the stiffness of the specimen decreases. Therefore, the amplitude of the control signal also decreases for a constant displacement amplitude with an increasing number of cycles as shown in Figure 8 b. The displacement increases suddenly at the final rapid failure stage indicating the complete failure of the specimen. While the stiffness of the test sample decreases at nucleation, propagation, and final failure stages, the rate of change in stiffness reduction is different at different stages. This gives us a unique comprehension of identifying nucleation and propagation phase applying a linear regression on the magnitude of the control signal and tracing the last peak of the signal near the line as ending of the nucleation phase. After identifying the nucleation and propagation, maximum nominal stress was calculated averaging the load amplitude up to the end of nucleation using Equation (3),

$$\sigma = \frac{3F}{2kh^2}, \tag{3}$$

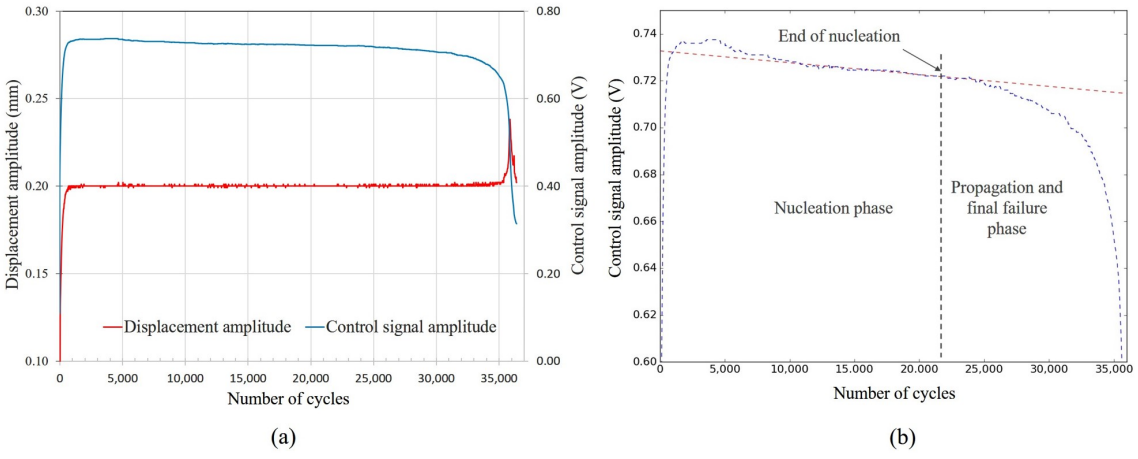

Figure 8. Amplitude of control signal and identification of the nucleation and propagation phase.

where, σ, F, h, and k are the nominal stress, load amplitude, thickness of the specimen, and the slope of the wedge shape. Figure 9 shows the Wohler curve of the specimens tested for different build orientations fabricated with nominal and optimized parameters. As we can see, for both the nominal and optimized parameters, horizontal specimens demonstrate higher fatigue strength than the inclined and vertical specimens while inclined specimens have higher strength than vertical ones.

The fatigue strength of the material in the horizontal direction is higher not only in the nucleation phase but also during propagation as we can see from the analysis of the control signal [52] shown in Figure 10. During the fatigue test, the crack initiates within the gauge and propagates across the cross-section. In inclined and vertical specimens, the loading direction is parallel to the layers while this is normal for horizontal specimens.

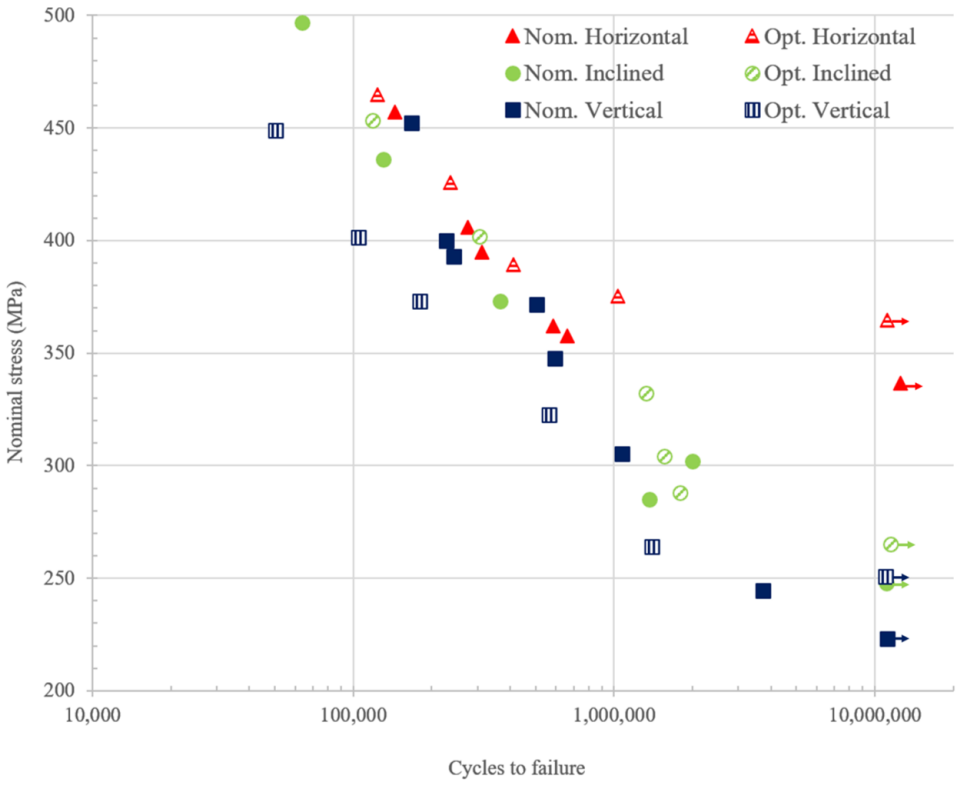

Figure 9. S-N plot of the specimens tested for horizontal, inclined, and vertical direction built with nominal and optimized parameters.

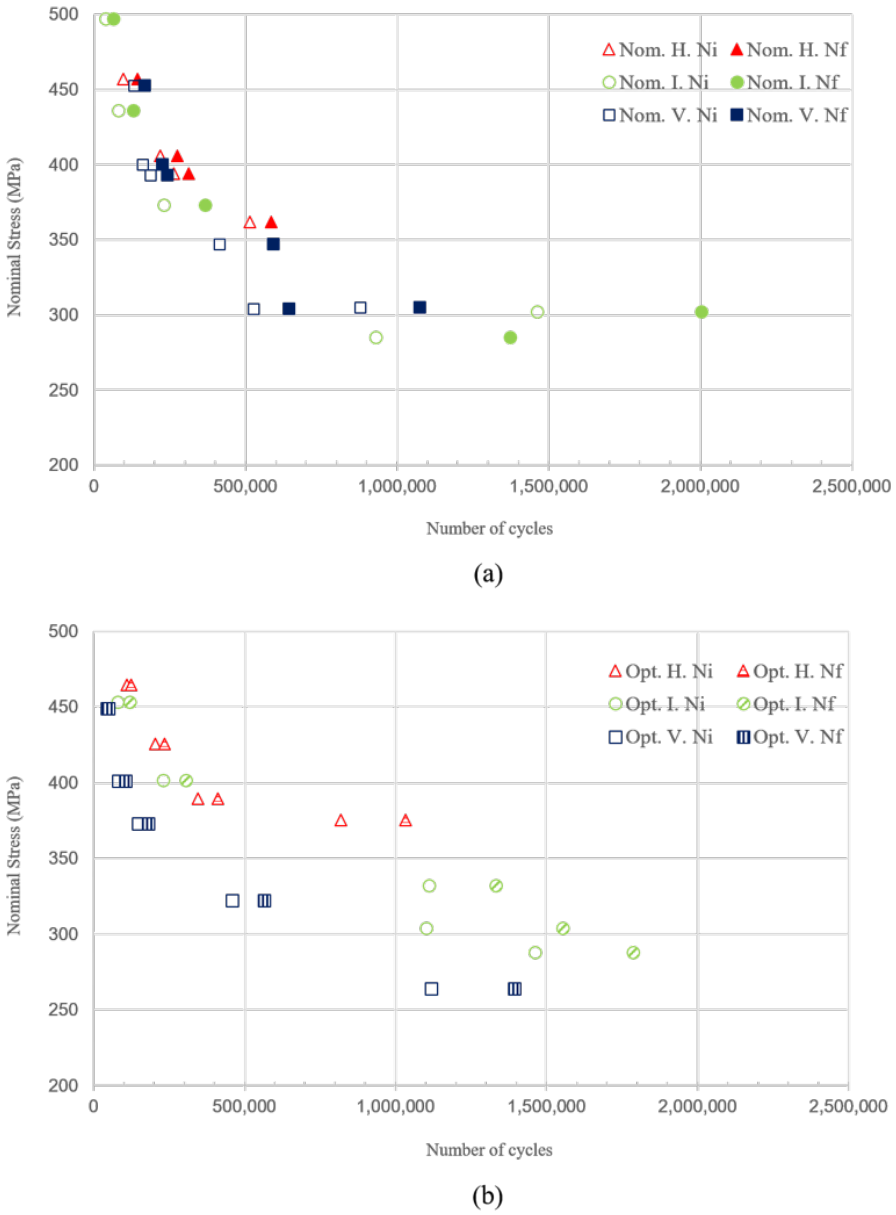

Figure 10. Nucleation phase and propagation and final failure phase of the specimens.

Moreover, inclined and vertical specimens consist of a larger number of layers hence interlayer within the gauges. In AM materials, interlayer strength is assumed to be weaker [9, 32]. Additionally, the inclined and vertical specimens have a higher defect probability since they accommodate a larger number of interlayer within the gauges. Including anisotropy, these are the possible reasons for horizontal specimens demonstrating higher fatigue strength

during nucleation and propagation. While comparing the inclined and vertical specimens, the crack in an inclined specimen has to travel through a large number of layers across the cross-section during propagation. Therefore the propagation cycle is longer in inclined specimens than in vertical specimens.

Scanning electron microscopic (SEM) images of fracture surfaces of the fatigue specimens fabricated with nominal and optimized parameters are shown in Figures 11 and 12, respectively. Figure 11 a, c, e exhibit the fracture surface of the horizontal, vertical, and inclined orientation specimens, respectively while the fracture surface for the horizontal and inclined specimens built with optimized parameters are shown in Figure 12 a, b, respectively. In Figure 11 b, d, f, nominal specimens with all orientations (horizontal, vertical, and incline) show that possible crack initiation sites are located around the lack-of-fusion defects close to the surface (circled by dashed lines). The initiation is a combined effect of higher nominal stress near the specimen surface and the stress concentration effect of defects. Especially in Figure 11 b, f, unmelted powder particles can be found. While for the specimens built with optimized parameters, there is no obvious sign of lack-of-fusion type defects near the possible crack initiation sites, since the higher energy density provided for the optimized parameters can reduce the probability of the generation of lack-of-fusion. The initiation sites of specimens for optimized parameters mainly locate at the surface defect such as surface cracks (shown in Figure 12 a, b). The fracture surface analysis reveals the possible reasons for the material fabricated with optimized parameters exhibiting higher fatigue strength at all different directions when compared with the material fabricated with nominal parameters.

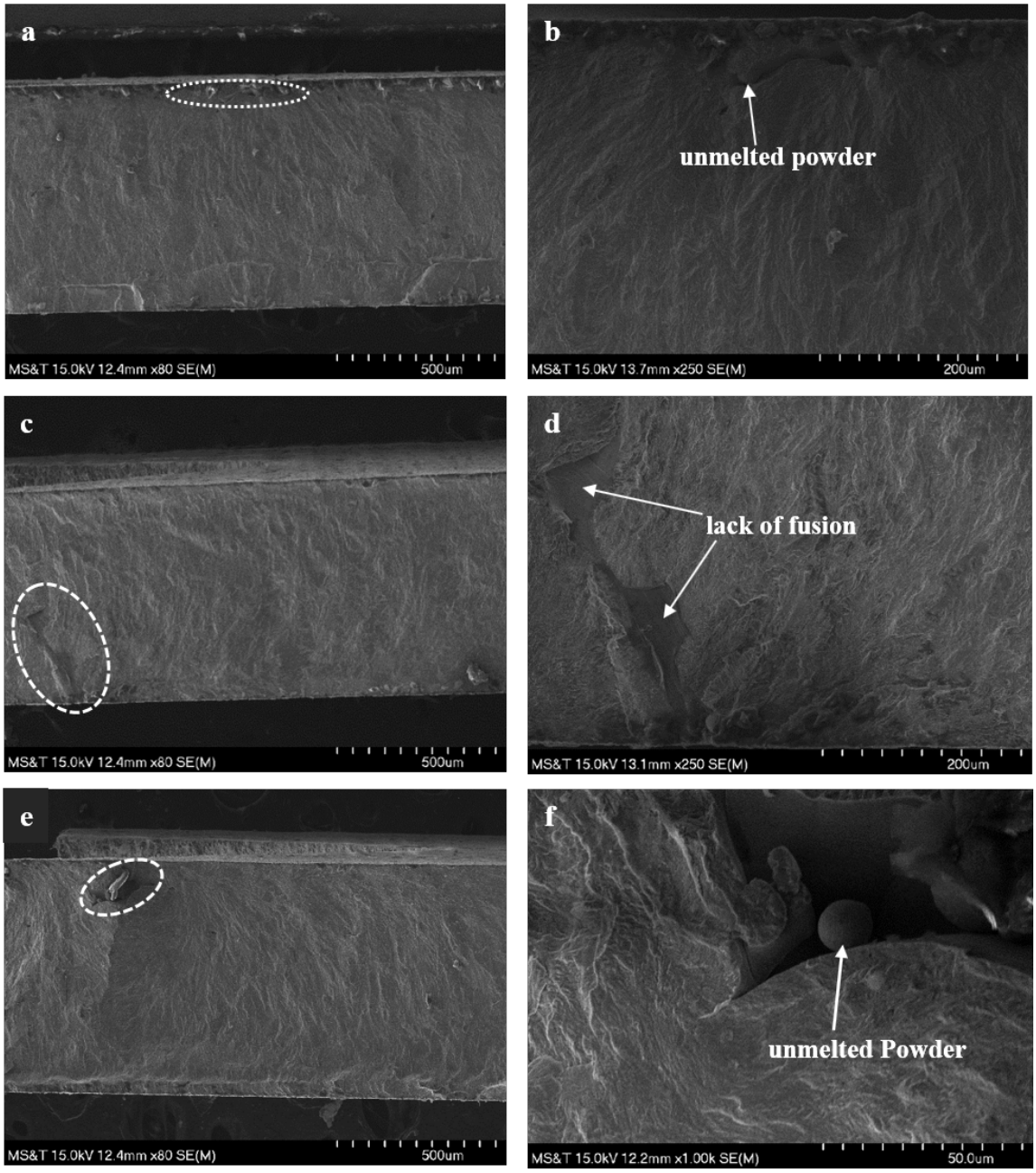

Figure 11. Scanning electron microscope (SEM) images of the fracture surfaces with possible crack initiation sites of the specimens.

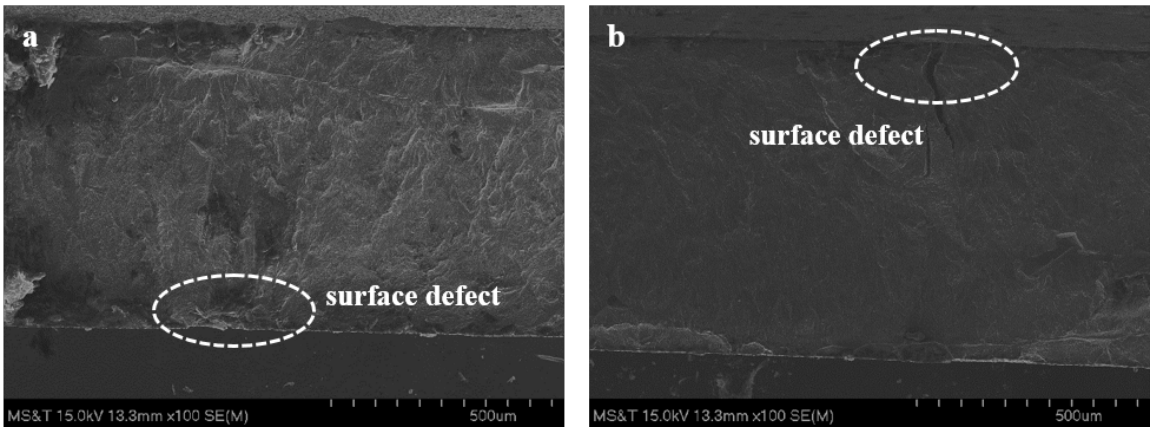

Figure 12. SEM images of the fracture surfaces with possible crack initiation sites of the specimens fabricated by the optimized parameters.

5. CONCLUSIONS

In this paper, the effect of build process parameters on fatigue strength of laser powder bed fused AISI 304L stainless steel was investigated. Nominal and optimized process parameters were chosen to fabricate the material based on the density, tensile, and toughness test results. The fatigue test was performed for displacement control on a Krouse type miniature specimen with a dual gauge. The nucleation and propagation phase was identified implementing the control signal monitoring method. The analyses and experimental results show that material fabricated with optimized parameters demonstrate a higher fatigue strength at horizontal, inclined, and vertical directions than the specimens built with nominal parameters. Materials built with nominal parameters consist of the lack of fusion type defects mostly while the materials for the optimized parameters are expected to have keyhole type defects most. For particular stress, horizontal specimens have higher strength both during nucleation and propagation compared to the inclined and vertical specimens while the inclined specimens have higher strength than the vertical ones. For both the parameters, this is in good agreement with the anisotropy issue. Future studies may include the investigation of the size effect on fatigue performance, and the comparison of the fatigue behavior of LPBF 304L SS between as-built and annealed specimens.

ACKNOWLEDGEMENT

This research was supported by National Science Foundation Grant CMMI-1625736. Part of the work was also funded by the Department of Energy's Kansas City National Security Campus which is operated and managed by Honeywell Federal Manufacturing Technologies, LLC under contract number DE-NA0002839, Intelligent Systems Center, and Material Research Center at Missouri University of Science and Technology. Their support is greatly appreciated.

REFERENCES

[1] W. E. Frazier, "Metal additive manufacturing: a review," *Journal of Materials Engineering and Performance*, vol. 23, no. 6, pp. 1917–1928, 2014.

[2] Y. Zhang, L. Wu, X. Guo, S. Kane, Y. Deng, Y.-G. Jung, J.-H. Lee, and J. Zhang, "Additive manufacturing of metallic materials: a review," *Journal of Materials Engineering and Performance*, vol. 27, no. 1, pp. 1–13, 2018.

[3] J. J. Lewandowski and M. Seifi, "Metal additive manufacturing: a review of mechanical properties," *Annual Review of Materials Research*, vol. 46, pp. 151–186, 2016.

[4] M. M. Parvez, S. Patel, S. P. Isanaka, and F. Liou, "A novel laser-aided machining and polishing process for additive manufacturing materials with multiple endmill emulating scan patterns," *Applied Sciences*, vol. 11, no. 20, p. 9428, 2021.

[5] J.-P. Kruth, L. Froyen, J. Van Vaerenbergh, P. Mercelis, M. Rombouts, and B. Lauwers, "Selective laser melting of iron-based powder," *Journal of materials processing technology*, vol. 149, no. 1-3, pp. 616–622, 2004.

[6] I. Yadroitsev, A. Gusarov, I. Yadroitsava, and I. Smurov, "Single track formation in selective laser melting of metal powders," *Journal of Materials Processing Technology*, vol. 210, no. 12, pp. 1624–1631, 2010.

[7] I. Serrano-Munoz, J.-Y. Buffiere, R. Mokso, C. Verdu, and Y. Nadot, "Location, location & size: defects close to surfaces dominate fatigue crack initiation," *Scientific reports*, vol. 7, p. 45239, 2017.

[8] V. Prithivirajan and M. D. Sangid, "The role of defects and critical pore size analysis in the fatigue response of additively manufactured in718 via crystal plasticity," *Materials & Design*, vol. 150, pp. 139–153, 2018.

[9] E. O. Olakanmi, R. Cochrane, and K. Dalgarno, "A review on selective laser sintering/melting (sls/slm) of aluminium alloy powders: Processing, microstructure, and properties," *Progress in Materials Science*, vol. 74, pp. 401–477, 2015.

[10] W. Schneller, M. Leitner, S. Pomberger, S. Springer, F. Beter, and F. Grün, "Effect of post treatment on the microstructure, surface roughness and residual stress regarding the fatigue strength of selectively laser melted alsi10mg structures," *Journal of Manufacturing and Materials Processing*, vol. 3, no. 4, p. 89, 2019.

[11] S. Romano, A. Brückner-Foit, A. Brandão, J. Gumpinger, T. Ghidini, and S. Beretta, "Fatigue properties of alsi10mg obtained by additive manufacturing: Defect-based modelling and prediction of fatigue strength," *Engineering Fracture Mechanics*, vol. 187, pp. 165–189, 2018.

[12] Z. Wang, W. Wu, G. Qian, L. Sun, X. Li, and J. A. Correia, "In-situ sem investigation on fatigue behaviors of additive manufactured al-si10-mg alloy at elevated temperature," *Engineering Fracture Mechanics*, vol. 214, pp. 149–163, 2019.

[13] E. W. Hovig, A. S. Azar, M. F. Sunding, E. Andreassen, and K. Sørby, "High cycle fatigue life estimation of materials processed by laser powder bed fusion," *Fatigue & Fracture of Engineering Materials & Structures*, vol. 42, no. 7, pp. 1454–1466, 2019.

[14] Y. Sun, S. Lu, S. Gulizia, C. Oh, D. Fraser, M. Leary, and M. Qian, "Fatigue performance of additively manufactured ti-6al-4v: Surface condition vs. internal defects," *JOM*, pp. 1–9.

[15] Z. Chen, S. Cao, X. Wu, and C. H. Davies, "Surface roughness and fatigue properties of selective laser melted ti–6al–4v alloy," in *Additive Manufacturing for the Aerospace Industry*, pp. 283–299, Elsevier, 2019.

[16] B. Vayssette, N. Saintier, C. Brugger, M. El May, and E. Pessard, "Numerical modelling of surface roughness effect on the fatigue behavior of ti-6al-4v obtained by additive manufacturing," *International Journal of Fatigue*, vol. 123, pp. 180–195, 2019.

[17] S. Tammas-Williams, P. Withers, I. Todd, and P. Prangnell, "The influence of porosity on fatigue crack initiation in additively manufactured titanium components," *Scientific reports*, vol. 7, no. 1, pp. 1–13, 2017.

[18] A. Vilardell, P. Krakhmalev, G. Fredriksson, F. Cabanettes, A. Sova, D. Valentin, and P. Bertrand, "Influence of surface topography on fatigue behavior of ti6al4v alloy by laser powder bed fusion," *Procedia CIRP*, vol. 74, pp. 49–52, 2018.

[19] P. Li, D. Warner, J. Pegues, M. Roach, N. Shamsaei, and N. Phan, "Towards predicting differences in fatigue performance of laser powder bed fused ti-6al-4v coupons from the same build," *International Journal of Fatigue*, vol. 126, pp. 284–296, 2019.

[20] S. Shao, M. Khonsari, S. Guo, W. J. Meng, and N. Li, "Overview: Additive manufacturing enabled accelerated design of ni-based alloys for improved fatigue life," *Additive Manufacturing*, p. 100779, 2019.

[21] S. Sarkar, C. S. Kumar, and A. K. Nath, "Effects of different surface modifications on the fatigue life of selective laser melted 15–5 ph stainless steel," *Materials Science and Engineering: A*, vol. 762, p. 138109, 2019.

[22] S. Afkhami, M. Dabiri, S. H. Alavi, T. Björk, and A. Salminen, "Fatigue characteristics of steels manufactured by selective laser melting," *International Journal of Fatigue*, vol. 122, pp. 72–83, 2019.

[23] M. Zhang, C.-N. Sun, X. Zhang, P. C. Goh, J. Wei, D. Hardacre, and H. Li, "High cycle fatigue life prediction of laser additive manufactured stainless steel: A machine learning approach," *International Journal of Fatigue*, vol. 128, p. 105194, 2019.

[24] M. Hamidi Nasab, A. Giussani, D. Gastaldi, V. Tirelli, and M. Vedani, "Effect of surface and subsurface defects on fatigue behavior of alsi10mg alloy processed by laser powder bed fusion (l-pbf)," *Metals*, vol. 9, no. 10, p. 1063, 2019.

[25] M. H. Nasab, S. Romano, D. Gastaldi, S. Beretta, and M. Vedani, "Combined effect of surface anomalies and volumetric defects on fatigue assessment of alsi7mg fabricated via laser powder bed fusion," *Additive Manufacturing*, p. 100918, 2019.

[26] S. Romano, P. Nezhadfar, N. Shamsaei, M. Seifi, and S. Beretta, "High cycle fatigue behavior and life prediction for additively manufactured 17-4 ph stainless steel: Effect of sub-surface porosity and surface roughness," *Theoretical and Applied Fracture Mechanics*, p. 102477, 2020.

[27] K. S. Chan and A. Peralta-Duran, "A methodology for predicting surface crack nucleation in additively manufactured metallic components," *Metallurgical and Materials Transactions A*, vol. 50, no. 9, pp. 4378–4387, 2019.

[28] Z. Zhan, H. Li, and K. Lam, "Development of a novel fatigue damage model with am effects for life prediction of commonly-used alloys in aerospace," *International Journal of Mechanical Sciences*, vol. 155, pp. 110–124, 2019.

[29] R. Biswal, X. Zhang, A. K. Syed, M. Awd, J. Ding, F. Walther, and S. Williams, "Criticality of porosity defects on the fatigue performance of wire+ arc additive manufactured titanium alloy," *International Journal of Fatigue*, vol. 122, pp. 208–217, 2019.

[30] L. Sheridan, J. E. Gockel, and O. E. Scott-Emuakpor, "Primary processing parameters, porosity production, and fatigue prediction for additively manufactured alloy 718," *Journal of Materials Engineering and Performance*, vol. 28, no. 9, pp. 5387–5397, 2019.

[31] N. M. Heckman, T. A. Ivanoff, A. M. Roach, B. H. Jared, D. J. Tung, H. J. Brown-Shaklee, T. Huber, D. J. Saiz, J. R. Koepke, J. M. Rodelas, *et al.*, "Automated high-throughput tensile testing reveals stochastic process parameter sensitivity," *Materials Science and Engineering: A*, vol. 772, p. 138632, 2020.

[32] B. Zhang, Y. Li, and Q. Bai, "Defect formation mechanisms in selective laser melting: a review," *Chinese Journal of Mechanical Engineering*, vol. 30, no. 3, pp. 515–527, 2017.

[33] E. Liverani, S. Toschi, L. Ceschini, and A. Fortunato, "Effect of selective laser melting (slm) process parameters on microstructure and mechanical properties of 316l austenitic stainless steel," *Journal of Materials Processing Technology*, vol. 249, pp. 255–263, 2017.

[34] K. Guan, Z. Wang, M. Gao, X. Li, and X. Zeng, "Effects of processing parameters on tensile properties of selective laser melted 304 stainless steel," *Materials & Design*, vol. 50, pp. 581–586, 2013.

[35] Z. Wang, T. A. Palmer, and A. M. Beese, "Effect of processing parameters on microstructure and tensile properties of austenitic stainless steel 304l made by directed energy deposition additive manufacturing," *Acta Materialia*, vol. 110, pp. 226–235, 2016.

[36] Y. Kok, X. P. Tan, P. Wang, M. Nai, N. H. Loh, E. Liu, and S. B. Tor, "Anisotropy and heterogeneity of microstructure and mechanical properties in metal additive manufacturing: A critical review," *Materials & Design*, vol. 139, pp. 565–586, 2018.

[37] B. E. Carroll, T. A. Palmer, and A. M. Beese, "Anisotropic tensile behavior of ti–6al–4v components fabricated with directed energy deposition additive manufacturing," *Acta Materialia*, vol. 87, pp. 309–320, 2015.

[38] H. Yu, J. Yang, J. Yin, Z. Wang, and X. Zeng, "Comparison on mechanical anisotropies of selective laser melted ti-6al-4v alloy and 304 stainless steel," *materials science and engineering: a*, vol. 695, pp. 92–100, 2017.

[39] D. B. Witkin, D. Patel, T. V. Albright, G. E. Bean, and T. McLouth, "Influence of surface conditions and specimen orientation on high cycle fatigue properties of inconel 718 prepared by laser powder bed fusion," *International Journal of Fatigue*, vol. 132, p. 105392, 2020.

[40] S. Karnati, A. Khiabhani, A. Flood, F. Liou, and J. Newkirk, "Anisotropy in impact toughness of powder bed fused aisi 304l stainless steel," *Material Design & Processing Communications*, p. e59, 2019.

[41] B. Blinn, M. Klein, and T. Beck, "Determination of the anisotropic fatigue behaviour of additively manufactured structures with short-time procedure phyballit," in *MATEC web of conferences*, vol. 165, p. 02006, EDP Sciences, 2018.

[42] S. Karnati, I. Axelsen, F. Liou, and J. W. Newkirk, "Investigation of tensile properties of bulk and slm fabricated 304l stainless steel using various gage length specimens," in *Proceedings of the 27th Annual International Solid Freeform Fabrication Symposium–An Additive Manufacturing Conference*, pp. 592–604, 2016.

[43] J. Dzugan, M. Sibr, P. Konopík, R. Procházka, and M. Rund, "Mechanical properties determination of am components," in *IOP Conference Series: Materials Science and Engineering*, vol. 179, p. 012019, IOP Publishing, 2017.

[44] H. Wan, G. Chen, C. Li, X. Qi, and G. Zhang, "Data-driven evaluation of fatigue performance of additive manufactured parts using miniature specimens," *Journal of Materials Science & Technology*, vol. 35, no. 6, pp. 1137–1146, 2019.

[45] ASTM, *B593-96(2014)e1 Standard Test Method for Bending Fatigue Testing for Copper-Alloy Spring Materials*. West Conshohocken, PA: ASTM International, 2009.

[46] A. S. Haidyrah, J. W. Newkirk, and C. H. Castaño, "Characterization a bending fatigue mini-specimen technique (krouse type) of nuclear materials," in *TMS 2015 144th Annual Meeting & Exhibition*, pp. 1225–1232, Springer, 2015.

[47] A. S. Haidyrah, C. Castano, and J. W. Newkirk, "An experimental study on bending fatigue test with a krouse-type fatigue specimen," in *2014 ANS Winter Meeting and Nuclear Technology Expo*, pp. 1–4, 2014.

[48] P. Gohil, H. N. Panchal, S. M. Sohail, and D. V. Mahant, "Experimental and fea prediction of fatigue life in sheet metal (is 2062)," *MH*, vol. 1, p. 1.

[49] A. S. Haidyrah, J. W. Newkirk, and C. H. Castaño, "Weibull statistical analysis of krouse type bending fatigue of nuclear materials," *Journal of Nuclear Materials*, vol. 470, pp. 244–250, 2016.

[50] P. De, C. Obermark, and R. Mishra, "Development of a reversible bending fatigue test bed to evaluate bulk properties using sub-size specimens," *Journal of Testing and Evaluation*, vol. 36, no. 4, pp. 402–405, 2008.

[51] T. L. Anderson and T. L. Anderson, *Fracture mechanics: fundamentals and applications*. CRC press, 2005.

[52] M. M. Parvez, Y. Chen, S. Karnati, C. Coward, J. W. Newkirk, and F. Liou, "A displacement controlled fatigue test method for additively manufactured materials," *Applied Sciences*, vol. 9, no. 16, p. 3226, 2019.

[53] M. Parvez, Y. Chen, J. Newkirk, and F. Liou, "Comparison of fatigue performance between additively manufactured and wrought 304l stainless steel using a novel fatigue test setup," in *Solid Freeform Fabrication 2019: Proceedings of the 30th Annual International Solid Freeform Fabrication Symposium – An Additive Manufacturing Conference*, pp. 353–363, 2019.

[54] B. Brown, "Characterization of 304l stainless steel by means of minimum input energy on the selective laser melting platform," Master's thesis, Missouri University of Science and Technology, 2014.

[55] S.-P. Zhu, S. Foletti, and S. Beretta, "Evaluation of size effect on strain-controlled fatigue behavior of a quench and tempered rotor steel: Experimental and numerical study," *Materials Science and Engineering: A*, vol. 735, pp. 423–435, 2018.

[56] C. Sun and Q. Song, "A method for predicting the effects of specimen geometry and loading condition on fatigue strength," *Metals*, vol. 8, no. 10, p. 811, 2018.

[57] M. Leitner, M. Vormwald, and H. Remes, "Statistical size effect on multiaxial fatigue strength of notched steel components," *International Journal of Fatigue*, vol. 104, pp. 322–333, 2017.

[58] M. Leitner, C. Garb, H. Remes, and M. Stoschka, "Microporosity and statistical size effect on the fatigue strength of cast aluminium alloys en ac-45500 and 46200," *Materials Science and Engineering: A*, vol. 707, pp. 567–575, 2017.

[59] T. Tomaszewski and J. Sempruch, "Verification of the fatigue test method applied with the use of mini specimen," in *Key Engineering Materials*, vol. 598, pp. 243–248, Trans Tech Publ, 2014.

[60] M. Nakajima, K. Tokaji, H. Itoga, and T. Shimizu, "Effect of loading condition on very high cycle fatigue behavior in a high strength steel," *International Journal of Fatigue*, vol. 32, no. 2, pp. 475–480, 2010.

[61] G. Härkegård and G. Halleraker, "Assessment of methods for prediction of notch and size effects at the fatigue limit based on test data by böhm and magin," *International Journal of Fatigue*, vol. 32, no. 10, pp. 1701–1709, 2010.

[62] A. Wormsen, B. Sjödin, G. Härkegård, and A. Fjeldstad, "Non-local stress approach for fatigue assessment based on weakest-link theory and statistics of extremes," *Fatigue & Fracture of Engineering Materials & Structures*, vol. 30, no. 12, pp. 1214–1227, 2007.

[63] Y. Akiniwa, N. Miyamoto, H. Tsuru, and K. Tanaka, "Notch effect on fatigue strength reduction of bearing steel in the very high cycle regime," *International Journal of Fatigue*, vol. 28, no. 11, pp. 1555–1565, 2006.

[64] S. Beretta, A. Ghidini, and F. Lombardo, "Fracture mechanics and scale effects in the fatigue of railway axles," *Engineering fracture mechanics*, vol. 72, no. 2, pp. 195–208, 2005.

[65] A. Diemar, R. Thumser, and J. Bergmann, "Determination of local characteristics for the application of the weakest-link model," *Materialwissenschaft und Werkstofftechnik: Entwicklung, Fertigung, Prüfung, Eigenschaften und Anwendungen technischer Werkstoffe*, vol. 36, no. 5, pp. 204–210, 2005.

[66] D. B. Lanning, T. Nicholas, and A. Palazotto, "Hcf notch predictions based on weakest-link failure models," *International journal of fatigue*, vol. 25, no. 9-11, pp. 835–841, 2003.

[67] M. Makkonen, "Statistical size effect in the fatigue limit of steel," *International journal of fatigue*, vol. 23, no. 5, pp. 395–402, 2001.

[68] Z. P. Bažant and D. Novák, "Probabilistic nonlocal theory for quasibrittle fracture initiation and size effect. i: Theory," *Journal of Engineering Mechanics*, vol. 126, no. 2, pp. 166–174, 2000.

[69] W. Findley, "An explanation of size effect in fatigue of metals," *Journal of Mechanical Engineering Science*, vol. 14, no. 6, pp. 424–428, 1972.

III. A NOVEL LASER-AIDED MACHINING AND POLISHING PROCESS FOR ADDITIVE MANUFACTURING MATERIALS WITH MULTIPLE ENDMILL EMULATING SCAN PATTERNS

Mohammad Masud Parvez[1,*], Sahil Patel[1], Sriram Praneeth Isanaka[1], and Frank Liou[1]

[1] Department of Mechanical and Aerospace Engineering

Missouri University of Science and Technology, Rolla, MO 65401, USA

[*] Correspondence: mphf2@umsystem.edu; Tel.: +1-573-202-1506

ABSTRACT

In additive manufacturing (AM), the surface roughness of the deposited parts remains significantly higher than the admissible range for most applications. Additionally, the surface topography of AM parts exhibits waviness profiles between tracks and layers. Therefore, post-processing is indispensable to improve surface quality. Laser-aided machining and polishing can be effective surface improvement processes that can be used due to their availability as the primary energy sources in many metal AM processes. While the initial roughness and waviness of the surface of most AM parts are very high, to achieve dimensional accuracy and minimize roughness, a high input energy density is required during machining and polishing processes although such high energy density may induce process defects and escalate the phenomenon of wavelength asperities. In this paper, we proposed a systematic approach to eliminate waviness and reduce surface roughness with the combination of laser-aided machining, macro-polishing, and micro-polishing process. While machining reduces the initial waviness, low energy density during polishing can minimize this further. The average roughness ($R_a = 1.11\mu m$) achieved in this study with optimized process parameters for both machining and polishing demonstrates a greater than 97% reduction in roughness when compared to the as-built part.

Keywords: additive manufacturing; direct energy deposition; aluminum deposition; laser aided machining; macro-polishing; micro-polishing

1. INTRODUCTION

Additive manufacturing (AM) is an emerging manufacturing process applied both in research and industrial fields such as aerospace, biomedical, space, defense, naval, energy sectors, automotive, oil and gas industries, and others [1, 2, 3]. This process can be used for the production of parts with complex geometries that are otherwise difficult to produce using conventional manufacturing processes [4, 5, 6]. The complex, lightweight, and customized parts manufactured by AM process can significantly minimize the consumption of raw materials and improve the competence in real field application. Therefore, AM is increasingly being used in different manufacturing fields. While AM has several advantages over conventional manufacturing processes, parts produced with such process exhibit poor surface roughness and geometric inaccuracy in their as-built state [7, 8, 9, 10]. Several studies have been recently carried out to investigate the factors for dimensional inaccuracy and poor surface quality of metal AM parts. Surface tension associated with temperature gradients of the melt pool can cause rapid hydrodynamic motions known as Marangoni flow, resulting in the dishing or humping [11, 12]. Balling of material caused by long thin melt pools degrade surface roughness [13, 14, 15]. Another process phenomenon degrading the surface quality of AM parts is the staircase effect, which is the result of layer-wise approximation of part geometry [16]. Fabrication process parameters also influence the surface roughness. High energy density helps reducing top and side surface roughness while repetitive laser melting and slow scan speed increases side surface roughness but decreases top surface roughness [17, 18]. Partially fused powder particles are also a common cause of high surface roughness in AM parts [19]. Due to all these factors mentioned above,

achieving an admissible range of surface roughness and geometric dimension and tolerance (GD&T) is very difficult in AM process. Therefore, post-processing especially surface treatment is required to qualify AM parts for final applications.

In most applications especially for the usages critical to fatigue [20], post-fabrication surface treatments such as machining, grinding, and polishing are preferred for AM metal parts. Conventional machining and polishing processes are usually employed to improve the part surface finish and bringing it within GD&T. Spierings et al. [21] utilized CNC lathe to finish AISI 316 and 15-5 HP steels parts built with AM techniques and improved the fatigue performance of the parts. Taminger et al. [22] applied high-speed milling (HSM) to finish AM aluminum parts and evaluated the effectiveness of the different surface finishing techniques to achieve a smooth surface finish. Löber et al. [23] reduced the as-built surface roughness of AISI 316L steel parts using different surface treatment processes such as grinding, sandblasting, and electrolytic and plasma polishing. They also compared and quantified the change in surface roughness after different surface treatments. Beauchamp et al. [24] introduced a novel shape-adaptive grinding process to finish AM Ti6Al4V parts and smoothed down the surface to less than 10 nm average roughness from 4 to 5 μm. Flynn et al. [25] implemented a hybrid manufacturing system by combining additive and subtractive methods to mitigate surface roughness.

Besides conventional surface quality improvement processes, laser aided machining and polishing (LAMP) can also be an effective method to achieve dimensional accuracy and minimize roughness [26, 27, 28, 29, 30]. LAMP offers a high processing rate, minimum heat-affected zone (HAZ), and easily adjustable process parameters [31, 32]. This method can also repair cracks and pores, ablate metallic globules, and improve the fatigue performance of AM materials [33, 34]. LAMP technique is also advantageous over commonly used processes since the size of the tools used in conventional methods for machining and polishing has limitations to reach critical locations. Additionally, while a hybrid manufacturing process combined with AM system makes the entire process unwieldy and

complicated, LAMP can be easily integrated with any existing laser-enabled AM process. Among different AM techniques available i.e. selective laser melting (SLM), electron beam melting (EBM), powder fed and wire fed direct energy deposition (DED), laser aided SLM and DED process are very popular methods to fabricate ferrous and nonferrous materials. Toward improving the surface finish and obtaining GD&T for AM parts, by utilizing the same laser employed to fabricate AM parts, surface roughness can be improved in the same build chamber or machine.

Toward modeling and developing the LAMP process and investigating the effect of this process on mechanical properties of AM materials, several studies have recently been carried out [35, 36, 37, 38, 39, 40, 41, 42, 43, 44, 45, 46]. Chow et al. [47] demonstrated the application of pulsed laser (PL) for both micro-milling and micro-polishing processes by changing the focal offset distance between the laser focus and the part surface. Perry et al. [48] investigated the effect of laser pulse duration and feed rate variation on surface polishing. Ramos et al. [49] studied the effect of shallow surface melting and surface over melting on the laser polishing process. Schneider et al. [50] discussed the general properties of PL machining relevant to solid-state physics such as the initial ablation process and the formation and properties of the plume. Brown et al. [51] performed a fundamental study on laser metal interaction and its application to surface modification without altering the part geometry. Marimuthu et al. [32] developed a numerical model based on a computational fluid dynamic formulation to understand the melt pool dynamics during laser polishing. They identified the input thermal energy as the key parameter affecting melt pool convection and controlling the surface quality. Rosa et al. [52] proposed a quadratic model taking into account the initial surface topography and polishing process parameters. Using the model, they predicted the polished surface quality and also experimentally determined the optimal parameters for polishing. Chen et al. [53] investigated the formation of bulge structure during laser polishing and the influence of processing parameters on the bulge structure

through parametric analyses. Yung et al. [54] made use of PL to polish complex geometries i.e. convex, concave, and slant geometries made of AM CoCr alloy and achieved 93% reduction in surface roughness with 8% hardness enhancement.

While PL has been reported to be applied for LAMP mostly, several researchers also employed continuous wave (CW) lasers alone or combined with PL and demonstrated improvement in surface roughness [40, 55, 56]. Solheid et al. [57] investigated the effect of using CW laser and PL on improving the surface roughness of AM 18Ni (300 grade) Maraging steel. A stable melt pool with fine surface finishing was observed for PL polishing at low power and low speed, while a significant improvement in surface quality was achieved with CW laser at high scan speed and laser power. By utilizing both CW laser and PL together, Nüsser et al. [58] deployed a dual beam technology for surface polishing. CW laser was used for preheating the surface and PL polished the preheated surface. The dual-beam polishing process demonstrated a higher reduction in surface roughness in comparison to the conventional laser polishing process. Caggiano et al. [59] introduced an innovative laser polishing process implementing wobble amplitude pattern during polishing and applied convolutional neural network (CNN) based artificial intelligence technique on polished surface images to identify optimal process parameters for polishing.

In previous studies, while different techniques and methods have been presented using both CW laser and/or PL for the laser aided polishing process [26, 27, 28, 29, 30, 47, 48, 59], further investigation is required to come up with a comprehensive and combined process while selecting the scan patterns and types of lasers for machining and polishing AM materials using lasers. In this study, we proposed a unique laser aided machining and polishing (LAMP) process with the combination of CW laser, pulsed laser, and a novel scan pattern that emulates end mill of different sizes while machining and fine polishing the material. For the LAMP process, the Scalmalloy aluminum alloy was fabricated using

the DED process and the process parameters were optimized in each step of machining (micro-milling) and polishing (macro-polishing and micro-polishing) to reduce the surface roughness and improve the surface quality of the material.

2. MATERIALS AND METHODS

2.1. MATERIALS

The material used in this study was Ar gas atomized aluminum alloy powder referred to as Scalmalloy purchased from APWORKS GmbH (Taufkirchen 82024, Germany). The powder was sieved to a particle size of 105 μm for powder fed DED process. Scalmalloy is a high-strength lightweight alloy widely used in AM process for aluminum deposition [60, 61, 62]. The material also exhibits excellent corrosion resistance. Because of its wide range of applications in robotics, aerospace, marine, and automotive industries, the material was chosen in this study. The chemical composition of the material is presented in Table 1.

2.2. METHODOLOGY

2.2.1. Experimental Setup. LAMP technique is advantageous over conventional machining and polishing processes because of the flexibility of integration with any existing laser enabled AM process. Additionally, the laser used for material deposition can also be employed for the LAMP process. Figure 1 shows the experimental setup designed and developed for this study. The LAMP system integrated with a powder-fed DED process

Table 1. Chemical composition of Scalmalloy powder particles in weight percentage (wt%).

Element	Al	Mg	Sc	Zr	Mn	Si	Fe	Zn	Cu	Ti	O	V
wt.%	bal.	4.00-4.90	0.60-0.80	0.20-0.50	0.30-0.80	<0.40	<0.40	<0.25	<0.10	<0.15	<0.05	<0.05

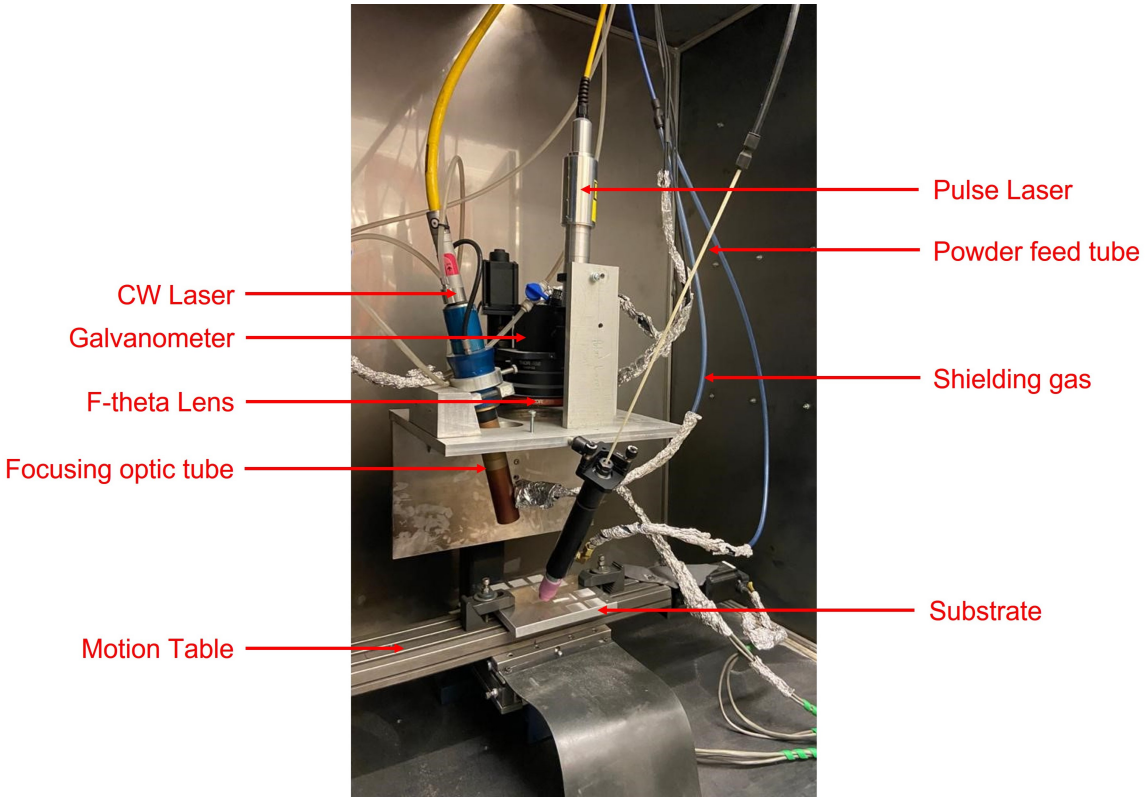

Figure 1. Experimental setup used in this study for direct energy deposition (DED) and laser aided machining and polishing (LAMP) processes.

consists of a stepper motor-driven gantry, a CW high power (2 KW) laser, a low power (100 W) PL, a galvanometer, an F-theta scan lens, and a servo-controlled powder feeder. In this paper, material deposition and macro-polishing were carried out with CW laser while PL was used for machining and micro-polishing processes. The CW laser was focused using a 200 mm focal length focusing optics. A 2-Axis scanning Galvanometer (GVS312) from Thorlabs combined with FTH254 F-Theta scanning lens was used for PL scanning. The effective focal length of the F-Theta lens was 254mm. A two-channel arbitrary signal generator (SDG2042X) from SIGLENT Technologies North America, Inc (Solon, Ohio 44139, USA) was used to generate a true waveform shape for PL scanning. The powder was fed using the X2W powder feeder from Powder Motions Labs (Rolla, Missouri 65401, USA) and focused on using an in-house custom-designed nozzle with a ceramic tube. The

standoff distance between the workpiece and the nozzle was kept at 12.5 mm for effective powder catchment. Argon gas was supplied as the shielding gas for the environment and the CW laser and carrier gas for the powder supply. All the hardware and peripherals were connected together with a LinuxCNC operating system to develop the hybrid manufacturing system integrated for AM and LAMP processes.

2.2.2. Fabrication. Aluminum is a highly reflective and thermally conductive material for any laser-enabled AM process. Therefore, a high-power TeraBlade-2000 direct-diode 949-1001 nm wavelength CW laser (TeraDiode, a Panasonic company, Wilmington, MA 01887, USA) was used in this study to fabricate Scalmalloy. Laser enabled AM process can be classified into three categories such as powder bed SLM, powder-fed DED, and wire-fed DED. In all these processes, the surface exhibits a waviness profile and roughness. The surface roughness and waviness are defined by ASME B46.1 [31, 63] as low frequency and high-frequency components, respectively. The surface roughness depends on the input energy density applied to fabricate the material. Poor energy density choices during deposition yields material defects that mimic bulge-like structures on the surface and increase the surface roughness [53] while high wavelength surface features (Waviness) exist on the surface of AM parts because of the layer width and thickness. These features are especially high in the DED process, where the beam size is larger compared to the SLM process beam size, and the track overlap leads to a wavy surface pattern. Therefore, in this study, the powder-fed DED process was employed with no raster rotation to obtain initially high surface roughness after deposition. Figure 2 (a) exhibits the schematic representation of the raster pattern used for material deposition. The fabrication process parameters used to deposit Scalmalloy is listed in Table 2. Based on the design of experiments, a total of 44 rectangular patches with dimensions of 27 mm $\times$ 27 mm $\times$ 1 mm were deposited to obtain optimized LAMP process parameters for good surface quality. All the samples were deposited on 5000 series aluminum alloy substrate (152.4 mm $\times$ 152.4 mm $\times$ 12.7 mm). Among 44 rectangular deposits, 12 samples were used for the machining process

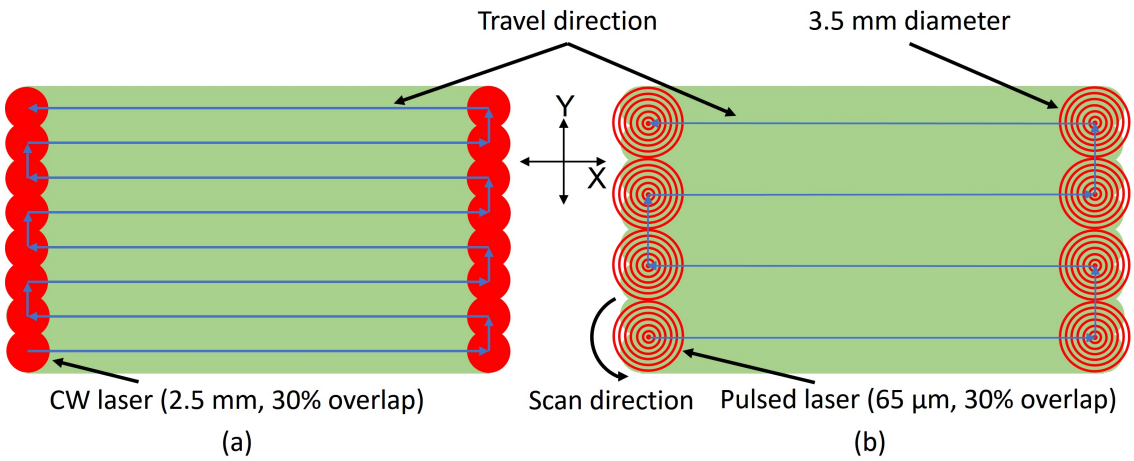

Figure 2. Schematic representation of the CW laser scan pattern for material deposition and macro-polishing and pulsed laser scan pattern for machining and micro-polishing.

while half of the remaining samples were used for macro-polishing and the rest for the micro-polishing process. Figure 3 (a) shows the first 12 samples deposited and used for optimizing the machining process.

2.2.3. Machining. In the laser-aided polishing process, the top surface of an AM part is remelted and the material is redistributed from peaks of the surface to the valleys because of surface tension and gravity [64, 65]. However, laser polishing alone cannot get rid of certain surface features with high wavelengths. A machining process before polishing can help to minimize high wavelength surface waviness. In order to ablate materials, the laser machining process may require high input energy, but higher input energy can originate additional wavy features because of the mass transport of the fluid flow in the melting pool.

Table 2. Fabrication process parameters used to deposit Scalmalloy.

Parameters	**Laser power** (W)	**Travel speed** (mm/min)	**Layer width** (mm)	**Layer thickness** (mm)	**Overlap between tracks** (%)	**Raster rotation rotation** (degree)	**Powder flow rate** (g/min)	**Shield gas flow rate** (L/min)
Value	1600	500	2.5	0.300	30	0	6	4

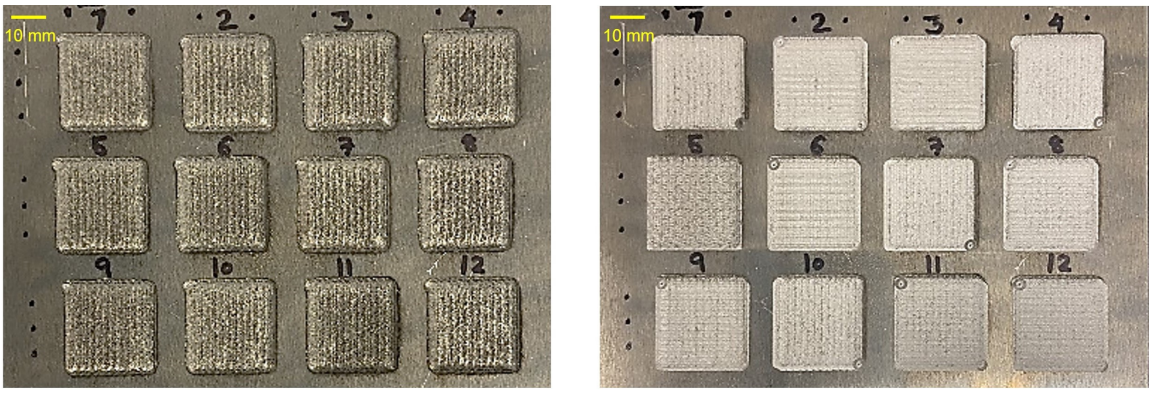

(a) (b)

Figure 3. Top view of Scalmalloy samples from #1 to #12 deposited with process parameters mentioned in Table 2 and machined with different process parameters presented in Table 3.

Therefore, we proposed a unique laser-enabled machining process that utilizes low input energy density to ablate materials. In this study, we introduced a novel PL scan pattern. Figure 2 (b) shows the schematic representation of the scan pattern and its travel direction used during machining cycles. The overall diameter of the scan pattern was set at 3.5 mm which is twice the layer width including hatch spacing during material deposition. This pattern is a modified version of the wobbling scan pattern introduced by Caggiano et al. [59]. The unique feature of this pattern is that while machining the top surface of the deposited samples, the pattern emulates end mills of multiple sizes commonly used in the CNC milling process. In such a way, these patterns offer a high processing rate with low thermal energy input during machining. The number of laser scanning passes on the top surface of the material depends on the scan speed, travel speed, total diameter of the scan, laser spot size, and the sum of the circumference of the scan pattern. Equation 1 was derived to calculate the number of passes per mm during PL scanning,

$$PPM = \frac{S_S}{S_T} \times \frac{2 \times N_C}{L_S} \tag{1}$$

where, S_S, S_T, PPM, N_C, and L_S are the scan speed, travel speed, number of laser scan passes per mm, number of circles in scan pattern, and total length PL scans in the pattern, respectively. The scan length is the sum of the circumference circles in a scan pattern given by Equation 2,

$$L_S = 2 \times \pi \times \sum_{i=0}^{N_C-1} (R - i \times r \times (1 - O_p)) \tag{2}$$

where, R and r are the radius of the scan pattern and laser spot size, respectively. O_p is the overlap. Number of circles in the scan pattern can be calculated using Equation 3.

$$N_C = \frac{R}{r \times (1 - O_p)} \tag{3}$$

In this study, a 100 W PL (YLP-V2, IPG Photonics, Oxford, MA 01540, USA) with 1055-1075 nm wavelength, 100 ns pulse duration, and 5 kHz frequency was used for the machining process. The depth of focus and spot size of the PL were $400\mu m$ and $65\mu m$, respectively. Figure 4 (a) shows the focal offset distance used for the machining process in this study. While the PL operates within the depth of focus, it ablates material acting like a machining process. In this work, the PL power and scanning speed were fixed at 100 W and 30 m/min, respectively, while varying the travel speed, the input energy density was changed for different experiments. A design of experiment presented in Table 3 was constructed to obtain the optimal process parameters for roughness and material removed by the machining process. While the laser power and scan speed was kept constant, the travel speed was varied from 150 mm/min to 375 mm/min with 75 mm/min increment. Since the low input energy density was used during polishing, the number of machining cycles was also varied in the experimental design. The first and third machining cycles were traveled along the X-axis while for the second and fourth cycles, the direction was set to travel along Y-axis. Among 44 deposited samples, the first 12 samples were used to obtain the optimal machining process parameters for surface roughness and material removal determination. Figure 3 (b) demonstrates the top surface texture of samples #1 to #12 after machining with

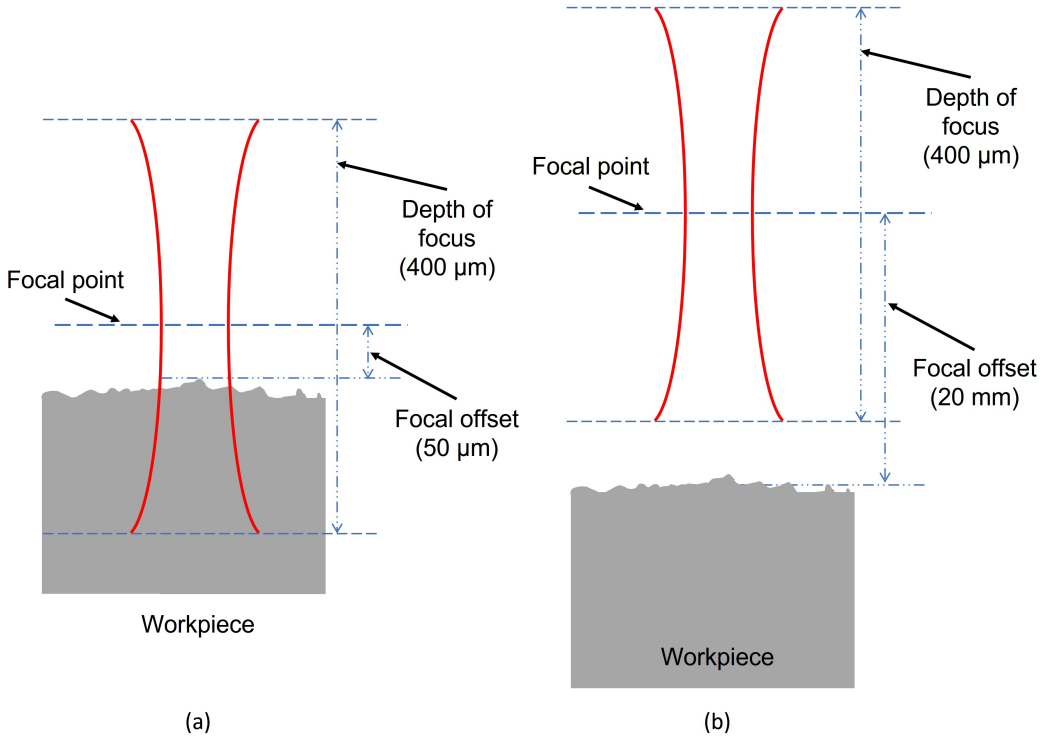

Figure 4. Schematic representation of the pulsed laser focal offset distance used for machining and micro-polishing.

different process parameters. Samples (#1, #4, #7, and #10) were machined for 1 cycle only with comparatively low input energy density. Therefore, the initial deposition hatching

Table 3. Design of experiments for the machining process of Scalmalloy samples #1 to #12.

Sample no.	**1**	**2**	**3**	**4**	**5**	**6**	**7**	**8**	**9**	**10**	**11**	**12**
Travel speed (mm/min)	150	150	150	225	225	225	300	300	300	375	375	375
Number of cycles	1	2	4	1	2	4	1	2	4	1	2	4
Number of scan passes per mm	72	144	288	48	96	192	36	72	144	29	58	116

pattern remains visible even after machining. The rest of the samples machined for 2 or 4 cycles depict the hatching pattern due to the machining process as we can see the pattern in both directions.

2.2.4. Polishing. Macro-polishing: Based on the previous study conducted by Ramos et al. [49] while investigating the effect of shallow surface melting and surface over melting during laser polishing, the process can be classified into two main categories, termed macro-polishing and micro-polishing. The difference between these two categories is primarily defined by the depth of the molten layer, which could be either "deep" or "shallow" with respect to the height of the asperities. The macro-polishing process can be used to polish the surface roughly, while micro-polishing can smooth the roughly polished surface. For the macro-polishing process in this study, the CW laser was used. During the polishing process, the CW laser power was varied from 1000 W to 1600 W with 200 W increment and the travel speed was varied from 300 to 750 mm/min. While the focal offset distance of CW laser and scan pattern for the macro-polishing process remained identical to the deposition offset distance and scan pattern, unlike the scanning deposition direction, the surface was scanned along Y-axis during macro-polishing. Table 4 represents different process parameters used for rough polishing the top surface of the sample #13 to #28. Before the polishing process, the samples were deposited and machined with optimal process parameters obtained from the laser-aided machining process. After macro-polishing, the surface roughness of each sample was measured and the optimal process parameters for the macro-polishing process were derived by analyzing the results.

Table 4. Different process parameters used for the macro-polishing of samples #13 to #28.

Sample no.	**13**	**14**	**15**	**16**	**17**	**18**	**19**	**20**	**21**	**22**	**23**	**24**	**25**	**26**	**27**	**28**
Travel speed (mm/min)	300	300	300	300	450	450	450	450	600	600	600	600	750	750	750	750
CW Laser power (W)	1000	1200	1400	1600	1000	1200	1400	1600	1000	1200	1400	1600	1000	1200	1400	1600

Micro-polishing: After obtaining the optimized process parameters for the machining and macro-polishing processes, samples #29 to #44 were deposited, machined, and roughly polished with the resultant process parameters to prepare the samples for further polishing process. An additional surface finishing process named micro-polishing was introduced in this study to fine finish the surface of the roughly finished part. The PL and scan pattern (shown in Figure 2 (b)) implemented in the machining process were also used for the micro-polishing process. Compared to the machining process, the travel speed, laser power, and focal offset distance were varied. While the scanning speed was equal to the speed used for the machining process, during micro-polishing, the focal offset distance of the PL was set at 20 mm as shown in Figure 4 (b). The PL power was varied from 40 to 100 W with a 20 W increment and the travel speed was changed from 300 to 750 mm/min with 150 mm/min increment in each step. Table 5 represents different process parameters used for micro-polishing process.

After the final polishing process, the surface roughness of the samples was measured to obtain the optimal process parameters for the micro-polishing process. Figure 5 (a) and (b) exhibit the surface texture of samples after final polishing process.

Table 5. Different process parameters used for the micro-polishing of sample #29 to #44.

Sample no.	**29**	**30**	**31**	**32**	**33**	**34**	**35**	**36**	**37**	**38**	**39**	**40**	**41**	**42**	**43**	**44**
Travel speed (mm/min)	300	300	300	300	450	450	450	450	600	600	600	600	750	750	750	750
Pulsed Laser power (W)	40	60	80	100	40	60	80	100	40	60	80	100	40	60	80	100

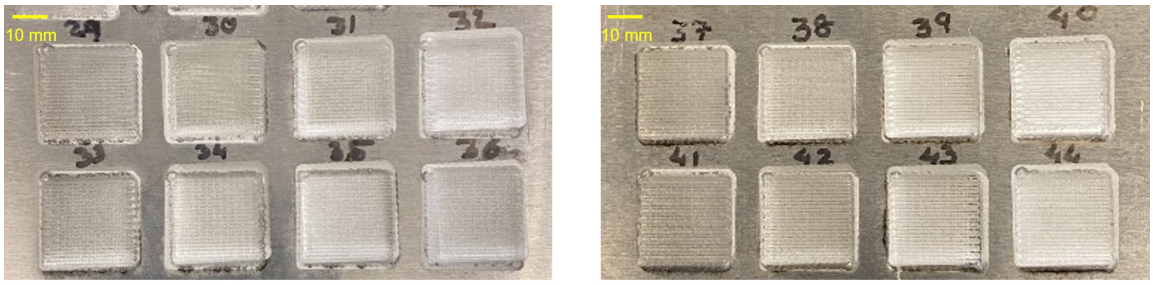

(a) (b)

Figure 5. Surface texture of samples #29 to #36 and #37 to #44 after micro-polishing process

2.3. SURFACE ROUGHNESS MEASUREMENT

In this study, a high-speed non-contact laser displacement sensor (Keyence LK-H052) with $0.025\mu m$ repeatability and $50\mu m$ spot size was used for surface scanning to determine the roughness of the as-built samples and materials removed after the machining process. The as-built samples had a very high roughness as shown in Figure 3 (a) and measuring the roughness using a surface profilometer may damage the touch probe. Therefore, the laser displacement sensor was employed. To scan the surface of the samples, the laser displacement sensor was mounted on the tool holder of a CNC milling machine. A point on the surface of the substrate was fixed as the reference point for scanning the surface both before and after the machining process. A CNC program for raster patterns with $50\mu m$ increment was written to automate the scanning process. The data acquisition rate for the sensor and the scan speed for the motion table were set for 1000 samples/sec and 1.25 mm/sec, respectively.

The common practice of laser line scanning is along one direction only. The average of the roughness remains the same regardless of the scanning direction. In this study, the as-built samples were scanned along the Y-axis of the deposition. Later, the data were processed to determine the surface roughness. The average roughness (Ra) was calculated according to the ASME B46.1 standard using the following Equation 4,

$$R_a = \frac{1}{n}\sum_{i=1}^{n} |Z_i - Z_{mean}| \tag{4}$$

where, n, i, and Z are the number of total data points, the data number, and the height measured. respectively. We also scanned a few surfaces along X-axis and compared them with the results obtained from Y-axis scanned. No significant difference was observed since Equation 4 uses millions of scan points and averaging them yields no significant difference. In this study, the laser scanning process was used for the as-built and machined surfaces while a surface profilometer (Mitutoyo Surftest-212) was utilized to measure the surface roughness after the macro-polishing and micro-polishing processes.

3. RESULTS AND DISCUSSION

The LAMP process is a three-step surface treatment method. Machining, macro-polishing, and micro-polishing together can yield a surface with significantly low roughness. While machining ablates some materials from the top surface to minimize high wavelength surface features (waviness), macro polishing and micro-polishing can do the rough and fine polishing of the surface, respectively. During the machining process with different process parameters, this is very important to determine the materials ablated due to laser-aided machining. In this study, while the PL power was kept constant to maintain a consistent Gaussian beam profile for the laser while the travel speed and number of cycles were varied according to the design of experiments. Figure 6 (a) shows the average material removed at different machining cycles with varying travel speed. This is obvious that the average material removed in laser-aided machining process decreases exponentially with the travel speed at different machining cycles while the average material removed increases linearly with the number of cycles at different travel speed (shown in Figure 6 (b)). Therefore, the

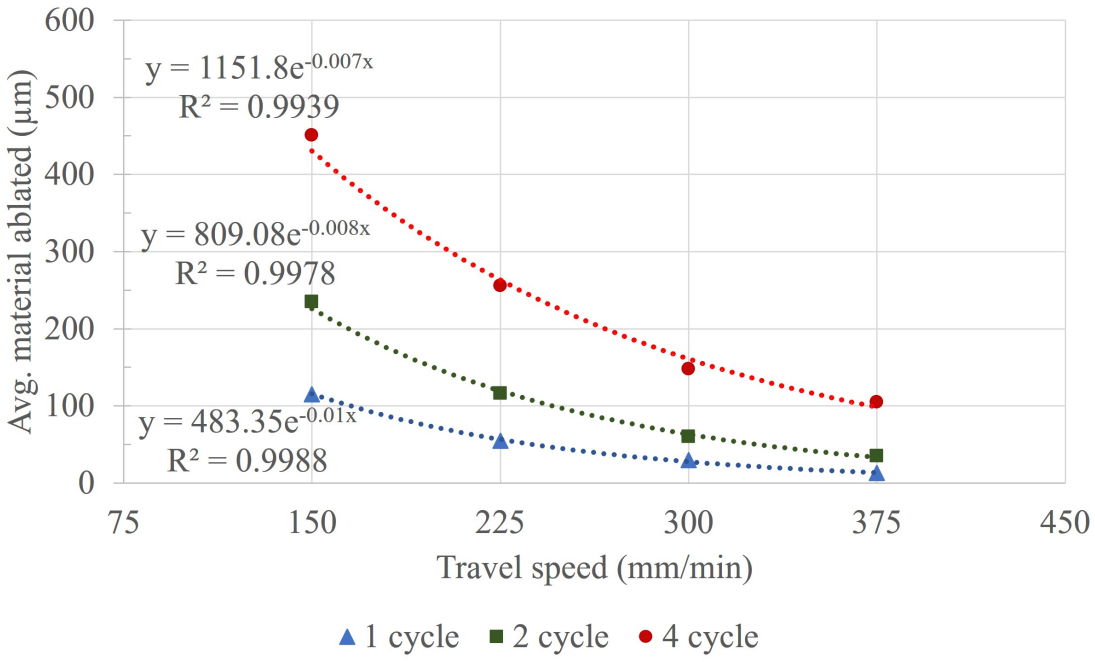

(a)

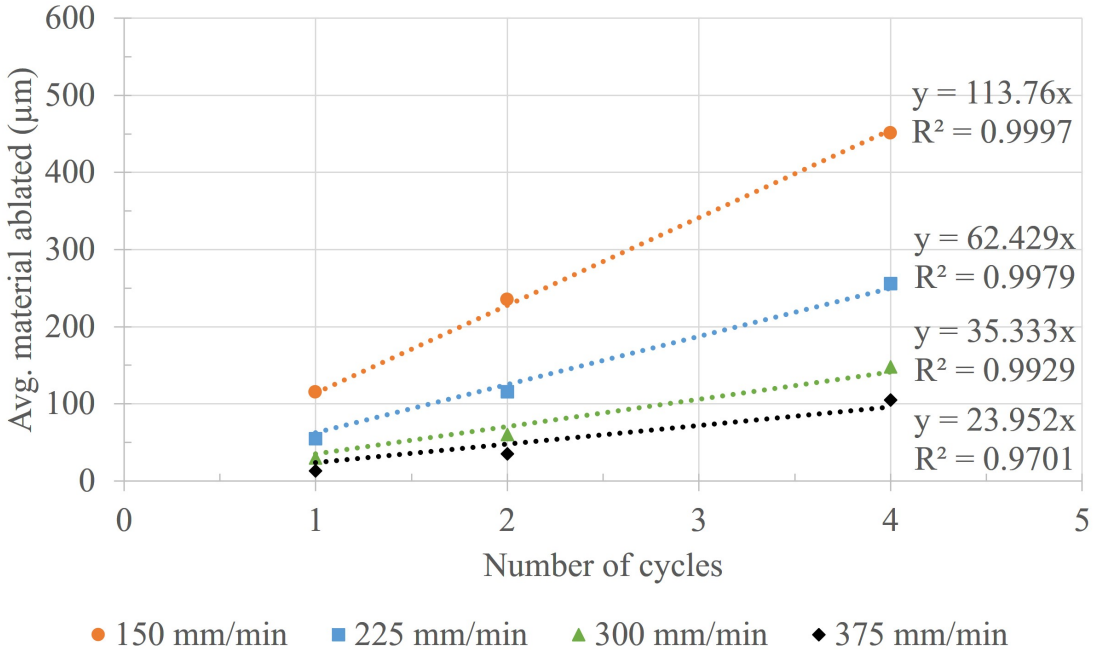

(b)

Figure 6. Average materials removed due to machining process at different travel speed and machining cycles.

average material removed can be expressed as Equation 5,

$$R_m = K \times N^{\alpha} \times e^{-\beta S} \tag{5}$$

where, R_m, N, S are the average material removed, number of machining cycles, and travel speed of the motion table, respectively, while K, α, and β are the coefficients assumed to be dependent on the material and laser properties. To determine the values of the coefficients in Equation 5 and predict the material removed based on the number of machining cycles and travel speed, a multiple linear regression analysis was performed on Equation 6 using the experimental results. A significant regression (Equation 7) was found with ($F(2, 9) = 308.537, p < 5.12 \times 10^{-9}$) and an $R^2 = 0.986$. This is evident that both the number of machining cycles and travel speed were significant to predict the material removed in the laser-aided machining process.

$$\ln R_m = K + \alpha \ln N + \beta \ln S \tag{6}$$

$$R_m = 0.927 \times N^{1.188} \times e^{-0.0036S} \tag{7}$$

The powder-fed DED parts initially exhibit a high surface roughness due to both the high and low wavelength surface characteristics. The surface roughness (R_a) of all the as-built samples in this study was more than $40\mu m$ on average. The machining process reduces the surface roughness by ablating some materials from the top surface and minimizes the waviness. Figure 7 shows the surface roughness of the samples machined at different travel speeds with varying numbers of cycles.

While the 4-cycle machining ablates a comparatively consistent amount of material following the mathematical model, the surface roughness increases while compared with the roughness achieved with 2 cycles. In conventional polishing processes, achieving an optimal roughness, over polishing increases the roughness of the surface instead of

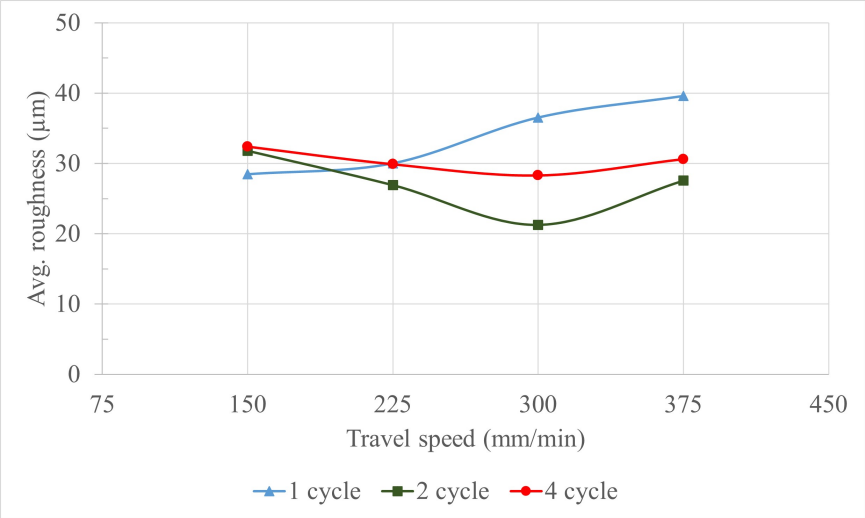

Figure 7. Average surface roughness of samples #1 to #12 after machining process.

decreasing. While a material is overly polished by an abrasive material, the polishing process creates additional peaks and valleys on the surface worsening the surface quality. In laser aided machining, repetitive laser melting or ablation may also create additional peaks and valleys due to the surface tension associated with the temperature gradient of repetitive laser remelting. The objective of these experiments was to determine the machining process parameters with minimal material removal but maximum surface roughness reduction. No significant surface roughness reduction was observed at the highest speed (375 mm/min) for the unit machining cycle though as the speed decreases, the roughness reduction increases. This is because the input energy density increases with the decreasing speed. The effect of the number of machining cycles shows that 2 cycle machining (both X and Y directions) exhibits improved surface quality at different speeds than 4 cycle machining. Additionally, 2 cycle machining ablates fewer materials than 4 cycle machining. Therefore, 2 cycle machining at 300 mm/min speed was chosen as the optimized machining process parameters. Later, these parameters were used to machine samples #13 to #44.

After machining, a reduction in surface roughness was observed. To further improve the surface quality, macro-polishing was performed using the CW laser at different power and travel speed. The surface roughness of samples #13 to #28 is shown in Figure 8. At all different laser powers, the surface roughness was reduced but a more than 90% reduction in roughness between machining and macro-polishing processes was observed between 450 and 600 mm/min speed and 1200 W laser power. Therefore, 500 mm/min travel speed with 1200 W power were selected as the optimized process parameters for the macro-polishing process.

While macro-polishing reduces the surface roughness mostly in the entire LAMP process, the micro-polishing process was implemented in this study for further smoothing the surface quality after the macro-polishing process. Figure 9 illustrates the roughness after micro-polishing the samples with different process parameters. Prior to implementing this process, all the samples were machined and macro-polished using the optimized parameters determined in this study. Increasing the scanning speed during fine polishing the surface did not help much in improving the surface quality since the laser could not originate a significant melt pool to polish the surface at higher speeds. As the PL power increases,

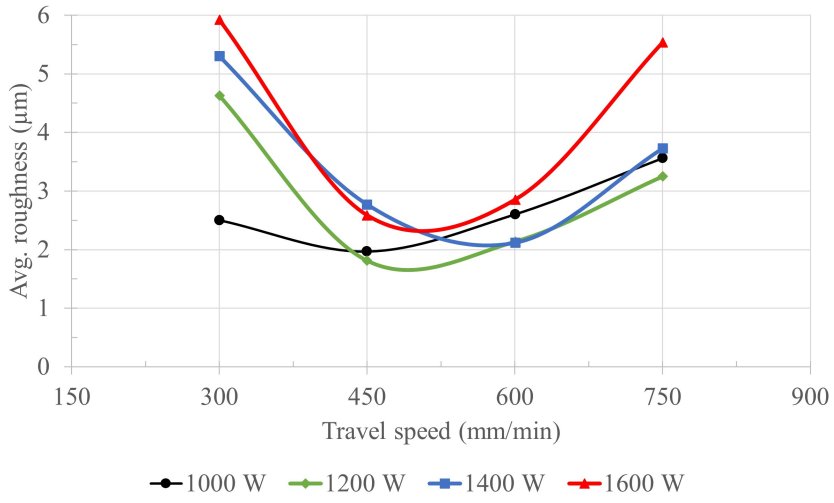

Figure 8. Average surface roughness of samples #13 to #28 after macro-polishing process.

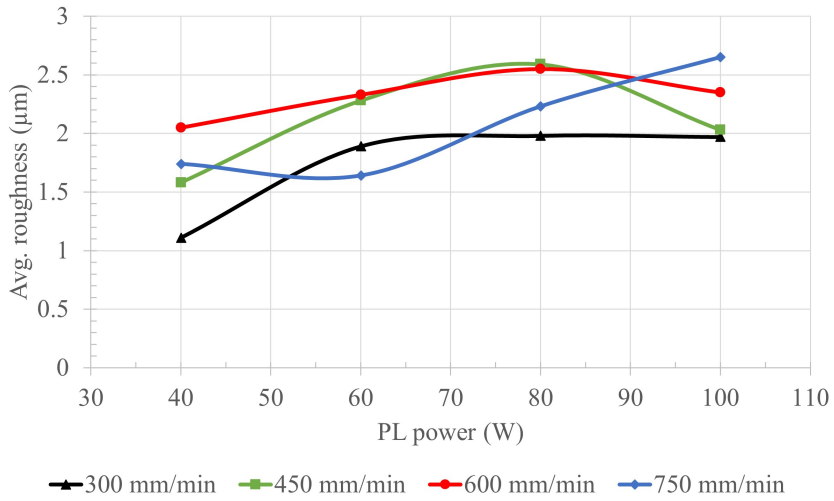

Figure 9. Average surface roughness of the samples #29 to #44 after micro-polishing process.

no significant improvement in surface quality was observed because increasing the laser power increases the melt pool depth and as a result creates additional roughness due to high energy input. A reduction in surface roughness was noticed only for 40 W PL power at all different speeds but the travel speed of 300 mm/min shows the highest improvement in surface quality. Though parameters for sample #29 show the nominal surface quality improvement within the boundary of the experimental design, The band of the process parameters chosen in this study does not confine the lower boundary of the parameters for optimal surface quality. As a future study, a new experimental design covering a wide range of PL power and higher scan speed can help to obtain optimized process parameters for improved surface quality.

For further investigation, to demonstrate the effectiveness of machining prior to polishing, an additional sample was deposited and polished with optimized parameters without machining. Figure 10 (a), (b), and (c) illustrate the line scanned surface profile of the as-built, LAMP processed, and polished sample. The as-built sample surface (shown in Figure 10 (a)) shows both the high and low waviness in surface topography while the LAMP processed surface in Figure 10 (b) demonstrates the least waviness compared to the

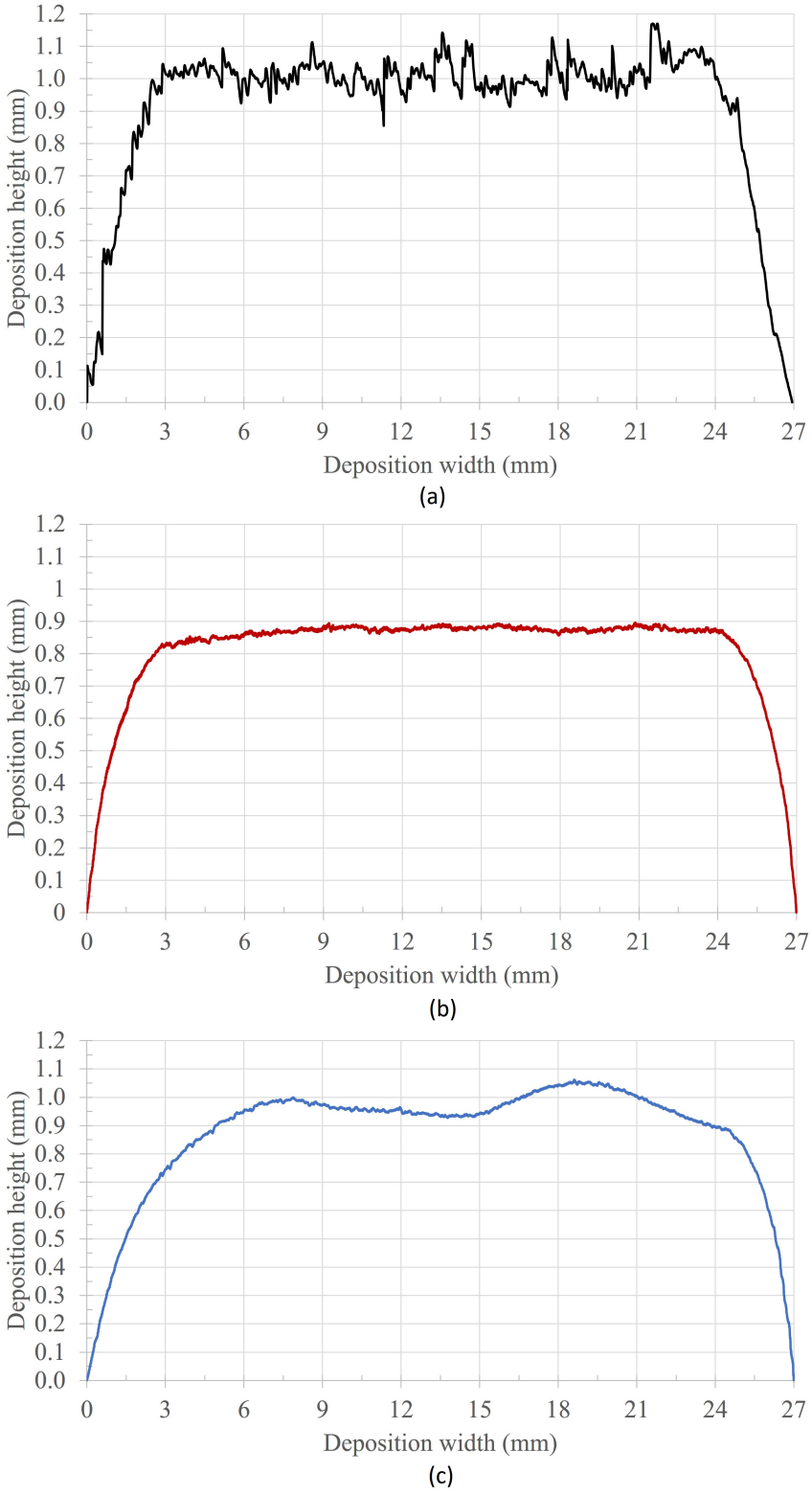

Figure 10. Surface profile (scanned line along Y axis) of as-built sample, sample machined and polished with optimized process parameters, and sample not machined but polished with optimized process parameters.

polished surface illustrated in Figure 10 (c). Therefore, the LAMP process (combination of laser-aided machining, macro-polishing, and micro-polishing) can be an effective method for improving the surface quality of AM metals due to minimizing the surface waviness and roughness and achieving an overall surface quality improvement of more than 97% when compared to the as-built part.

Due to the limitation in the degree of freedom of the CNC motion table, in this study, the LAMP process was applied only on the XY (horizontal) plane of the deposited materials. But a five-axis machine or a robotic AM system can facilitate the process with the advantage of machining and polishing at different planes as well.

4. CONCLUSION

AM metal parts exhibit a high surface roughness. To improve the surface quality of AM materials, post-processing is required. In this paper, we proposed a laser-aided machining and polishing process to reduce the surface roughness of AM metals. The conclusion of this research work can be summarized as follows.

- In this study, multiple lasers were integrated together for fabrication, machining, and polishing of AM materials in the same build chamber. A unique scan pattern was also introduced to implement low energy input for machining and polishing of metals. A two-step polishing process using CW and pulsed laser was employed for rough and fine polishing.

- A systematic approach was discussed and implemented to obtain optimal process parameters for machining and polishing of AM aluminum alloy. A regression analysis was performed, and a mathematical model was derived from the experimental results to predict the material removed during the machining process.

- The roughness and waviness in the surface topography were minimized using the combined machining and polishing process and a more than 97% improvement in surface quality was achieved.

Future works may include implementing the process to obtain geometric dimension and tolerances (GD&T) for custom parts, applying the method for other AM processes, materials, and alloys. The influence of the laser-aided machining and polishing process on the microstructure and mechanical properties such as hardness, corrosion resistance, and fatigue performance can also be a part of future studies.

ACKNOWLEDGEMENT

This research was supported by National Science Foundation Grants CMMI-1625736 and EEC 1937128. Part of the work was also funded by the Department of Energy's Kansas City National Security Campus which is operated and managed by Honeywell Federal Manufacturing Technologies, LLC under contract number DE-NA0002839, Intelligent Systems Center, and Material Research Center at Missouri University of Science and Technology. Their support is greatly appreciated.

REFERENCES

[1] Y. Zhang, L. Wu, X. Guo, S. Kane, Y. Deng, Y.-G. Jung, J.-H. Lee, and J. Zhang, "Additive manufacturing of metallic materials: a review," *Journal of Materials Engineering and Performance*, vol. 27, no. 1, pp. 1–13, 2018.

[2] W. E. Frazier, "Metal additive manufacturing: a review," *Journal of Materials Engineering and Performance*, vol. 23, no. 6, pp. 1917–1928, 2014.

[3] J. J. Lewandowski and M. Seifi, "Metal additive manufacturing: a review of mechanical properties," *Annual Review of Materials Research*, vol. 46, pp. 151–186, 2016.

[4] I. Gibson, D. Rosen, B. Stucker, and M. Khorasani, "Design for additive manufacturing," in *Additive manufacturing technologies*, pp. 555–607, Springer, 2021.

[5] K. V. Wong and A. Hernandez, "A review of additive manufacturing," *International scholarly research notices*, vol. 2012, 2012.

[6] M. Parvez, Y. Chen, J. Newkirk, and F. Liou, "Comparison of fatigue performance between additively manufactured and wrought 304l stainless steel using a novel fatigue test setup," *Proceedings of the Solid Freeform Fabrication*, pp. 353–363, 2019.

[7] J. Ramos-Grez and D. Bourell, "Reducing surface roughness of metallic freeform-fabricated parts using non-tactile finishing methods," *International Journal of Materials and Product Technology*, vol. 21, no. 4, pp. 297–316, 2004.

[8] E. Abele and M. Kniepkamp, "Analysis and optimisation of vertical surface roughness in micro selective laser melting," *Surface Topography: Metrology and Properties*, vol. 3, no. 3, p. 034007, 2015.

[9] F. Calignano, D. Manfredi, E. Ambrosio, L. Iuliano, and P. Fino, "Influence of process parameters on surface roughness of aluminum parts produced by dmls," *The International Journal of Advanced Manufacturing Technology*, vol. 67, no. 9-12, pp. 2743–2751, 2013.

[10] M. M. Parvez, T. Pan, Y. Chen, S. Karnati, J. W. Newkirk, and F. Liou, "High cycle fatigue performance of lpbf 304l stainless steel at nominal and optimized parameters," *Materials*, vol. 13, no. 7, p. 1591, 2020.

[11] K. Mills, B. Keene, R. Brooks, and A. Shirali, "Marangoni effects in welding," *Philosophical Transactions of the Royal Society of London. Series A: Mathematical, Physical and Engineering Sciences*, vol. 356, no. 1739, pp. 911–925, 1998.

[12] M. H. Cho and D. F. Farson, "Understanding bead hump formation in gas metal arc welding using a numerical simulation," *Metallurgical and materials transactions B*, vol. 38, no. 2, pp. 305–319, 2007.

[13] C. Hauser, T. Childs, and K. Dalgamo, "Selective laser sintering of stainless steel 314s hc processed using room temperature powder beds," in *1999 International Solid Freeform Fabrication Symposium*, 1999.

[14] F. Klocke and C. Wagner, "Coalescence behaviour of two metallic particles as base mechanism of selective laser sintering," *CIRP Annals*, vol. 52, no. 1, pp. 177–180, 2003.

[15] R. Li, J. Liu, Y. Shi, L. Wang, and W. Jiang, "Balling behavior of stainless steel and nickel powder during selective laser melting process," *The International Journal of Advanced Manufacturing Technology*, vol. 59, no. 9, pp. 1025–1035, 2012.

[16] J.-P. Kruth, B. Vandenbroucke, J. Van Vaerenbergh, and P. Mercelis, "Benchmarking of different sls/slm processes as rapid manufacturing techniques," in *Proceedings of the International Conference Polymers & Moulds Innovations PMI 2005*, 2005.

[17] K. Mumtaz and N. Hopkinson, "Top surface and side roughness of inconel 625 parts processed using selective laser melting," *Rapid Prototyping Journal*, 2009.

[18] G. Strano, L. Hao, R. M. Everson, and K. E. Evans, "Surface roughness analysis, modelling and prediction in selective laser melting," *Journal of Materials Processing Technology*, vol. 213, no. 4, pp. 589–597, 2013.

[19] R. M. Vilar, "Laser cladding," in *ALT'02 International Conference on Advanced Laser Technologies*, vol. 5147, pp. 385–392, International Society for Optics and Photonics, 2003.

[20] M. M. Parvez, Y. Chen, S. Karnati, C. Coward, J. W. Newkirk, and F. Liou, "A displacement controlled fatigue test method for additively manufactured materials," *Applied Sciences*, vol. 9, no. 16, p. 3226, 2019.

[21] A. B. Spierings, T. L. Starr, and K. Wegener, "Fatigue performance of additive manufactured metallic parts," *Rapid prototyping journal*, 2013.

[22] K. Taminger, R. A. Hafley, D. T. Fahringer, and R. E. Martin, "Effect of surface treatments on electron beam freeform fabricated aluminum structures," in *2004 International Solid Freeform Fabrication Symposium*, 2004.

[23] L. Löber, C. Flache, R. Petters, U. Kühn, and J. Eckert, "Comparison of different post processing technologies for slm generated 316l steel parts," *Rapid Prototyping Journal*, 2013.

[24] A. T. Beaucamp, Y. Namba, P. Charlton, S. Jain, and A. A. Graziano, "Finishing of additively manufactured titanium alloy by shape adaptive grinding (sag)," *Surface Topography: Metrology and Properties*, vol. 3, no. 2, p. 024001, 2015.

[25] J. M. Flynn, A. Shokrani, S. T. Newman, and V. Dhokia, "Hybrid additive and subtractive machine tools–research and industrial developments," *International Journal of Machine Tools and Manufacture*, vol. 101, pp. 79–101, 2016.

[26] T. Ermergen and F. Taylan, "Review on surface quality improvement of additively manufactured metals by laser polishing," *Arabian Journal for Science and Engineering*, pp. 1–17, 2021.

[27] A. Krishnan and F. Fang, "Review on mechanism and process of surface polishing using lasers," *Frontiers of Mechanical Engineering*, vol. 14, no. 3, pp. 299–319, 2019.

[28] T. Deng, J. Li, and Z. Zheng, "Fundamental aspects and recent developments in metal surface polishing with energy beam irradiation," *International Journal of Machine Tools and Manufacture*, vol. 148, p. 103472, 2020.

[29] L. Giorleo, E. Ceretti, and C. Giardini, "Ti surface laser polishing: effect of laser path and assist gas," *Procedia Cirp*, vol. 33, pp. 446–451, 2015.

[30] E. V. Bordatchev, A. M. Hafiz, and O. R. Tutunea-Fatan, "Performance of laser polishing in finishing of metallic surfaces," *The International Journal of Advanced Manufacturing Technology*, vol. 73, no. 1-4, pp. 35–52, 2014.

[31] S. Mohajerani, E. V. Bordatchev, and O. R. Tutunea-Fatan, "Recent developments in modeling of laser polishing of metallic materials," *Lasers in Manufacturing and Materials Processing*, vol. 5, no. 4, pp. 395–429, 2018.

[32] S. Marimuthu, A. Triantaphyllou, M. Antar, D. Wimpenny, H. Morton, and M. Beard, "Laser polishing of selective laser melted components," *International Journal of Machine Tools and Manufacture*, vol. 95, pp. 97–104, 2015.

[33] C. Liang, Y. Hu, N. Liu, X. Zou, H. Wang, X. Zhang, Y. Fu, and J. Hu, "Laser polishing of ti6al4v fabricated by selective laser melting," *Metals*, vol. 10, no. 2, p. 191, 2020.

[34] S. Lee, Z. Ahmadi, J. W. Pegues, M. Mahjouri-Samani, and N. Shamsaei, "Laser polishing for improving fatigue performance of additive manufactured ti-6al-4v parts," *Optics & Laser Technology*, vol. 134, p. 106639, 2021.

[35] E. Willenborg, "Polishing with laser radiation," *Kunststoffe international*, vol. 97, no. 6, p. 37, 2007.

[36] T. L. Perry, D. Werschmoeller, X. Li, F. E. Pfefferkorn, and N. A. Duffie, "Micromelting for laser micro polishing of meso/micro metallic components," in *International Manufacturing Science and Engineering Conference*, vol. 42908, pp. 363–369, 2007.

[37] H.-Y. Wang, D. Bourell, and J. Beaman, "Laser polishing of silica slotted rods," *Materials science and technology*, vol. 19, no. 3, pp. 382–387, 2003.

[38] S. Mohajerani, J. D. Miller, O. R. Tutunea-Fatan, and E. V. Bordatchev, "Thermophysical modelling of track width during laser polishing of h13 tool steel," *Procedia Manufacturing*, vol. 10, pp. 708–719, 2017.

[39] S. Vatsya and S. Nikumb, "Modeling of fluid dynamical processes during pulsed-laser texturing of material surfaces," *Physical Review B*, vol. 68, no. 3, p. 035410, 2003.

[40] W. S. Gora, Y. Tian, A. P. Cabo, M. Ardron, R. R. Maier, P. Prangnell, N. J. Weston, and D. P. Hand, "Enhancing surface finish of additively manufactured titanium and cobalt chrome elements using laser based finishing," *Physics Procedia*, vol. 83, pp. 258–263, 2016.

[41] M. Ćwikła, R. Dziedzic, and J. Reiner, "Influence of overlap on surface quality in the laser polishing of 3d printed inconel 718 under the effect of air and argon," *Materials*, vol. 14, no. 6, p. 1479, 2021.

[42] D. Zhang, J. Yu, H. Li, X. Zhou, C. Song, C. Zhang, S. Shen, L. Liu, and C. Dai, "Investigation of laser polishing of four selective laser melting alloy samples," *Applied Sciences*, vol. 10, no. 3, p. 760, 2020.

[43] J. Lambarri, J. Leunda, C. Soriano, and C. Sanz, "Laser surface smoothing of nickel-based superalloys," *Physics Procedia*, vol. 41, pp. 255–265, 2013.

[44] L. Chen and X. Zhang, "Modification the surface quality and mechanical properties by laser polishing of al/pla part manufactured by fused deposition modeling," *Applied Surface Science*, vol. 492, pp. 765–775, 2019.

[45] C. Ma, M. Vadali, N. A. Duffie, F. E. Pfefferkorn, and X. Li, "Melt pool flow and surface evolution during pulsed laser micro polishing of ti6al4v," *Journal of Manufacturing Science and Engineering*, vol. 135, no. 6, 2013.

[46] J. D. Miller, O. R. Tutunea-Fatan, and E. V. Bordatchev, "Experimental analysis of laser and scanner control parameters during laser polishing of h13 steel," *Procedia Manufacturing*, vol. 10, pp. 720–729, 2017.

[47] M. T. Chow, E. V. Bordatchev, and G. K. Knopf, "Experimental study on the effect of varying focal offset distance on laser micropolished surfaces," *The International Journal of Advanced Manufacturing Technology*, vol. 67, no. 9-12, pp. 2607–2617, 2013.

[48] T. L. Perry, D. Werschmoeller, X. Li, F. E. Pfefferkorn, and N. A. Duffie, "The effect of laser pulse duration and feed rate on pulsed laser polishing of microfabricated nickel samples," *Journal of manufacturing science and engineering*, vol. 131, no. 3, 2009.

[49] J. Ramos, D. Bourell, and J. Beaman, "Surface over-melt during laser polishing of indirect-sls metal parts," *MRS Online Proceedings Library (OPL)*, vol. 758, 2002.

[50] C. W. Schneider and T. Lippert, "Laser ablation and thin film deposition," in *Laser processing of materials*, pp. 89–112, Springer, 2010.

[51] M. S. Brown and C. B. Arnold, "Fundamentals of laser-material interaction and application to multiscale surface modification," in *Laser precision microfabrication*, pp. 91–120, Springer, 2010.

[52] B. Rosa, J. Y. Hascoet, and P. Mognol, "Modeling and optimization of laser polishing process," in *Applied Mechanics and Materials*, vol. 575, pp. 766–770, Trans Tech Publ, 2014.

[53] C. Chen and H.-L. Tsai, "Fundamental study of the bulge structure generated in laser polishing process," *Optics and Lasers in Engineering*, vol. 107, pp. 54–61, 2018.

[54] K. Yung, T. Xiao, H. Choy, W. Wang, and Z. Cai, "Laser polishing of additive manufactured cocr alloy components with complex surface geometry," *Journal of Materials Processing Technology*, vol. 262, pp. 53–64, 2018.

[55] J. Kumstel and B. Kirsch, "Polishing titanium-and nickel-based alloys using cw-laser radiation," *Physics procedia*, vol. 41, pp. 362–371, 2013.

[56] W. Dai, J. Li, W. Zhang, and Z. Zheng, "Evaluation of fluences and surface characteristics in laser polishing skd 11 tool steel," *Journal of Materials Processing Technology*, vol. 273, p. 116241, 2019.

[57] J. dos Santos Solheid, H. J. Seifert, and W. Pfleging, "Laser surface modification and polishing of additive manufactured metallic parts," *Procedia Cirp*, vol. 74, pp. 280–284, 2018.

[58] C. Nüsser, H. Sändker, and E. Willenborg, "Pulsed laser micro polishing of metals using dual-beam technology," *Physics procedia*, vol. 41, pp. 346–355, 2013.

[59] A. Caggiano, R. Teti, V. Alfieri, and F. Caiazzo, "Automated laser polishing for surface finish enhancement of additive manufactured components for the automotive industry," *Production Engineering*, vol. 15, no. 1, pp. 109–117, 2021.

[60] M. Awd, J. Tenkamp, M. Hirtler, S. Siddique, M. Bambach, and F. Walther, "Comparison of microstructure and mechanical properties of scalmalloy® produced by selective laser melting and laser metal deposition," *Materials*, vol. 11, no. 1, p. 17, 2018.

[61] S. Baig, S. R. Ghiaasiaan, and N. Shamsaei, "Effect of heat treatment on the microstructure and mechanical properties of lb-pbf alsi10mg and scalmalloy," in *Light Metals 2021: 50th Anniversary Edition*, pp. 119–125, Springer International Publishing, 2021.

[62] L. Cordova, E. Macia, M. Campos, and T. Tinga, "Mechanical properties of aluminum alloys produced by metal additive manufacturing," in *Euro PM 2018 Congress & Exhibition*, 2018.

[63] S. Texture, "Ansi/asme b46. 1," *American Society of Mechanical Engineers, NY, New York*, vol. 10017, 1995.

[64] C. Ma, Y. Guan, and W. Zhou, "Laser polishing of additive manufactured ti alloys," *Optics and Lasers in Engineering*, vol. 93, pp. 171–177, 2017.

[65] D. Bhaduri, P. Penchev, A. Batal, S. Dimov, S. L. Soo, S. Sten, U. Harrysson, Z. Zhang, and H. Dong, "Laser polishing of 3d printed mesoscale components," *Applied Surface Science*, vol. 405, pp. 29–46, 2017.

SECTION

2. CONCLUSION AND FUTURE WORK

Considering a great application of additive manufacturing in rapid prototyping and complex parts manufacturing, this research targets at several key issues associated with fatigue testing and property characterization of AM materials including the fabrication, machining, and polishing using lasers. Based on these research tasks, the conclusions can be summarized as follows.

At first, the constraints on the implementation of miniature specimens in fatigue testing were addressed and the effectiveness of the dual gauge miniature specimen to overcome these limitations was demonstrated. The implementation of miniature specimens minimizes the material cost and build time of AM test samples. Additionally, fatigue test setup for miniature specimens reduces the test equipment cost and power consumption requirements. The dual gauge Krouse type specimen captures many surfaces and microstructural defects with the increased surface area. Uniform stress distribution within gauges and symmetric loading conditions during the test reduce the stress gradient effect on miniature specimens. Finite element analysis and sensitivity analysis performed in this study evaluates the validity of the specimen in conducting fatigue tests. The random failure location of the samples within the gauges confirms the uniform nominal stress distribution. The new control signal monitoring (CSM) method introduces a simple but effective approach to identifying the nucleation and propagation phase during fatigue testing without incorporating any additional sensor. In this task, the fatigue test was performed with a simply supported loading mechanism on wrought and AM 304L stainless steel materials using a unique adaptive displacement controlled mini fatigue test setup. The adaptive PD controller has been proven to be a useful controller design approach in displacement-controlled high cycle fatigue

testing of miniature specimens. The test results and analyses illustrate that AM materials demonstrate lower fatigue strength in terms of both the nucleation and propagation cycles compared to bulk wrought material. The comparative study of the fatigue performance of wrought and AM material reveals that the presence of surface defects and other internal defects are the major reasons for AM materials exhibiting lower fatigue strength both in terms of nucleation and propagation life cycles compared to wrought materials.

To further extend the research, the effect of build process parameters and build orientation on fatigue strength of LPBF 304L stainless steel was investigated. Samples were deposited based on an experimental design to determine nominal and optimized parameters from part density, tensile, and toughness tests. These parameters were chosen to fabricate specimens for fatigue testing. The feasibility of determining the nominal and optimized fabrication process parameters was demonstrated effectively in this study. The fatigue test was performed for displacement control on a Krouse-type miniature specimen with a dual gauge. The nucleation and propagation phase was identified by implementing the control signal monitoring method. The analyses and experimental results show that material fabricated with optimized parameters demonstrate a higher fatigue strength at horizontal, inclined, and vertical directions than the specimens built with nominal parameters. Materials built with nominal parameters consist of the lack of fusion type defects mostly while the materials for the optimized parameters are expected to have keyhole type defects most. For particular stress, horizontal specimens have higher strength both during nucleation and propagation compared to the inclined and vertical specimens while the inclined specimens have higher strength than the vertical ones. For both the parameters, this is in good agreement with the anisotropy issue. For a dense part, the AM material built with higher energy density during fabrication yields a higher fatigue strength at all orientations due to the lower probability of the presence of lack of fusion type defects. Additionally, lack of fusion type defects compared to the keyhole defects are found to be critical in the high cycle fatigue of AM materials. In bending fatigue, the horizontal fatigue specimens demonstrate

a higher fatigue strength compared to the inclined and vertical specimens at all different process parameters due to the anisotropy issue and the presence of fewer layers within gauges.

AM metal parts exhibit a high surface roughness which influences the fatigue characteristics. To improve the surface quality of AM materials, post-processing is required. In the final task, a unique laser-aided machining and polishing process was presented to reduce the surface roughness of AM metals. Multiple lasers were integrated together for direct energy deposition, machining, and polishing of Scalmalloy AM materials in the same build chamber. A unique scan pattern was introduced to implement low energy input for machining and polishing. A two-step polishing process using a continuous-wave and pulsed laser was employed for rough and fine polishing. A systematic approach was discussed and implemented to obtain optimal process parameters for machining and polishing of AM aluminum alloy. A regression analysis was performed, and a mathematical model was derived from the experimental results to predict the material removed during the machining process. The roughness and waviness in the surface topography were minimized using the combined machining and polishing process and a more than 97% improvement in surface quality was achieved. Studying the effect of LAMP process parameters in machining and polishing AM materials helps reduce the surface roughness of AM parts. Additionally, investigations performed on the LAMP process may introduce new scientific approaches to improving the surface quality of AM parts.

The research findings of this dissertation add a significant scientific and knowledge-based contribution in the advancement of the fundamental understanding of the high cycle bending fatigue characterization of AM materials and laser-aided machining and polishing besides additive manufacturing. The fatigue test method and LAMP process can be applied in the extensive study on other AM materials. This research has broader impact on the fatigue characterization of AM materials. Using multiple units of equipment, high throughput fatigue test results can be obtained for AM materials. The statistical distribution of fatigue

behavior can be achieved with much less effort compared to the standard test equipment and samples. Furthermore, the work may inspire other researchers to employ the equipment and implement data-driven approaches in process parameter optimization and life cycle prediction models. The LAMP process can also be applied to obtain geometric dimension and tolerances (GD&T) for custom parts and for other AM processes, materials, and alloys. The influence of the laser-aided machining and polishing process on the microstructure and mechanical properties such as hardness, corrosion resistance, and fatigue performance can also be a part of future studies. The overall outcome of this dissertation provided with methodologies for high cycle fatigue characterization and machining and polishing of AM materials could benefit many industries.

REFERENCES

[1] Jean-Pierre Kruth, Ludo Froyen, Jonas Van Vaerenbergh, Peter Mercelis, Marleen Rombouts, and Bert Lauwers. Selective laser melting of iron-based powder. *Journal of materials processing technology*, 149(1-3):616–622, 2004.

[2] Yitao Chen, Xinchang Zhang, Mohammad Masud Parvez, and Frank Liou. A review on metallic alloys fabrication using elemental powder blends by laser powder directed energy deposition process. *Materials*, 13(16):3562, 2020.

[3] I Yadroitsev, A Gusarov, I Yadroitsava, and I Smurov. Single track formation in selective laser melting of metal powders. *Journal of Materials Processing Technology*, 210(12):1624–1631, 2010.

[4] Itziar Serrano-Munoz, Jean-Yves Buffiere, Rajmund Mokso, Catherine Verdu, and Yves Nadot. Location, location & size: defects close to surfaces dominate fatigue crack initiation. *Scientific reports*, 7:45239, 2017.

[5] Veerappan Prithivirajan and Michael D Sangid. The role of defects and critical pore size analysis in the fatigue response of additively manufactured in718 via crystal plasticity. *Materials & Design*, 150:139–153, 2018.

[6] Eyitayo Olatunde Olakanmi, RF Cochrane, and KW Dalgarno. A review on selective laser sintering/melting (sls/slm) of aluminium alloy powders: Processing, microstructure, and properties. *Progress in Materials Science*, 74:401–477, 2015.

[7] Mohammad Masud Parvez, Sahil Patel, Sriram Praneeth Isanaka, and Frank Liou. A novel laser-aided machining and polishing process for additive manufacturing materials with multiple endmill emulating scan patterns. *Applied Sciences*, 11(20): 9428, 2021.

[8] Yitao Chen, Xinchang Zhang, Mohammad Masud Parvez, Joseph W Newkirk, and Frank Liou. Fabricating tinicu ternary shape memory alloy by directed energy deposition via elemental metal powders. *Applied Sciences*, 11(11):4863, 2021.

[9] Wolfgang Schneller, Martin Leitner, Sebastian Pomberger, Sebastian Springer, Florian Beter, and Florian Grün. Effect of post treatment on the microstructure, surface roughness and residual stress regarding the fatigue strength of selectively laser melted alsi10mg structures. *Journal of Manufacturing and Materials Processing*, 3(4):89, 2019.

[10] S Romano, A Brückner-Foit, A Brandão, J Gumpinger, T Ghidini, and S Beretta. Fatigue properties of alsi10mg obtained by additive manufacturing: Defect-based modelling and prediction of fatigue strength. *Engineering Fracture Mechanics*, 187: 165–189, 2018.

[11] Zhen Wang, Wenwang Wu, Guian Qian, Lijuan Sun, Xide Li, and José AFO Correia. In-situ sem investigation on fatigue behaviors of additive manufactured al-si10-mg alloy at elevated temperature. *Engineering Fracture Mechanics*, 214:149–163, 2019.

[12] Even W Hovig, Amin S Azar, Martin F Sunding, Erik Andreassen, and Knut Sørby. High cycle fatigue life estimation of materials processed by laser powder bed fusion. *Fatigue & Fracture of Engineering Materials & Structures*, 42(7):1454–1466, 2019.

[13] YY Sun, SL Lu, S Gulizia, CH Oh, D Fraser, M Leary, and M Qian. Fatigue performance of additively manufactured ti-6al-4v: Surface condition vs. internal defects. *JOM*, pages 1–9.

[14] Zhuoer Chen, Sheng Cao, Xinhua Wu, and Chris HJ Davies. Surface roughness and fatigue properties of selective laser melted ti–6al–4v alloy. In *Additive Manufacturing for the Aerospace Industry*, pages 283–299. Elsevier, 2019.

[15] Bastien Vayssette, Nicolas Saintier, Charles Brugger, Mohamed El May, and Etienne Pessard. Numerical modelling of surface roughness effect on the fatigue behavior of ti-6al-4v obtained by additive manufacturing. *International Journal of Fatigue*, 123: 180–195, 2019.

[16] S Tammas-Williams, PJ Withers, I Todd, and PB Prangnell. The influence of porosity on fatigue crack initiation in additively manufactured titanium components. *Scientific reports*, 7(1):1–13, 2017.

[17] AM Vilardell, Pavel Krakhmalev, Gunnel Fredriksson, F Cabanettes, A Sova, D Valentin, and P Bertrand. Influence of surface topography on fatigue behavior of ti6al4v alloy by laser powder bed fusion. *Procedia CIRP*, 74:49–52, 2018.

[18] P Li, DH Warner, JW Pegues, MD Roach, N Shamsaei, and N Phan. Towards predicting differences in fatigue performance of laser powder bed fused ti-6al-4v coupons from the same build. *International Journal of Fatigue*, 126:284–296, 2019.

[19] Shuai Shao, Michael Khonsari, Shengmin Guo, Wen Jin Meng, and Nan Li. Overview: Additive manufacturing enabled accelerated design of ni-based alloys for improved fatigue life. *Additive Manufacturing*, page 100779, 2019.

[20] Sagar Sarkar, Cheruvu Siva Kumar, and Ashish Kumar Nath. Effects of different surface modifications on the fatigue life of selective laser melted 15–5 ph stainless steel. *Materials Science and Engineering: A*, 762:138109, 2019.

[21] Shahriar Afkhami, Mohammad Dabiri, S Habib Alavi, Timo Björk, and Antti Salminen. Fatigue characteristics of steels manufactured by selective laser melting. *International Journal of Fatigue*, 122:72–83, 2019.

[22] Meng Zhang, Chen-Nan Sun, Xiang Zhang, Phoi Chin Goh, Jun Wei, David Hardacre, and Hua Li. High cycle fatigue life prediction of laser additive manufactured stainless steel: A machine learning approach. *International Journal of Fatigue*, 128:105194, 2019.

[23] Milad Hamidi Nasab, Alessandro Giussani, Dario Gastaldi, Valeria Tirelli, and Maurizio Vedani. Effect of surface and subsurface defects on fatigue behavior of alsi10mg alloy processed by laser powder bed fusion (l-pbf). *Metals*, 9(10):1063, 2019.

[24] Milad Hamidi Nasab, Simone Romano, Dario Gastaldi, Stefano Beretta, and Maurizio Vedani. Combined effect of surface anomalies and volumetric defects on fatigue assessment of alsi7mg fabricated via laser powder bed fusion. *Additive Manufacturing*, page 100918, 2019.

[25] Simone Romano, PD Nezhadfar, Nima Shamsaei, Mohsen Seifi, and Stefano Beretta. High cycle fatigue behavior and life prediction for additively manufactured 17-4 ph stainless steel: Effect of sub-surface porosity and surface roughness. *Theoretical and Applied Fracture Mechanics*, page 102477, 2020.

[26] Romali Biswal, Xiang Zhang, Abdul Khadar Syed, Mustafa Awd, Jialuo Ding, Frank Walther, and Stewart Williams. Criticality of porosity defects on the fatigue performance of wire+ arc additive manufactured titanium alloy. *International Journal of Fatigue*, 122:208–217, 2019.

[27] Luke Sheridan, Joy E Gockel, and Onome E Scott-Emuakpor. Primary processing parameters, porosity production, and fatigue prediction for additively manufactured alloy 718. *Journal of Materials Engineering and Performance*, 28(9):5387–5397, 2019.

[28] Nathan M Heckman, Thomas A Ivanoff, Ashley M Roach, Bradley H Jared, Daniel J Tung, Harlan J Brown-Shaklee, Todd Huber, David J Saiz, Josh R Koepke, Jeffrey M Rodelas, et al. Automated high-throughput tensile testing reveals stochastic process parameter sensitivity. *Materials Science and Engineering: A*, 772:138632, 2020.

[29] Bi Zhang, Yongtao Li, and Qian Bai. Defect formation mechanisms in selective laser melting: a review. *Chinese Journal of Mechanical Engineering*, 30(3):515–527, 2017.

[30] E Liverani, S Toschi, L Ceschini, and A Fortunato. Effect of selective laser melting (slm) process parameters on microstructure and mechanical properties of 316l austenitic stainless steel. *Journal of Materials Processing Technology*, 249:255–263, 2017.

[31] Kai Guan, Zemin Wang, Ming Gao, Xiangyou Li, and Xiaoyan Zeng. Effects of processing parameters on tensile properties of selective laser melted 304 stainless steel. *Materials & Design*, 50:581–586, 2013.

[32] Zhuqing Wang, Todd A Palmer, and Allison M Beese. Effect of processing parameters on microstructure and tensile properties of austenitic stainless steel 304l made by directed energy deposition additive manufacturing. *Acta Materialia*, 110:226–235, 2016.

[33] Yihong Kok, Xi Peng Tan, P Wang, MLS Nai, Ngiap Hiang Loh, Erjia Liu, and Shu Beng Tor. Anisotropy and heterogeneity of microstructure and mechanical properties in metal additive manufacturing: A critical review. *Materials & Design*, 139:565–586, 2018.

[34] Beth E Carroll, Todd A Palmer, and Allison M Beese. Anisotropic tensile behavior of ti–6al–4v components fabricated with directed energy deposition additive manufacturing. *Acta Materialia*, 87:309–320, 2015.

[35] Hanchen Yu, Jingjing Yang, Jie Yin, Zemin Wang, and Xiaoyan Zeng. Comparison on mechanical anisotropies of selective laser melted ti-6al-4v alloy and 304 stainless steel. *materials science and engineering: a*, 695:92–100, 2017.

[36] David B Witkin, Dhruv Patel, Thomas V Albright, Glenn E Bean, and Tait McLouth. Influence of surface conditions and specimen orientation on high cycle fatigue properties of inconel 718 prepared by laser powder bed fusion. *International Journal of Fatigue*, 132:105392, 2020.

[37] Sreekar Karnati, Atoosa Khiabhani, Aaron Flood, Frank Liou, and Joseph Newkirk. Anisotropy in impact toughness of powder bed fused aisi 304l stainless steel. *Material Design & Processing Communications*, page e59, 2019.

[38] Bastian Blinn, Marcus Klein, and Tilmann Beck. Determination of the anisotropic fatigue behaviour of additively manufactured structures with short-time procedure phyballit. In *MATEC web of conferences*, volume 165, page 02006. EDP Sciences, 2018.

[39] Janusz Sempruch and Tomasz Tomaszewski. Application of mini specimens to high-cycle fatigue tests. *Journal of Polish CIMAC*, 6(3):279–287, 2011.

[40] Tomasz Tomaszewski and Janusz Sempruch. Verification of the fatigue test method applied with the use of mini specimen. In *Key Engineering Materials*, volume 598, pages 243–248. Trans Tech Publ, 2014.

[41] Zdeněk P Bažant. Size effect in blunt fracture: concrete, rock, metal. *Journal of Engineering Mechanics*, 110(4):518–535, 1984.

[42] T Hirose, H Sakasegawa, A Kohyama, Y Katoh, and H Tanigawa. Effect of specimen size on fatigue properties of reduced activation ferritic/martensitic steels. *Journal of Nuclear Materials*, 283:1018–1022, 2000.

[43] Haftirman Haftirman. The size effect on fatigue strength of structural steel materials in high-humidity environment. *Jurnal Mekanikal*, 32(1), 2011.

[44] Sreekar Karnati, I Axelsen, FF Liou, and Joseph William Newkirk. Investigation of tensile properties of bulk and slm fabricated 304l stainless steel using various gage length specimens. In *Proceedings of the 27th Annual International Solid Freeform Fabrication Symposium–An Additive Manufacturing Conference*, pages 592–604, 2016.

[45] J Dzugan, M Sibr, P Konopík, R Procházka, and M Rund. Mechanical properties determination of am components. In *IOP Conference Series: Materials Science and Engineering*, volume 179, page 012019. IOP Publishing, 2017.

[46] HY Wan, GF Chen, CP Li, XB Qi, and GP Zhang. Data-driven evaluation of fatigue performance of additive manufactured parts using miniature specimens. *Journal of Materials Science & Technology*, 35(6):1137–1146, 2019.

[47] ME Biancolini, Carlo Brutti, Gabriele Paparo, and Alessandro Zanini. Fatigue cracks nucleation on steel, acoustic emission and fractal analysis. *International Journal of Fatigue*, 28(12):1820–1825, 2006.

[48] J Meriaux, M Boinet, S Fouvry, and JC Lenain. Identification of fretting fatigue crack propagation mechanisms using acoustic emission. *Tribology International*, 43 (11):2166–2174, 2010.

[49] Li Lin and Fulei Chu. Hht-based ae characteristics of natural fatigue cracks in rotating shafts. *Mechanical Systems and Signal Processing*, 26:181–189, 2012.

[50] J Meriaux, S Fouvry, KJ Kubiak, and S Deyber. Characterization of crack nucleation in ta6v under fretting–fatigue loading using the potential drop technique. *International Journal of Fatigue*, 32(10):1658–1668, 2010.

[51] Akira Todoroki, Yoshihiro Mizutani, Yoshiro Suzuki, and Daichi Haruyama. Fatigue damage detection of cfrp using the electrical resistance change method. *International Journal of Aeronautical and Space Sciences*, 14(4):350–355, 2013.

[52] Vladimir Zilberstein, Darrell Schlicker, Karen Walrath, Volker Weiss, and Neil Goldfine. Mwm eddy current sensors for monitoring of crack initiation and growth during fatigue tests and in service. *International Journal of Fatigue*, 23:477–485, 2001.

[53] SA Grammatikos, EZ Kordatos, TE Matikas, and AS Paipetis. Real-time debonding monitoring of composite repaired materials via electrical, acoustic, and thermographic methods. *Journal of materials engineering and performance*, 23(1): 169–180, 2014.

[54] Mohammad Masud Parvez, Yitao Chen, Sreekar Karnati, Connor Coward, Joseph W Newkirk, and Frank Liou. A displacement controlled fatigue test method for additively manufactured materials. *Applied Sciences*, 9(16):3226, 2019. doi: https://doi.org/10.3390/app9163226.

[55] Tolgahan Ermergen and Fatih Taylan. Review on surface quality improvement of additively manufactured metals by laser polishing. *Arabian Journal for Science and Engineering*, pages 1–17, 2021.

[56] Arun Krishnan and Fengzhou Fang. Review on mechanism and process of surface polishing using lasers. *Frontiers of Mechanical Engineering*, 14(3):299–319, 2019.

[57] Tiantian Deng, Jianjun Li, and Zhizhen Zheng. Fundamental aspects and recent developments in metal surface polishing with energy beam irradiation. *International Journal of Machine Tools and Manufacture*, 148:103472, 2020.

[58] L Giorleo, Elisabetta Ceretti, and Claudio Giardini. Ti surface laser polishing: effect of laser path and assist gas. *Procedia Cirp*, 33:446–451, 2015.

[59] Evgueni V Bordatchev, Abdullah MK Hafiz, and O Remus Tutunea-Fatan. Performance of laser polishing in finishing of metallic surfaces. *The International Journal of Advanced Manufacturing Technology*, 73(1-4):35–52, 2014.

[60] Shirzad Mohajerani, Evgueni V Bordatchev, and O Remus Tutunea-Fatan. Recent developments in modeling of laser polishing of metallic materials. *Lasers in Manufacturing and Materials Processing*, 5(4):395–429, 2018.

[61] Sundar Marimuthu, A Triantaphyllou, M Antar, D Wimpenny, H Morton, and M Beard. Laser polishing of selective laser melted components. *International Journal of Machine Tools and Manufacture*, 95:97–104, 2015.

[62] Chunyong Liang, Yazhou Hu, Ning Liu, Xianrui Zou, Hongshui Wang, Xinping Zhang, Yulan Fu, and Jingyun Hu. Laser polishing of ti6al4v fabricated by selective laser melting. *Metals*, 10(2):191, 2020.

[63] Seungjong Lee, Zabihollah Ahmadi, Jonathan W Pegues, Masoud Mahjouri-Samani, and Nima Shamsaei. Laser polishing for improving fatigue performance of additive manufactured ti-6al-4v parts. *Optics & Laser Technology*, 134:106639, 2021.

[64] Michael TC Chow, Evgueni V Bordatchev, and George K Knopf. Experimental study on the effect of varying focal offset distance on laser micropolished surfaces. *The International Journal of Advanced Manufacturing Technology*, 67(9-12):2607–2617, 2013.

[65] Tyler L Perry, Dirk Werschmoeller, Xiaochun Li, Frank E Pfefferkorn, and Neil A Duffie. The effect of laser pulse duration and feed rate on pulsed laser polishing of microfabricated nickel samples. *Journal of manufacturing science and engineering*, 131(3), 2009.

[66] Alessandra Caggiano, Roberto Teti, Vittorio Alfieri, and Fabrizia Caiazzo. Automated laser polishing for surface finish enhancement of additive manufactured components for the automotive industry. *Production Engineering*, 15(1):109–117, 2021.

[67] HT Brown, CR Mischke, and JE Shigley. Standard handbook of machine design. *Raleigh, North Carolina*, 2004.

[68] Yung-Li Lee, Jwo Pan, Richard Hathaway, and Mark Barkey. *Fatigue testing and analysis: theory and practice*, volume 13. Butterworth-Heinemann, 2005.

[69] Yoshikazu Nakai, Akihisa Hashimoto, Takeshi Imanishi, and Chiaki Hiwa. Size effect on fatigue strength of metallic micro-materials. In *Proceedings of Asian-Pacific Conference on Fracture and Strength*, volume 99, 1999.

[70] E Santecchia, AMS Hamouda, F Musharavati, E Zalnezhad, M Cabibbo, M El Mehtedi, and S Spigarelli. A review on fatigue life prediction methods for metals. *Advances in Materials Science and Engineering*, 2016, 2016.

[71] Flake C Campbell. *Elements of metallurgy and engineering alloys*. ASM International, 2008.

[72] S Beretta, A Ghidini, and F Lombardo. Fracture mechanics and scale effects in the fatigue of railway axles. *Engineering fracture mechanics*, 72(2):195–208, 2005.

[73] Masaki Nakajima, Keiro Tokaji, Hisatake Itoga, and Toshihiro Shimizu. Effect of loading condition on very high cycle fatigue behavior in a high strength steel. *International Journal of Fatigue*, 32(2):475–480, 2010.

[74] Yoshiaki Akiniwa, Nobuyuki Miyamoto, Hirotaka Tsuru, and Keisuke Tanaka. Notch effect on fatigue strength reduction of bearing steel in the very high cycle regime. *International Journal of Fatigue*, 28(11):1555–1565, 2006.

[75] A Wormsen, B Sjödin, G Härkegård, and A Fjeldstad. Non-local stress approach for fatigue assessment based on weakest-link theory and statistics of extremes. *Fatigue & Fracture of Engineering Materials & Structures*, 30(12):1214–1227, 2007.

[76] WN Findley. An explanation of size effect in fatigue of metals. *Journal of Mechanical Engineering Science*, 14(6):424–428, 1972.

[77] Shun-Peng Zhu, Stefano Foletti, and Stefano Beretta. Evaluation of size effect on strain-controlled fatigue behavior of a quench and tempered rotor steel: Experimental and numerical study. *Materials Science and Engineering: A*, 735:423–435, 2018.

[78] A Diemar, R Thumser, and JW Bergmann. Determination of local characteristics for the application of the weakest-link model. *Materialwissenschaft und Werkstofftechnik: Entwicklung, Fertigung, Prüfung, Eigenschaften und Anwendungen technischer Werkstoffe*, 36(5):204–210, 2005.

[79] Martin Leitner, Christian Garb, Heikki Remes, and Michael Stoschka. Microporosity and statistical size effect on the fatigue strength of cast aluminium alloys en ac-45500 and 46200. *Materials Science and Engineering: A*, 707:567–575, 2017.

[80] Chengqi Sun and Qingyuan Song. A method for predicting the effects of specimen geometry and loading condition on fatigue strength. *Metals*, 8(10):811, 2018.

[81] Martin Leitner, Michael Vormwald, and Heikki Remes. Statistical size effect on multiaxial fatigue strength of notched steel components. *International Journal of Fatigue*, 104:322–333, 2017.

[82] David B Lanning, Theodore Nicholas, and Anthony Palazotto. Hcf notch predictions based on weakest-link failure models. *International journal of fatigue*, 25(9-11): 835–841, 2003.

[83] Zdeněk P Bažant and Drahomír Novák. Probabilistic nonlocal theory for quasibrittle fracture initiation and size effect. i: Theory. *Journal of Engineering Mechanics*, 126 (2):166–174, 2000.

[84] M Makkonen. Statistical size effect in the fatigue limit of steel. *International journal of fatigue*, 23(5):395–402, 2001.

[85] G Härkegård and G Halleraker. Assessment of methods for prediction of notch and size effects at the fatigue limit based on test data by böhm and magin. *International Journal of Fatigue*, 32(10):1701–1709, 2010.

[86] Engineering ToolBox. Beams-fixed at both ends-continuous and point loads, 2004. URL `https://www.engineeringtoolbox.com/beams-fixed-both-ends-support-loads-deflection-d_809.html`.

[87] Engineering ToolBox. Beams-supported at both ends-continuous and point loads, 2009. URL `https://www.engineeringtoolbox.com/beam-stress-deflection-d_1312.html`.

[88] ASTM. *B593-96(2014)e1 Standard Test Method for Bending Fatigue Testing for Copper-Alloy Spring Materials*. ASTM International, West Conshohocken, PA, 2009. doi: https://doi.org/10.1520/B0593-96R14E01.

[89] PS De, CM Obermark, and RS Mishra. Development of a reversible bending fatigue test bed to evaluate bulk properties using sub-size specimens. *Journal of Testing and Evaluation*, 36(4):402–405, 2008.

[90] Piyush Gohil, Hemant N Panchal, Siddiqi Mahmud Sohail, and Devang V Mahant. Experimental and fea prediction of fatigue life in sheet metal (is 2062). *MH*, 1:1.

[91] Ahmed S Haidyrah, CH Castano, and Joseph William Newkirk. An experimental study on bending fatigue test with a krouse-type fatigue specimen. In *2014 ANS Winter Meeting and Nuclear Technology Expo*, pages 1–4, 2014.

[92] Ahmed S Haidyrah, Joseph W Newkirk, and Carlos H Castaño. Characterization a bending fatigue mini-specimen technique (krouse type) of nuclear materials. In *TMS 2015 144th Annual Meeting & Exhibition*, pages 1225–1232. Springer, 2015.

[93] Ahmed S Haidyrah, Joseph W Newkirk, and Carlos H Castaño. Weibull statistical analysis of krouse type bending fatigue of nuclear materials. *Journal of Nuclear Materials*, 470:244–250, 2016.

[94] Ferdinand Pierre Beer, Elwood Russell Johnston, John T DeWolf, and David F Mazurek. *Statics and mechanics of materials*. McGraw-Hill Education, 2017.

[95] William Thomson. *Theory of vibration with applications*. CrC Press, 2018.

[96] Xiaojun Wang and DDL Chung. Real-time monitoring of fatigue damage and dynamic strain in carbon fiber polymer-matrix composite by electrical resistance measurement. *Smart materials and structures*, 6(4):504, 1997.

[97] Ralph I Stephens, Ali Fatemi, Robert R Stephens, and Henry O Fuchs. *Metal fatigue in engineering*. John Wiley & Sons, 2000.

[98] Haël Mughrabi. Microstructural mechanisms of cyclic deformation, fatigue crack initiation and early crack growth. *Philosophical Transactions of the Royal Society A: Mathematical, Physical and Engineering Sciences*, 373(2038):20140132, 2015.

[99] S Al-Shahrani and TJ Marrow. Effect of surface finish on fatigue of stainless steels. In *ICF12, Ottawa 2009*, 2009.

[100] William E Frazier. Metal additive manufacturing: a review. *Journal of Materials Engineering and Performance*, 23(6):1917–1928, 2014.

[101] Yi Zhang, Linmin Wu, Xingye Guo, Stephen Kane, Yifan Deng, Yeon-Gil Jung, Je-Hyun Lee, and Jing Zhang. Additive manufacturing of metallic materials: a review. *Journal of Materials Engineering and Performance*, 27(1):1–13, 2018.

[102] John J Lewandowski and Mohsen Seifi. Metal additive manufacturing: a review of mechanical properties. *Annual Review of Materials Research*, 46:151–186, 2016.

[103] Kwai S Chan and Alonso Peralta-Duran. A methodology for predicting surface crack nucleation in additively manufactured metallic components. *Metallurgical and Materials Transactions A*, 50(9):4378–4387, 2019.

[104] Zhixin Zhan, Hua Li, and KY Lam. Development of a novel fatigue damage model with am effects for life prediction of commonly-used alloys in aerospace. *International Journal of Mechanical Sciences*, 155:110–124, 2019.

[105] Ted L Anderson and Ted L Anderson. *Fracture mechanics: fundamentals and applications*. CRC press, 2005.

[106] MM Parvez, Y Chen, JW Newkirk, and FF Liou. Comparison of fatigue performance between additively manufactured and wrought 304l stainless steel using a novel fatigue test setup. In *Solid Freeform Fabrication 2019: Proceedings of the 30th Annual International Solid Freeform Fabrication Symposium – An Additive Manufacturing Conference*, pages 353–363, 2019.

[107] Ben Brown. Characterization of 304l stainless steel by means of minimum input energy on the selective laser melting platform. Master's thesis, Missouri University of Science and Technology, 2014.

[108] Ian Gibson, David Rosen, Brent Stucker, and Mahyar Khorasani. Design for additive manufacturing. In *Additive manufacturing technologies*, pages 555–607. Springer, 2021.

[109] Kaufui V Wong and Aldo Hernandez. A review of additive manufacturing. *International scholarly research notices*, 2012, 2012.

[110] M Parvez, Y Chen, J Newkirk, and F Liou. Comparison of fatigue performance between additively manufactured and wrought 304l stainless steel using a novel fatigue test setup. *Proceedings of the Solid Freeform Fabrication*, pages 353–363, 2019.

[111] JA Ramos-Grez and DL Bourell. Reducing surface roughness of metallic freeform-fabricated parts using non-tactile finishing methods. *International Journal of Materials and Product Technology*, 21(4):297–316, 2004.

[112] Eberhard Abele and Michael Kniepkamp. Analysis and optimisation of vertical surface roughness in micro selective laser melting. *Surface Topography: Metrology and Properties*, 3(3):034007, 2015.

[113] Flaviana Calignano, D Manfredi, EP Ambrosio, Luca Iuliano, and Paolo Fino. Influence of process parameters on surface roughness of aluminum parts produced by dmls. *The International Journal of Advanced Manufacturing Technology*, 67(9-12): 2743–2751, 2013.

[114] Mohammad Masud Parvez, Tan Pan, Yitao Chen, Sreekar Karnati, Joseph W Newkirk, and Frank Liou. High cycle fatigue performance of lpbf 304l stainless steel at nominal and optimized parameters. *Materials*, 13(7):1591, 2020.

[115] KC Mills, BJ Keene, RF Brooks, and A Shirali. Marangoni effects in welding. *Philosophical Transactions of the Royal Society of London. Series A: Mathematical, Physical and Engineering Sciences*, 356(1739):911–925, 1998.

[116] Min Hyun Cho and Dave F Farson. Understanding bead hump formation in gas metal arc welding using a numerical simulation. *Metallurgical and materials transactions B*, 38(2):305–319, 2007.

[117] C Hauser, THC Childs, and KW Dalgamo. Selective laser sintering of stainless steel 314s hc processed using room temperature powder beds. In *1999 International Solid Freeform Fabrication Symposium*, 1999.

[118] F Klocke and C Wagner. Coalescence behaviour of two metallic particles as base mechanism of selective laser sintering. *CIRP Annals*, 52(1):177–180, 2003.

[119] Ruidi Li, Jinhui Liu, Yusheng Shi, Li Wang, and Wei Jiang. Balling behavior of stainless steel and nickel powder during selective laser melting process. *The International Journal of Advanced Manufacturing Technology*, 59(9):1025–1035, 2012.

[120] Jean-Pierre Kruth, Ben Vandenbroucke, Jonas Van Vaerenbergh, and Peter Mercelis. Benchmarking of different sls/slm processes as rapid manufacturing techniques. In *Proceedings of the International Conference Polymers & Moulds Innovations PMI 2005*, 2005.

[121] Kamran Mumtaz and Neil Hopkinson. Top surface and side roughness of inconel 625 parts processed using selective laser melting. *Rapid Prototyping Journal*, 2009.

[122] Giovanni Strano, Liang Hao, Richard M Everson, and Kenneth E Evans. Surface roughness analysis, modelling and prediction in selective laser melting. *Journal of Materials Processing Technology*, 213(4):589–597, 2013.

[123] Rui M Vilar. Laser cladding. In *ALT'02 International Conference on Advanced Laser Technologies*, volume 5147, pages 385–392. International Society for Optics and Photonics, 2003.

[124] Adriaan B Spierings, Thomas L Starr, and Konrad Wegener. Fatigue performance of additive manufactured metallic parts. *Rapid prototyping journal*, 2013.

[125] Karen Taminger, Robert A Hafley, David T Fahringer, and Richard E Martin. Effect of surface treatments on electron beam freeform fabricated aluminum structures. In *2004 International Solid Freeform Fabrication Symposium*, 2004.

[126] Lukas Löber, Christoph Flache, Romy Petters, Uta Kühn, and Jürgen Eckert. Comparison of different post processing technologies for slm generated 316l steel parts. *Rapid Prototyping Journal*, 2013.

[127] Anthony T Beaucamp, Yoshiharu Namba, Phillip Charlton, Samyak Jain, and Arthur A Graziano. Finishing of additively manufactured titanium alloy by shape adaptive grinding (sag). *Surface Topography: Metrology and Properties*, 3(2): 024001, 2015.

[128] Joseph M Flynn, Alborz Shokrani, Stephen T Newman, and Vimal Dhokia. Hybrid additive and subtractive machine tools–research and industrial developments. *International Journal of Machine Tools and Manufacture*, 101:79–101, 2016.

[129] E Willenborg. Polishing with laser radiation. *Kunststoffe international*, 97(6):37, 2007.

[130] Tyler L Perry, Dirk Werschmoeller, Xiaochun Li, Frank E Pfefferkorn, and Neil A Duffie. Micromelting for laser micro polishing of meso/micro metallic components. In *International Manufacturing Science and Engineering Conference*, volume 42908, pages 363–369, 2007.

[131] H-Y Wang, DL Bourell, and JJ Beaman. Laser polishing of silica slotted rods. *Materials science and technology*, 19(3):382–387, 2003.

[132] Shirzad Mohajerani, Joshua D Miller, O Remus Tutunea-Fatan, and Evgueni V Bordatchev. Thermo-physical modelling of track width during laser polishing of h13 tool steel. *Procedia Manufacturing*, 10:708–719, 2017.

[133] SR Vatsya and SK Nikumb. Modeling of fluid dynamical processes during pulsed-laser texturing of material surfaces. *Physical Review B*, 68(3):035410, 2003.

[134] Wojciech S Gora, Yingtao Tian, Aldara Pan Cabo, Marcus Ardron, Robert RJ Maier, Philip Prangnell, Nicholas J Weston, and Duncan P Hand. Enhancing surface finish of additively manufactured titanium and cobalt chrome elements using laser based finishing. *Physics Procedia*, 83:258–263, 2016.

[135] Michał Ćwikła, Robert Dziedzic, and Jacek Reiner. Influence of overlap on surface quality in the laser polishing of 3d printed inconel 718 under the effect of air and argon. *Materials*, 14(6):1479, 2021.

[136] Dongqi Zhang, Jie Yu, Hui Li, Xin Zhou, Changhui Song, Chen Zhang, Shengnan Shen, Linqing Liu, and Chengyuan Dai. Investigation of laser polishing of four selective laser melting alloy samples. *Applied Sciences*, 10(3):760, 2020.

[137] J Lambarri, J Leunda, C Soriano, and C Sanz. Laser surface smoothing of nickel-based superalloys. *Physics Procedia*, 41:255–265, 2013.

[138] Lan Chen and Xinzhou Zhang. Modification the surface quality and mechanical properties by laser polishing of al/pla part manufactured by fused deposition modeling. *Applied Surface Science*, 492:765–775, 2019.

[139] Chao Ma, Madhu Vadali, Neil A Duffie, Frank E Pfefferkorn, and Xiaochun Li. Melt pool flow and surface evolution during pulsed laser micro polishing of ti6al4v. *Journal of Manufacturing Science and Engineering*, 135(6), 2013.

[140] Joshua D Miller, O Remus Tutunea-Fatan, and Evgueni V Bordatchev. Experimental analysis of laser and scanner control parameters during laser polishing of h13 steel. *Procedia Manufacturing*, 10:720–729, 2017.

[141] JA Ramos, DL Bourell, and JJ Beaman. Surface over-melt during laser polishing of indirect-sls metal parts. *MRS Online Proceedings Library (OPL)*, 758, 2002.

[142] Christof W Schneider and Thomas Lippert. Laser ablation and thin film deposition. In *Laser processing of materials*, pages 89–112. Springer, 2010.

[143] Matthew S Brown and Craig B Arnold. Fundamentals of laser-material interaction and application to multiscale surface modification. In *Laser precision microfabrication*, pages 91–120. Springer, 2010.

[144] Benoit Rosa, Jean Yves Hascoet, and Pascal Mognol. Modeling and optimization of laser polishing process. In *Applied Mechanics and Materials*, volume 575, pages 766–770. Trans Tech Publ, 2014.

[145] Chen Chen and Hai-Lung Tsai. Fundamental study of the bulge structure generated in laser polishing process. *Optics and Lasers in Engineering*, 107:54–61, 2018.

[146] KC Yung, TY Xiao, HS Choy, WJ Wang, and ZX Cai. Laser polishing of additive manufactured cocr alloy components with complex surface geometry. *Journal of Materials Processing Technology*, 262:53–64, 2018.

[147] J Kumstel and B Kirsch. Polishing titanium-and nickel-based alloys using cw-laser radiation. *Physics procedia*, 41:362–371, 2013.

[148] Wei Dai, Jianjun Li, Weikang Zhang, and Zhizhen Zheng. Evaluation of fluences and surface characteristics in laser polishing skd 11 tool steel. *Journal of Materials Processing Technology*, 273:116241, 2019.

[149] Juliana dos Santos Solheid, Hans Jürgen Seifert, and Wilhelm Pfleging. Laser surface modification and polishing of additive manufactured metallic parts. *Procedia Cirp*, 74:280–284, 2018.

[150] C Nüsser, H Sändker, and E Willenborg. Pulsed laser micro polishing of metals using dual-beam technology. *Physics procedia*, 41:346–355, 2013.

[151] Mustafa Awd, Jochen Tenkamp, Markus Hirtler, Shafaqat Siddique, Markus Bambach, and Frank Walther. Comparison of microstructure and mechanical properties of scalmalloy® produced by selective laser melting and laser metal deposition. *Materials*, 11(1):17, 2018.

[152] Shaharyar Baig, Seyed R Ghiaasiaan, and Nima Shamsaei. Effect of heat treatment on the microstructure and mechanical properties of lb-pbf alsi10mg and scalmalloy. In *Light Metals 2021: 50th Anniversary Edition*, pages 119–125. Springer International Publishing, 2021.

[153] Laura Cordova, Eric Macia, Monica Campos, and Tiedo Tinga. Mechanical properties of aluminum alloys produced by metal additive manufacturing. In *Euro PM 2018 Congress & Exhibition*, 2018.

[154] Surface Texture. Ansi/asme b46. 1. *American Society of Mechanical Engineers, NY, New York*, 10017, 1995.

[155] CP Ma, YC Guan, and Wei Zhou. Laser polishing of additive manufactured ti alloys. *Optics and Lasers in Engineering*, 93:171–177, 2017.

[156] Debajyoti Bhaduri, Pavel Penchev, Afif Batal, Stefan Dimov, Sein Leung Soo, Stella Sten, Urban Harrysson, Zhenxue Zhang, and Hanshan Dong. Laser polishing of 3d printed mesoscale components. *Applied Surface Science*, 405:29–46, 2017.

VITA

Mohammad Masud Parvez was born in Bangladesh, a beautiful country in South Asia. He graduated from Khulna University of Engineering and Technology, Bangladesh in 2011 with a B.Sc. in Electrical and Electronic Engineering. After graduation, he started working as a product development officer at Bestway Powertech Limited and later as a senior system designer at Embedtheta in Dhaka, Bangladesh. He worked for about 3 years in industry and designed solar power systems from small to medium scale for rural and urban setups.

In 2014, he joined the lab of Dr. Frank Liou at Missouri University of Science and Technology for M.Sc. in Manufacturing Engineering. In this program, he studied the fundamentals of robotics and controls in manufacturing and worked on the development of a compliant robotic polishing process for additive manufacturing (AM) parts.

After the completion of M.Sc. in 2016, Parvez continued his research work in the same lab. He designed and developed several advanced Laser Metal Deposition (LMD) systems. His works included programming robots and controllers for metal AM systems, developing software, designing embedded electromechanical systems. His field of study covered fabricating metals and alloys using different AM processes, designing experiments for metal deposition, optimizing deposition process parameters to achieve good mechanical strength, characterizing mechanical properties such as tensile, toughness, hardness, fatigue strength, and studying the microstructure of printed parts to analyze the relationship between the microstructure and mechanical properties.

He received a PhD in Mechanical Engineering from Missouri University of Science and Technology in May 2022.